AN ABSTRACT OF THE THESIS OF

Clayton David Gosmeyer for the degree of Master of Science in Chemical Engineering presented on September 14, 1979

Title: AN EXPERIMENTAL STUDY OF HEAT TRANSFER IN A LARGE PARTICLE HEATED FLUIDIZED BED

Abstract approved: Redacted for privacy
Thomas J. Fitzgerald

In recent years there has been considerable interest in the potential uses of large particle fluidized beds. One of these uses is the combustion of coal in a fluidized bed of relatively large limestone particles, the result being reduced emission of sulphur oxides. Little or no literature data exist for either minimum fluidization velocities or local heat transfer coefficients in such large particle high temperature beds.

This thesis presents data for minimum fluidization velocities of large particles in a 0.31 m by 0.61 m cross-section bed. The data are presented for temperatures ranging between 570 K and 1090 K. The bed consisted of inert particles of a size distribution ranging between about 1 mm and 6 mm with a surface average diameter of 3.21 mm and a solids density of 2610 kg/m^3.

Minimum fluidization data were collected with no immersed tubes (here called an open bed) and with an immersed tube array.

The open bed data are found to be well correlated by the previously published equation of Wen and Yu. The bed depth was about 0.56 m during the experiments. The bed is operated near atmospheric pressure.

The thesis presents design, construction, testing and operating data for a transducer capable of measuring transient heat flux in high temperature fluidized beds. The device presented has a measured response time for 63.2% of a step change in flux of between 0.055 and 0.075 seconds. The device presented has a working surface of 2 mm diameter or less and a total diameter of 3.2 mm so that local flux measurements are obtained. The device output is typically 7.5 mV/$[MJ/m^2\text{-}s]$ to 15 mV/$[MJ/m^2\text{-}s]$ and the device DC resistance is typically 0.42Ω so that it is possible to obtain clean signals in electrically noisy environments with relatively simple electronics.

As a final test of the device operation and usefulness some local transient heat transfer data have been collected in a fluidized bed of inert particles of average diameter of 3.21 mm. The bed temperature was about 1080 K during the runs and most of the data presented are for $U_o/U_{mf} \tilde{=} 1.2$. The heat transfer to a single horizontal tube was measured. The data are presented as a function of radial position and the time averaged total heat transfer coefficient is found to vary

between 101 and 218 J/m^2-s-K. The range in instantaneous values of the heat transfer coefficient is found to be typically +300 J/m^2-s-K and -100 J/m^2-s-K.

An Experimental Study of Heat Transfer in a Large Particle Heated Fluidized Bed

by

Clayton David Gosmeyer

A THESIS

submitted to

Oregon State University

in partial fulfillment of
the requirements for the
degree of

Master of Science

Completed September 1979

Commencement June 1980

APPROVED:

Redacted for privacy

Professor of Chemical Engineering
in charge of major

Redacted for privacy

Head of Department of Chemical Engineering

Redacted for privacy

Dean of Graduate School

Date thesis is presented September 14, 1979

Typed by Opal Grossnicklaus for Clayton David Gosmeyer

ACKNOWLEDGMENTS

It is difficult to properly express gratitude to those who have helped me fulfill my desire to experiment and learn. I feel it is not possible to mention all who have helped me and to list what I consider to be their greatest contributions. Should I try I am certain to disappoint some and offend others. Consequentially I will mention only a few by name and I offer only my thanks to you who I neglect here.

My thanks go to Mrs. Louis Richter who provided a roof for my head at a price I could afford. They go also to Mr. Don Johnson, manager of the Memorial Union Craft Center, who provided employment and very kind moral support during my undergraduate years.

My thanks to Professor Charles Wicks for taking a chance on me and likewise to my major professor, Professor Thomas Fitzgerald who has given me the leeway to learn and expand. I hope that this work will be of benefit to both of them in some way.

Thanks to Mr. Chan who has taken me from the world of vacuum tubes and 100 lb power supplies into modern electronics.

Thanks to Adonis for dragging me away from this "addiction," at least on occasion.

Thanks to Richard, my office mate and collaborator, for being willing to work with me and to trade discussions.

Thanks to Professor Welty who has cooperated in every way and

made me feel at home in his department.

Thanks to the U. S. Department of Energy which has been largely responsible for financing my graduate work.

Thanks to Professor Binney, my minor professor, and to his department for accepting me so kindly.

Most of all, thanks to Mom and Dad for giving me this dream that has lasted for such a long time. I find it hard to believe.

TABLE OF CONTENTS

LIST OF FIGURES

LIST OF TABLES

NOTATION

Symbol		Description	Units
A_o	=	superficial area, no immersed internals	m^2
A'_o	=	equivalent superficial area of bed with immersed internals, $A'_o = A_o - A_{te}$	m^2
A_{te}	=	equivalent area of immersed internals	m^2
Ar	=	Archimedes number, $\bar{d}_p^{\,3} \rho_f(\rho_s - \rho_f) g / \mu_f^2$	dimensionless
C_1, C_2	=	integration constants	arbitrary
C_p	=	foil heat capacity	J/kg-K
D	=	average foil diameter	m
$\bar{dp}$	=	average bed particle diameter, $[\Sigma' X_i / dp_{mi}]^{-1}$	mm
dp_{mi}	=	mean of adjacent sieve openings	mm
E	=	thermocouple EMF	mV
E_{out}	=	circular foil transducer EMF	mV
g	=	acceleration of gravity	m/s^2
h_o	=	total heat transfer coefficient	J/m^2-s-K
h_R	=	radiative part of h_o	J/m^2-s-K
J_o, J_1	=	Bessel's functions	dimensionless
k	=	foil thermal conductivity	J/m-s-K

Symbol		Description	Units
k_o	=	foil thermal conductivity coefficient	J/m-s-K
L_s	=	slumped bed depth	m
Δp	=	fluidized bed pressure drop	kPa
$\dot{q}''$	=	total heat flux = $\dot{q}_l''+\dot{q}_c''$	J/m^2-s
$\dot{q}_l''$	=	radiative heat flux	J/m^2-s
$\dot{q}_c''$	=	convective heat flux	J/m^2-s
R	=	active foil radius	m
r	=	radial position from center of foil disk	m
r'	=	dimensionless radial position, r/R	dimensionless
Δr	=	incremental radial position	m
Re_{mf}	=	particle Reynolds number, $\overline{d}pU_{mf}\rho_f/u_f$	dimensionless
S	=	foil thickness	m
T	=	foil temperature	K
T_B	=	fluidized bed temperature as indicated by an immersed thermocouple	K
T_c	=	temperature at the center of foil disk	K
T_{LM}	=	average foil temperature	K
T_o	=	initial uniform foil disk temperature	K
T'	=	dimensionless foil temperature	dimensionless

Symbol		Description	Units
T''	=	dimensionless foil temperature	dimensionless
t	=	time	s
t'	=	dimensionless time	dimensionless
U_{mf}	=	minimum fluidization velocity based on superficial bed area, A_o	m/s
U'_{mf}	=	false minimum fluidization velocity based on A_o but with actual open area being $A_o - A_{te} = A'_o$	m/s
U_o	=	superficial velocity based on A_o	m/s
V_{eq}	=	equivalent volume of immersed internals	m^3
V_{im}	=	actual volume of immersed internals	m^3
V_{ls}	=	total volume of lee stacks supported by immersed internals	m^3
W_B	=	weight of bed	kg
X_i	=	weight fraction of particles of size equal to dp_{mi}	dimensionless

Greek Letters

α_n	=	eigenvalues for series solution	dimensionless
β	=	foil thermal conductivity coefficient	K^{-1}
ε	=	radiant emissivity	dimensionless
μ_f	=	fluid viscosity	Pa-s
ρ	=	foil density	kg/m^3
ρ_f	=	fluid density	kg/m^3
ρ_s	=	solids density	kg/m^3

Symbol		Description	Units
σ	=	Stefan-Boltzmann constant, 5.676E-8	$J/S\text{-}m^2\text{-}K^4$
τ	=	time constant	s
τ'	=	dimensionless time constant	dimensionless

AN EXPERIMENTAL STUDY OF HEAT TRANSFER IN A LARGE PARTICLE HEATED FLUIDIZED BED

I. INTRODUCTION

In recent years there has been considerable interest in the potential uses of large particle fluidized beds. One of these uses is the combustion of coal in a fluidized bed of limestone, with a consequential reduction of sulphur emissions. Some of the beds under consideration consist of particles ranging from very fine to 6 mm or more in diameter.

Since the interest in large particle fluidization has become widespread the United States Department of Energy has funded this basic research in the field. This thesis deals with the development and testing of equipment that is used to collect local transient heat transfer measurements to a cooled tube. The tube is immersed in a high temperature large particle fluidized bed of inert material.

In the course of the development it was found that there are few published data for the minimum fluidization velocity of particles in high temperature fluidized beds and apparently none at all for particles as large as used in this work ($\overline{d}_p$=3.21 mm). This latter fact, as well as the apparent discrepancies in the published data for smaller particles at high temperatures, led to the collection of data with the current equipment. The methods and results of this work are presented in Chapter II.

Just as there are little or no minimum fluidization velocity data there are apparently no published data on local transient heat transfer coefficients in large particle high temperature beds. Catapovic (1979) has recently published experimental results for such particles in a room temperature bed. Adams and Welty (1979) have recently published a theoretical model for heat transfer in large particle beds which Catapovic's results seem to verify. However, as Catapovic noted, at high temperatures the Adams and Welty theory predicts that radiative heat transfer becomes important. Catapovic's results are for low temperatures and so the radiative portion of the theory remained untested.

Chapter III of this thesis presents the method and a limited set of results for local transient heat transfer coefficient determination in this large particle high temperature fluidized bed. These results are compared to Catapovic's cold bed results.

Some of the data may be of use to those who design large particle high temperature fluidized beds.

II. MINIMUM FLUIDIZATION VELOCITY

A. Introduction

The design of gas fluidized bed combustors or reactors requires a reasonably accurate estimate of the necessary compressor capacity. A useful starting point for this estimate is the minimum fluidization velocity, defined as shown in Figure 2.1.

A large amount of literature data exist for U_{mf} for many different gas-solid combinations. Most of these experiments were carried out near room temperature and pressure. Various correlations have been proposed to fit these data, some are entirely empirical and some are empirical fits to packed bed pressure drop theory. Of the latter group, the Wen and Yu (1966a, b) correlation has been mentioned by Kunii and Levenspiel (1962) among others.

The Wen and Yu correlation is derived from the Ergun correlation for packed bed pressure drop and the above definition of U_{mf}. A very convenient feature of this correlation is that it includes observed empirical correlations for bed voidage versus particle sphericity at minimum fluidization conditions. The result is that only fluid properties and particle size and density information need be known.

The Wen and Yu correlation in dimensionless form is

$$Re_{mf} = \{(33.7)^2 + 0.0408\ Ar\}^{\frac{1}{2}} - 33.7 \qquad (2.1)$$

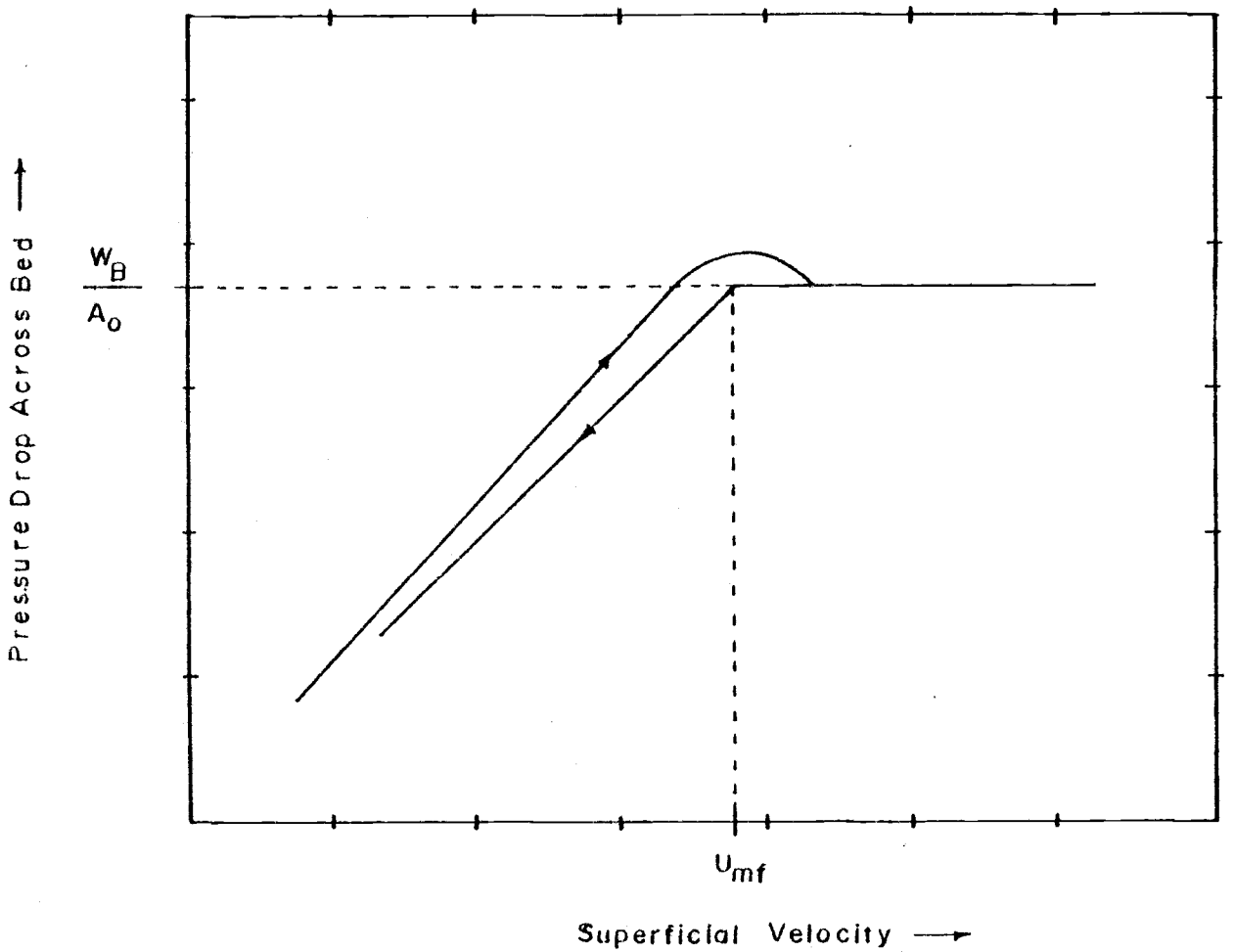

Figure 2.1 Minimum Fluidization Velocity Definition.

where

$$Re_{mf} = \frac{U_{mf}\bar{d}_p\rho_f}{\mu_f} \tag{2.2}$$

$$Ar = \frac{\bar{d}_p^{\,3}\rho_f(\rho_s-\rho_f)g}{\mu_f^{\,2}} \tag{2.3}$$

$$\bar{d}_p = \frac{1}{\Sigma \frac{X_i}{dp_{mi}}} \tag{2.4}$$

Figure 2.2 shows the Wen and Yu predictions of U_{mf} for different temperatures and average particle diameters for a 101.325kPa air-solid system.

A few workers have published data for minimum fluidization velocities at higher pressures and/or temperatures. Table 2.1 summarizes these works.

Figure 2.3 shows the experimental results of Avedesian and Davidson (1973) as well as the Wen and Yu predictions for their work. The deviation of the experimental results from the Wen and Yu correlation averages about ±5%.

Figure 2.4 shows one set of experimental results published by Saxena and Vogel (1976) as well as the Wen and Yu predictions. The experimental results cover a range of operating pressures (refer to Table 2.1 and the figure). The bed used in these experiments

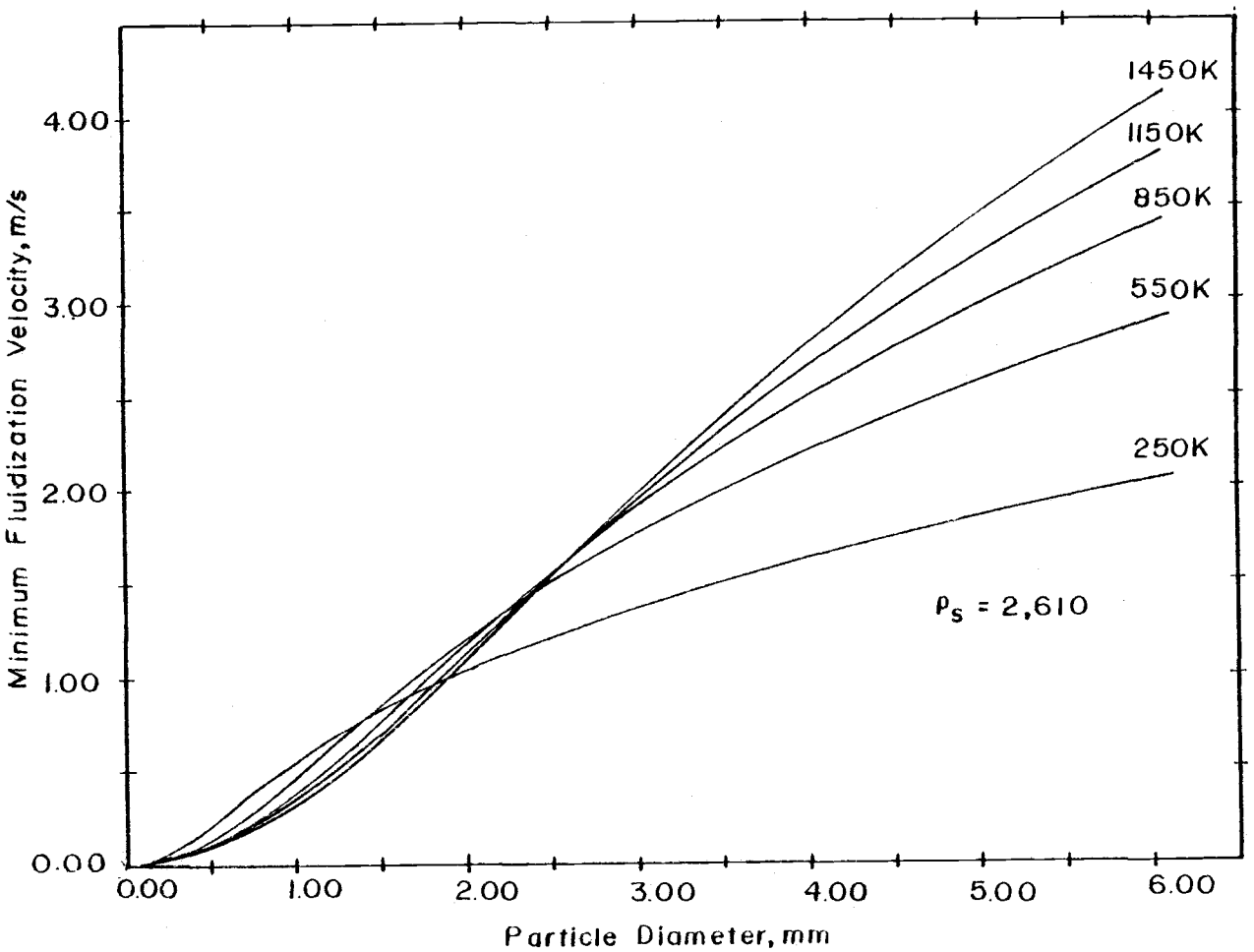

Figure 2.2 Wen and Yu Correlation for Various Temperatures.

Table 2.1. Summary of experimental conditions.

Experimenters	Temp., K	Press, kPa	Approx. Size Range	$\bar{d}_p$, mm	ρ_s, kg/m^3
Saxena and Vogel (1976)	294-655	179-827	88-1410 μm	0.717	~2750
Sazens and Vogel (1977	291-666	165-875	88-2000 μm	1.18-1.05	2750
	291-705	159-827	44-2000 μm	0.555-0.963	2750
Avedsian and Davidson (1973)	290-870	atmospheric	not given	0.39	2360
	290-870	atmospheric	not given	0.65	2360
Doheim and Collinge (1978)	293-650	atmospheric	66-124 μm	0.095	not given
Present Work	561-1091	atmospheric	2120-5520 μm	3.21	2610

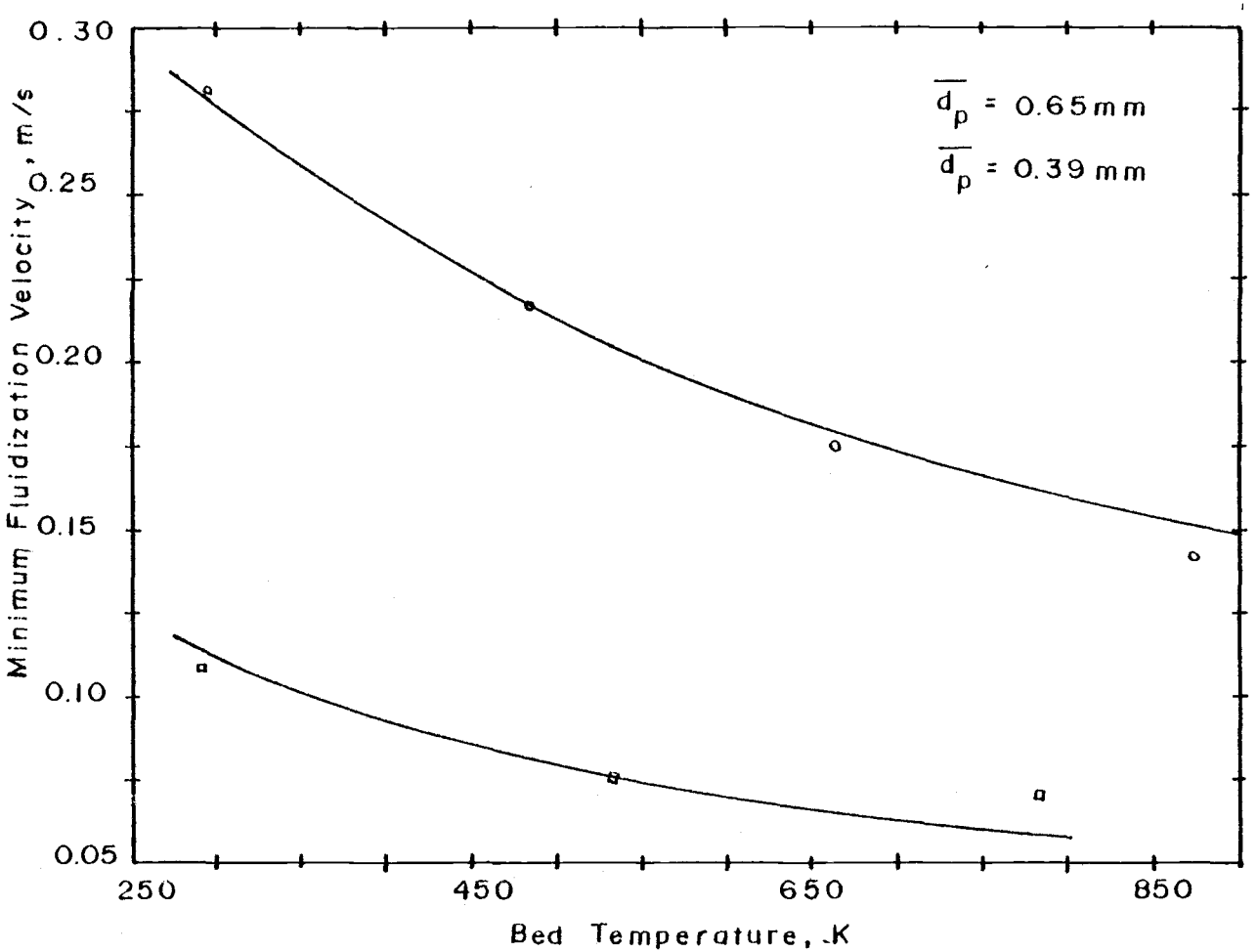

Figure 2.3 Avedesian and Davidson Results Compared to the Wen and Yu Correlation (Solid Lines).

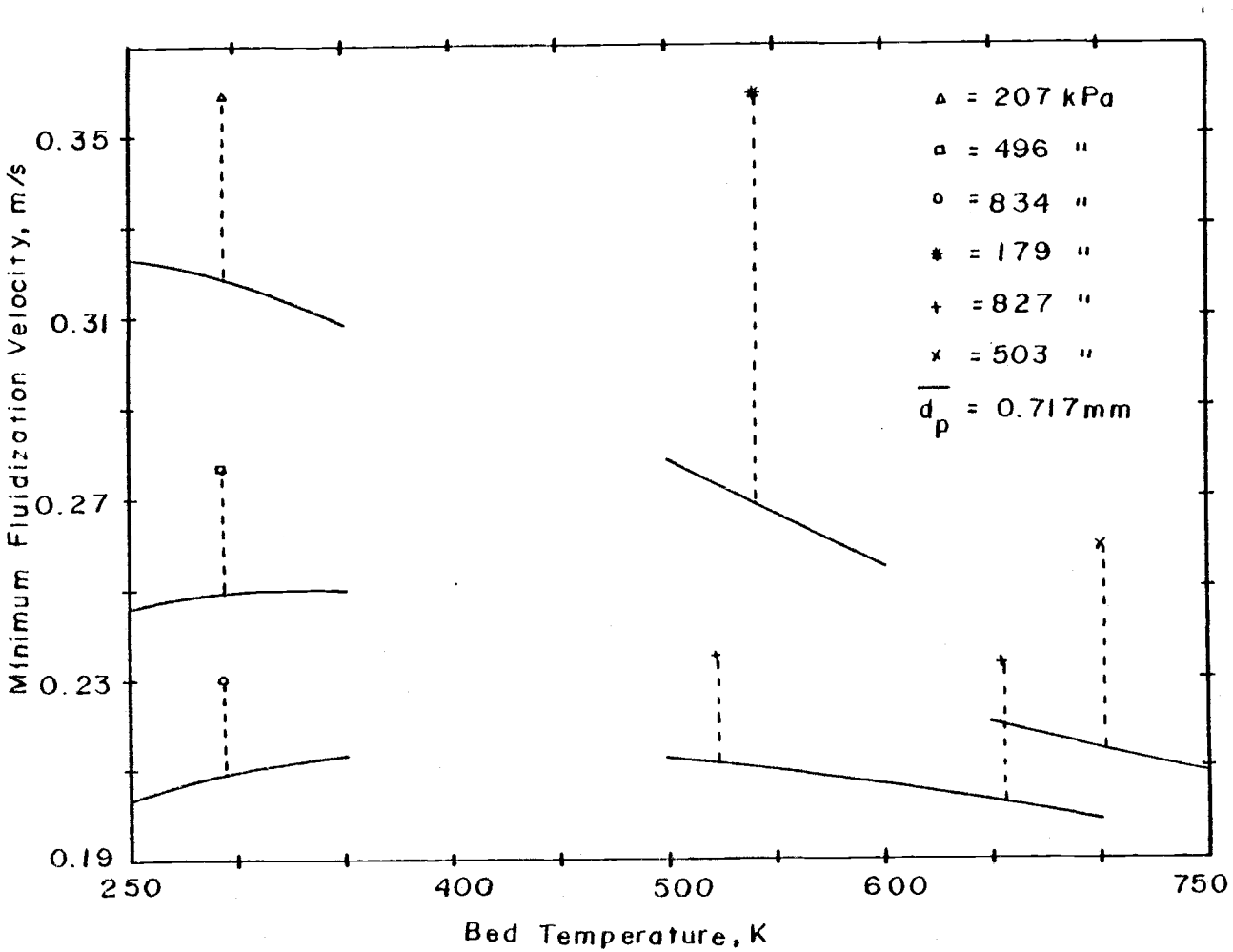

Figure 2.4 Saxena and Vogel Results Compared to the Wen and Yu Correlation (Solid Lines).

contained a relatively wide range of particle sizes (again refer to Table 2.1).

Saxena and Vogel (1977) have published further high temperature and pressure data. These latter data are not included in the figures as the mean particle diameters are not well defined in the published work.

The work of Doheim and Collinge (1978) covers the 293-650K temperature range for particles of 95 μm average diameter. It is not presented in the figures as the solids density is not defined in the published work so that the Wen and Yu curves could not be generated.

The present work covers the 561-1091K range for a 3.21 mm mean particle size bed.

B. Experimental Equipment

Figure 2.5 shows the experimental facility layout. More detail is given in Appendix A. Air is supplied by a 22.4 kW electric blower. Propane is metered into the air stream and combustion is completed in the firebox. The air distribution plate assembly is of stainless steel, perforated plate design.

The fluidized zone has a superficial cross-section of 0.31 by 0.61 m. Gas exiting the transport disengaging zone passes through a cyclone. Solids from the cyclone collect in a small bucket.

The air which enters the firebox is metered by a venturi tube. The venturi inlet pressure and the venturi differential pressure are

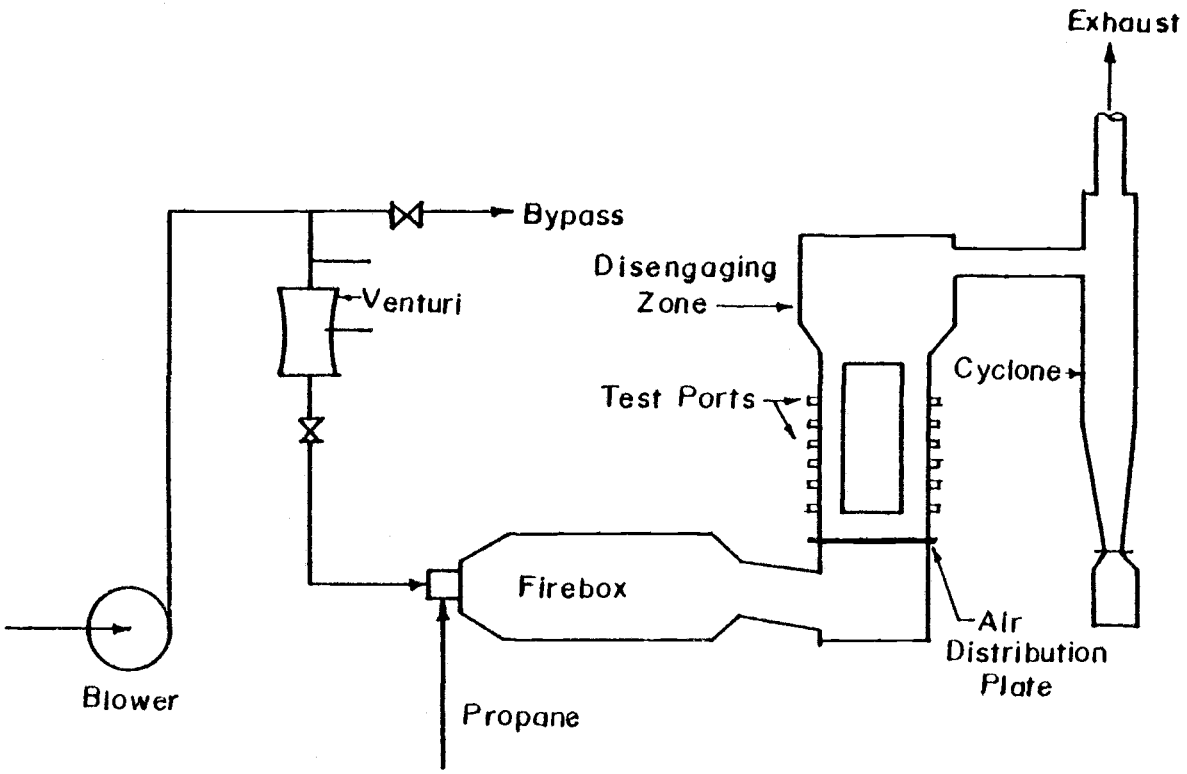

Figure 2.5 Experimental Facility Layout.

monitored by mercury and water manometers respectively. Each manometer is connected in parallel with a National Semiconductor brand solid state differential pressure gage.

The walls of the fluidized zone of the bed are supplied with instrument ports of several types. The locations of the various pressure, temperature, and tube array ports germane to these experiments are shown in Figure 2.6. The tube array crosses the bed parallel to the 0.31 m dimension.

The upper pressure tap, not shown in Figure 2.6, is located at the top of the transport disengaging zone. Both pressure taps are equipped with purge air meters and are connected across a water manometer in parallel with a solid state differential pressure transducer.

The thermocouple is a type K with a stainless steel well and is connected to a Honeywell pyrometer. The array tubes are uncooled, thin wall stainless steel tube of 50.8 mm o.d.

The bed material is a silica-alumina compound with the trade name Ione Grain. Before the first fluidization it was roughed to +3.2, -6.4 mm. There is some size degradation of this material when first fluidized at high temperature. Successive samples indicate that the size stabilizes after this first run. Typical size and density data are given in Table 2.2.

During the experimental runs with the array in place the slumped

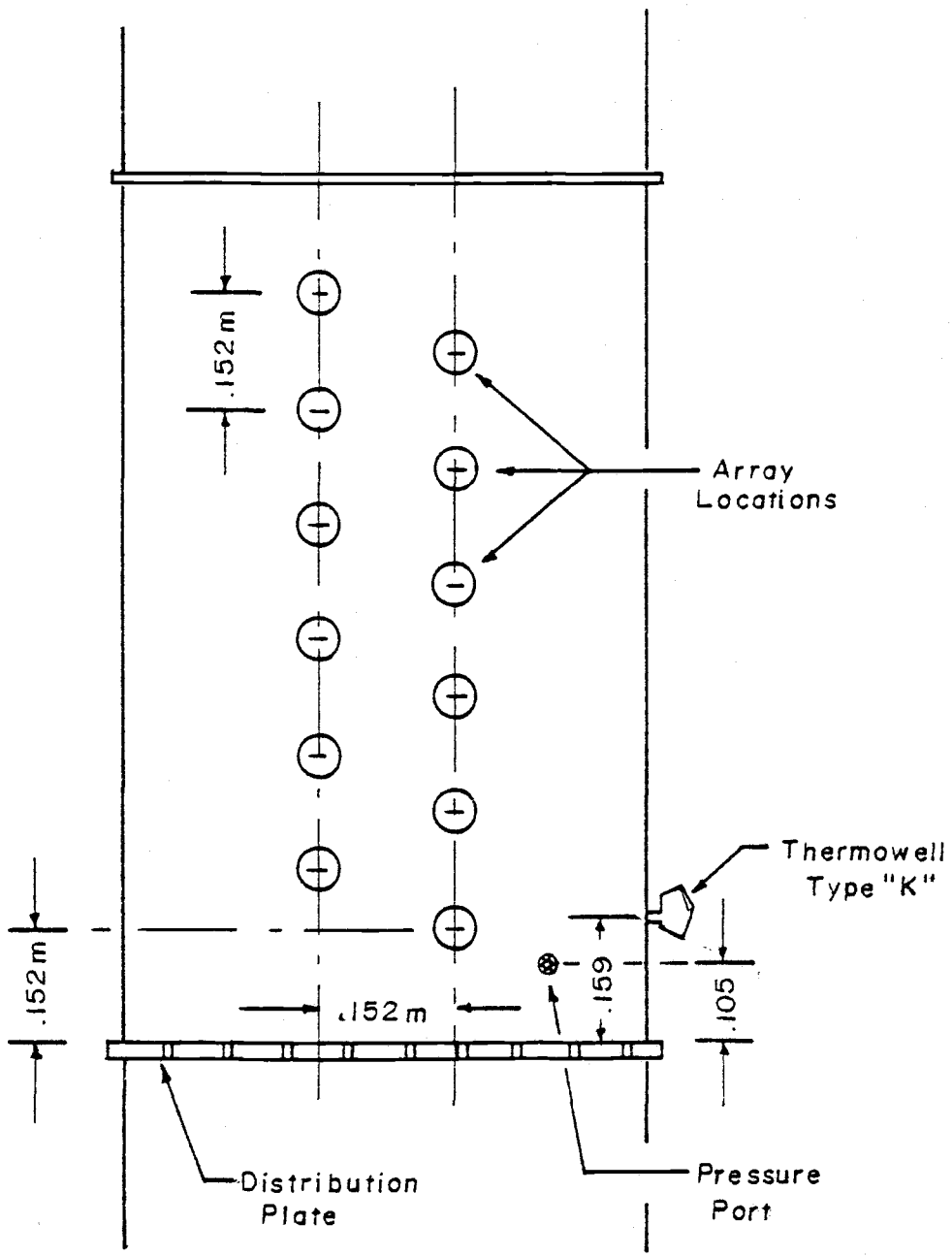

Figure 2.6 Tube Array and Test Port Locations.

Table 2.2. Bed material characteristics.

dp_{mi}, mm	fraction	
larger	trace	bulk density = 1500 kg/m^3
5.52	0.051	
4.03	0.344	solids density = 2610 kg/m^3
2.86	0.564	
2.12	0.041	
1.54	0.000	$\overline{d}_p$ = 3.21 mm
smaller	trace	

bed depth was about 0.58m. During the open bed (i.e. no tube array) runs the slumped depth was 0.56 m.

C. Experimental Procedures

Data collection is accomplished by the following procedures.

The bed is brought to temperature as indicated by the thermocouple. The bed is well mixed (U_o/U_{mf} = 1.3-1.4) at all times except for brief intervals during the actual data recording. When the bed thermocouple indicates no further change with time (about 45 minutes after a 56 K step in inlet temperature) the Visicorder chart drive is engaged and several cycles of lowering and then raising the air velocity are recorded. The velocity changes are accomplished by varying the bypass fraction of the blower output.

Since falling pressures and velocities are used to determine U_{mf}, the runs are always started from a strongly bubbling condition.

The venturi inlet pressure, the venturi differential pressure, and the partial bed differential pressure are recorded simultaneously.

The bed temperature is noted immediately before and after recording the data. In general there is no change in bed temperature as long as the runs are made without extended periods of low air velocity conditions.

Immediately after the above actions are carried out the air flow is set to several constant values and these conditions are recorded

with the Visicorder. The manometer readings corresponding to these conditions are noted for calibration purposes. The particular constant values which air flows are set at are chosen to bracket the expected U_{mf} values.

The calibration data with each group of experimental data were found useful as the electronic pressure transducers are sensitive to changes in the temperature of the environment. For the most part these drifts are small.

The array runs were made with one of the previously mentioned tubes in each of the twelve possible locations. Individual run calibrations were not made on the array data runs.

D. Data Analysis

A sample Visicorder trace copy is shown in Figure 2.7. Time proceeds from right to left. The air flow rate first increases and then decreases. The lines drawn in are the points that were used as occurring at minimum fluidizing conditions.

Since the lower pressure tap is several centimeters above the distributor plate, the measured bed differential pressure at U_{mf} is not equal to the weight of the bed divided by the superficial area, rather it is somewhat less. Pruden et al. (1976) found that taking the pressure drop across only the top 10% of the bed gave sharper drops in the pressure drop curve than taking the whole bed. In any case

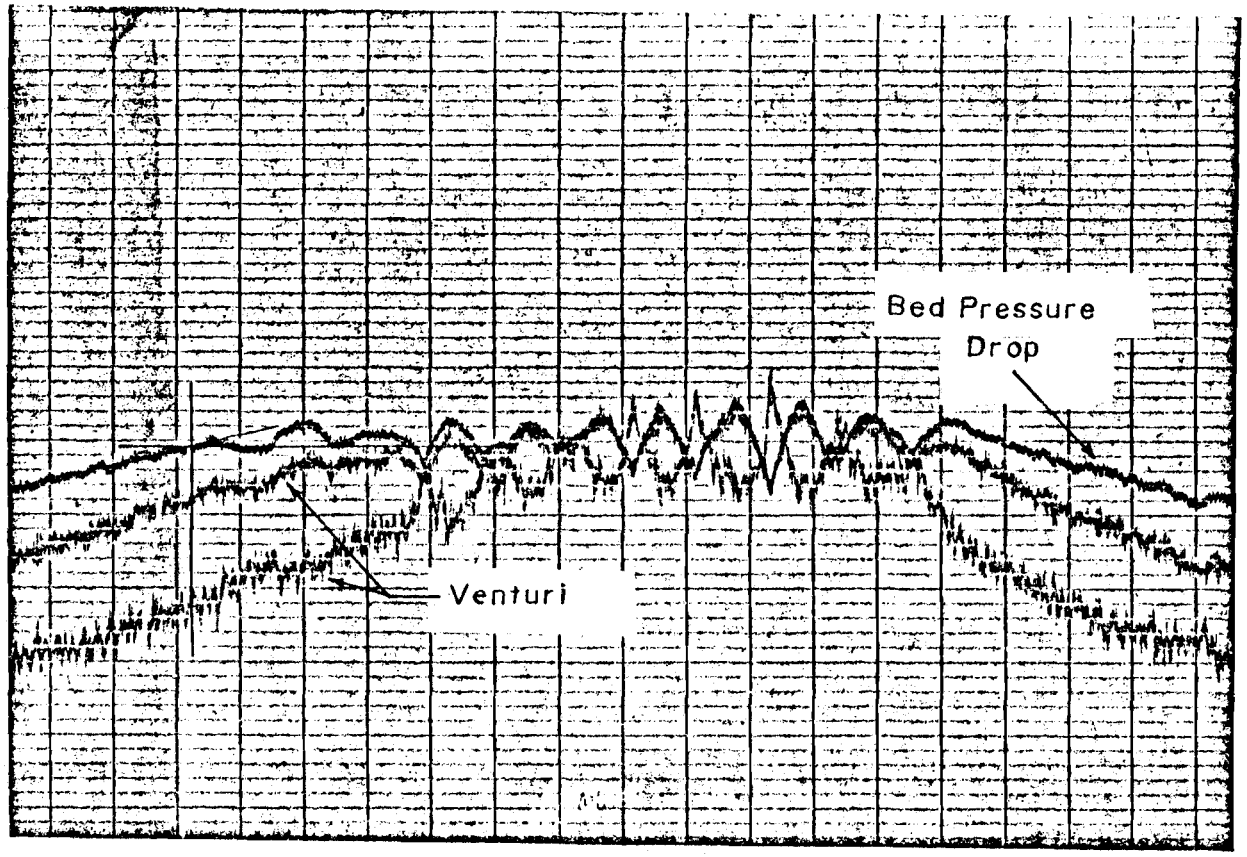

Figure 2.7 Sample Visicorder Chart Copy.

the break in the curve is fairly apparent and the observed pressure drop is consistent from run to run, showing a few percent increase from the lowest to highest temperatures recorded.

Data collected from the Visicorder charts at the falling pressure break points are then used to calculate the bed air velocity.

It is estimated that the accuracy of the given bed temperatures is better than ±20K. This estimate is based on comparison between the permanent thermowell and another which was temporarily installed at a location near the top of the bed. The upper thermocouple read 5-10K lower than the lower one at higher temperatures. This may be due to the considerable radiant loss from the top of the bed at higher temperatures.

The fluid properties of the bed gas are modified to account for the presence of combustion products, but are fairly close to those of pure air at the same temperature and pressure.

The major source of error is thought to be the Visicorder value for the venturi differential pressure. An error of 1 chart division in reading or recording this value results in an error in U_{mf} of about 3% at the lowest temperature up to about 10% at the highest.

The venturi itself was calibrated with a pitot tube-micromanometer apparatus. The results are found to agree well with the data published in A. S. M. E. (1959). Appendix B has some details.

The overall accuracy of the U_{mf} values reported here is expected

to be about ±12%, allowing ±10% for recording error, ±5% for temperature measurement, and ±5% for flow calibration. The precision of the 38 trials reported for the open bed case is ±2.9%.

E. Results and Discussion

The experimental results for the runs with the tube array in place are shown in Figure 2.8, and Table 2.3. The results for the open bed runs are shown in Figure 2.9 and Table 2.4. In both figures the solid curves are the Wen and Yu predictions for U_{mf}.

The indicated U_{mf} with the array in place is lower than those of the open bed as may be expected. At least a major part of this difference is due to calculating the superficial velocity as if the bed open area is that of the no array case, even when the array is present. Minimum fluidization air velocity requirements per unit of true open area are probably the same in either case.

Advance theoretical prediction of the equivalent area of the immersed bodies, to be used in estimating the true U_{mf} from experimental data, is complicated. However it is possible to get an estimate of the effective area when both array and open bed data are available, as in the present case.

Figure 2.10 shows three bed configurations. Figure 2.10a shows the open bed configuration, Figure 2.10b shows the case where there are immersed bodies, and Figure 2.10 c shows a fraction of the immersed volume lumped into a rectangular solid, V_{eq}, which extends

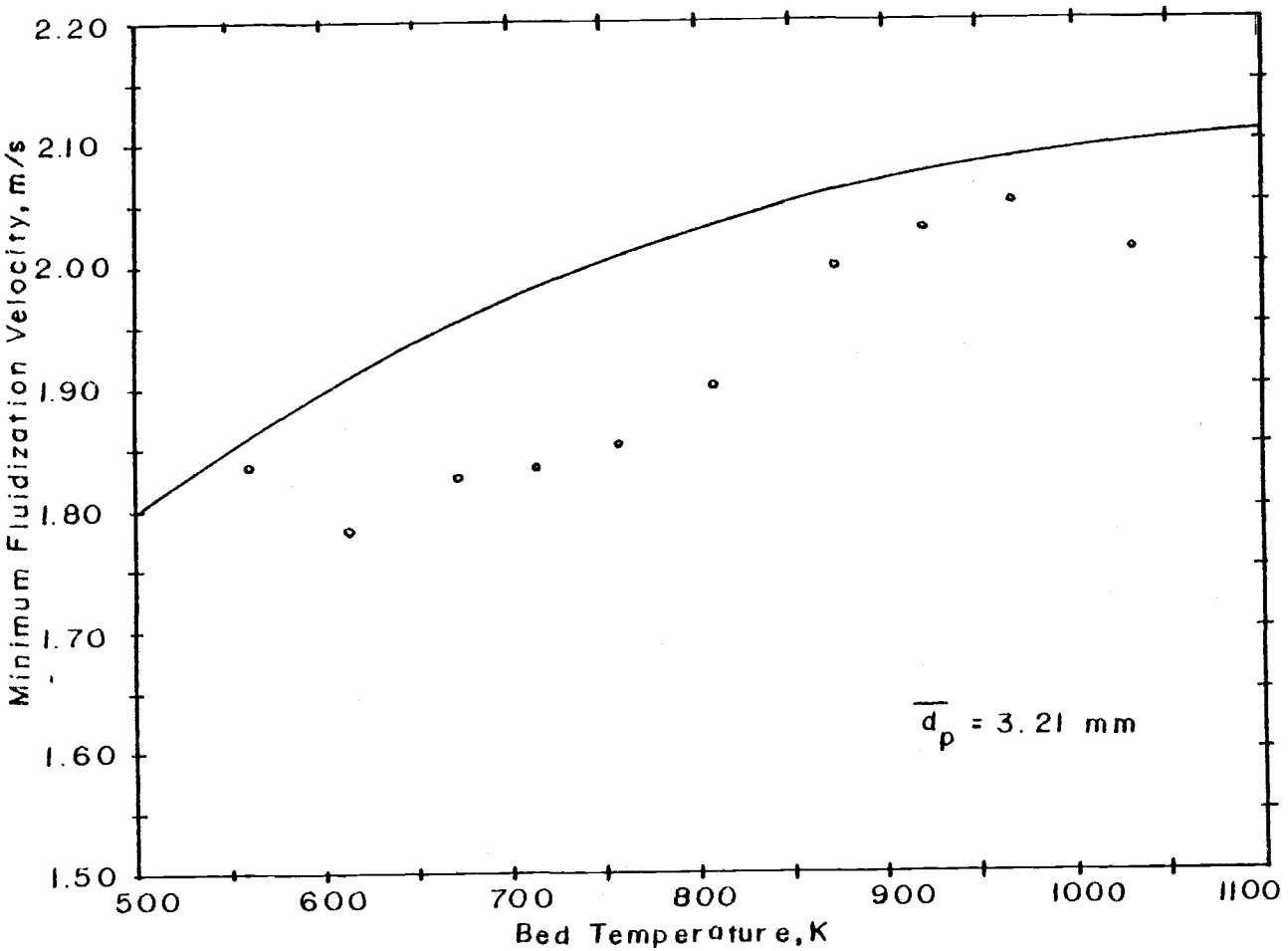

Figure 2.8 Experimental Results for the Immersed Tube Array Situation Compared to the Wen and Yu Correlation (Solid Line).

Table 2.3. Experimental results with tube array in place.

Temp., K.	U'_{mf}, m/sec
561	1.83
614	1.78
672	1.83
714	1.83
758	1.85
808	1.90
872	2.00
919	2.03
966	2.05
1030	2.01

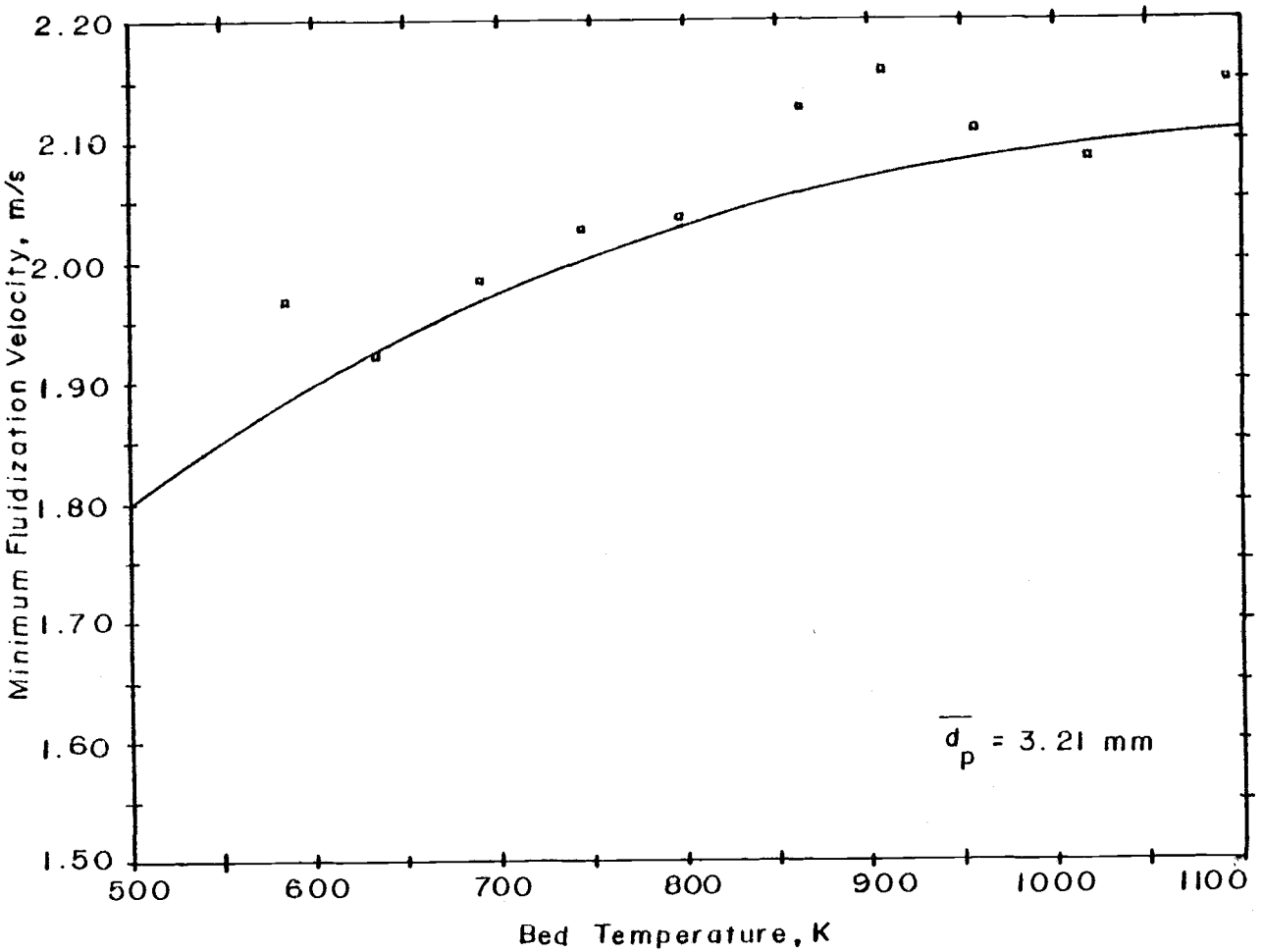

Figure 2.9 Experimental Results for the Open Bed Situation Compared to the Wen and Yu Correlation (Solid Line).

Table 2.4. Experimental results for the open bed situation.

Temp., K	U_{mf}, m/sec
583	1.97
633	1.92
689	1.98
744	2.03
797	2.04
861	2.13
905	2.16
955	2.11
1016	2.08
1091	2.15

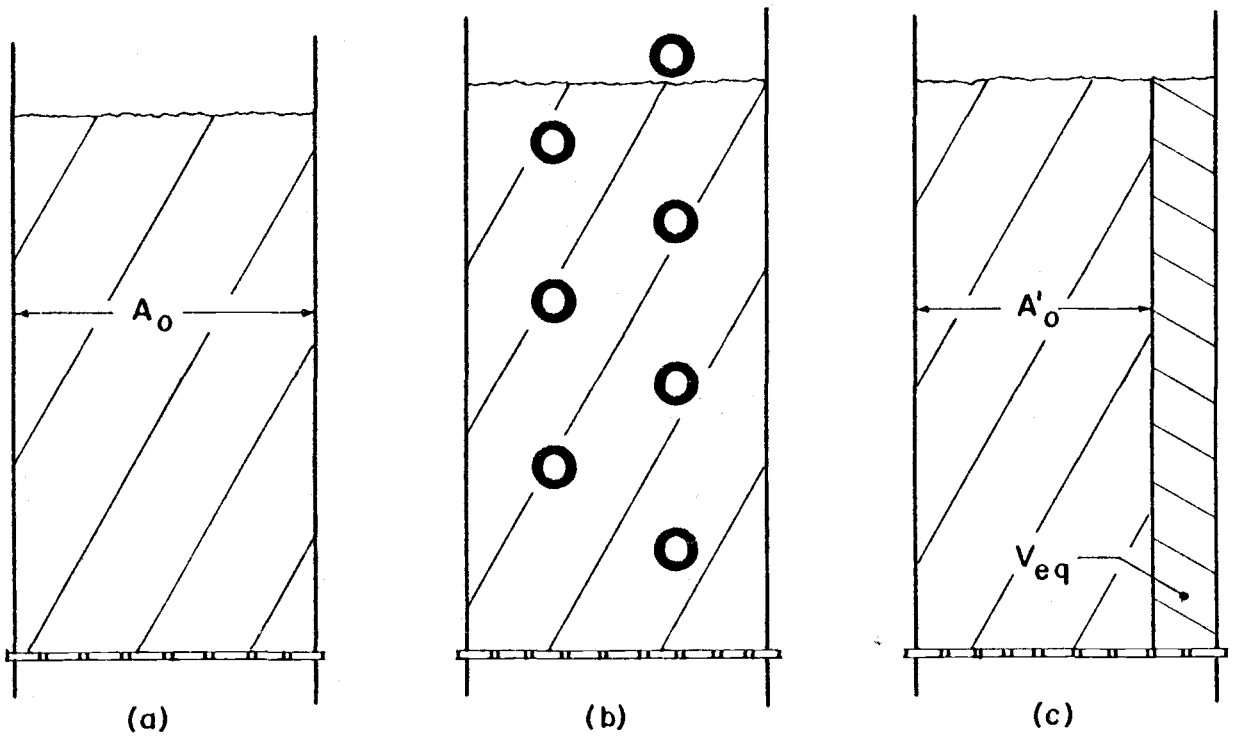

Figure 2.10 Equivalent Immersed Volume.

the depth and height of the bed.

If V_{im} is the actual immersed volume of the internals then in general it is expected that

$$V_{eq} \neq V_{im} \tag{2.7}$$

If A_{te} is the cross-sectional area of V_{eq} in the direction of bulk gas flow, then the equivalent open area is given by

$$A_o' = A_o - A_{te} \tag{2.8}$$

If, as previously mentioned, U_{mf} and U_{mf}' are both based on the superficial area, A_o, and if it is further taken that the actual minimum fluidization velocity for a particular size and specific gravity of particles is the same whether or not there are adjacent walls, then a material balance gives

$$A_o' = \frac{U_{mf}'}{U_{mf}} A_o \tag{2.9}$$

Now Equation 2.10 follows from (2.8)

$$A_{te} = A_o - A_o' \tag{2.10}$$

Applying these results to the present experimental situation (an average of 6 array tubes are immersed at U_{mf}') the following results are obtained:

$$\frac{U'_{mf}}{U_{mf}} = 0.939$$

$$A'_o = 0.174 \text{ m}^2$$

$$A_{te} = 0.0113 \text{ m}^2$$

$$V_{eq} = 0.00635 \text{ m}^3$$

$$V_{im} = 0.00371 \text{ m}^3$$

The fact that $V_{eq} > V_{im}$ may be taken as a qualitative measure of the average lee stack volume which the array supports at U'_{mf}, i.e.:

$$V_{ls} \tilde{=} V_{eq} - V_{im} \qquad (2.11)$$

For these experiments V_{ls} is about 71% of the immersed tube volume as calculated by Equation (2.11).

F. Summary

Experimental data for minimum fluidization velocity for a large particle bed have been presented for a range of temperatures. The open bed results are found to justify the use of the Wen and Yu correlation over the range of experimental conditions.

The accuracy of the experimental results is proposed as ±12% overall. The Wen and Yu correlation is a maximum of 4% lower and 1% higher than the data. The data averages 1.5% higher than the correlation predicts.

III. LOCAL TRANSIENT HEAT TRANSFER COEFFICIENT

A. Introduction

Fluidized beds are noted for the high rates of heat transfer between the bed and an immersed surface. However in the past most beds have been operated with particles that averaged less than 1 mm or so in diameter. An examination of the literature shows that the observed overall heat transfer coefficient is a decreasing function of particle diameter for particle diameters less than about 3 mm. Since larger particle fluidized beds are under active development for use as coal fired steam generators it has become necessary to be able to predict the heat transfer coefficients with some accuracy.

A model which predicts the local heat transfer coefficients in beds of larger particles has been developed and presented by Adams and Welty (1979). Unfortunately there is little literature data available to test the model. Table 3.1 summarizes some of the published data.

The present work investigates local heat transfer coefficients in a large particle high temperature fluidized bed.

B. Experimental Equipment

The fluidized bed facility is described in Appendix A. The bed material used in the heat transfer studies is the same as that used

Table 3.1. Some Previous Larger Particle Heat Transfer Studies.

Investigators	$\bar{d}_p$, mm	Bed Material	Bed Temp., K	Gas or Mass Velocity	Tube Dia., mm	Tube Temp., K	h J/m^2-s-K	Comments
		glass		0.136-0.679	12.7	>300	426-568	vertical, single tube
Chen and Withers	0.127	beads	~300	kg/m^2-s	22.0			
(1978)	0.254	"	"	0.136-0.814	"	"	312-511	"
"	0.610	"	"	0.270-0.814	"	"	210-341	"
			322-		15.9	339-		
Bartel and Genetti	0.203	"	377	0.163-0.678	15.9	394	596-710	horizontal, tube array
(1973)	0.279	"	"	0.163-0.950	"	"	539-596	"
	0.470	"	"	0.407-1.120	"	"	~397	"
Genetti et al.	0.114	"	~300	0.0679-0.407	12.7	>300	681-795	horiz., single tube
(1971)	0.203	"	"	0.136-0.679	"	"	625-738	"
"	0.470	"	"	0.407-1.090	"	"	~397	"
McLaren and Williams	-10 +240 BSS	coal, mostly ash	1073	0.6 m/s	60.3	~370	534 avg.	coal combustor, single horiz. tube
Wright et al.	2.9	coal, mostly ash	1073-1173	2.3-4.0 m/s	50.8	~370	220-250	coal combustor, horiz. array
Catapovic (1979)	0.37	sand	308	0.1-1.1 m/s	60.3	>308	15-240	horiz., single tube and tube array
	0.8	"	"	0.2-2.0	"		15-165	
	1.3	"	"	0.2-2.6	"		20-155	
	2.0	dolomite	"	0.2-3.4	"		25-135	
	2.85	"	"	0.4-4.3	"		40-140	
	4.0	"	"	0.6-5.3	"		65-140	
	6.6	"	"	1.0-5.5	"		75-145	

in the previously described minimum fluidization velocity work. Table 3.2 gives the important characteristics.

Local, transient heat transfer rates are measured with the circular foil heat flux gage. This gage was originally described by Gardon (1953, 1960).

The physical essentials of a working device are shown in Figure (3.1a). Heat flux is applied to the outer surface of the disk. The inner surface is relatively adiabatic. Also the disk radius is much larger than the thickness so that the temperature difference between the inside and outside surface is negligible. In addition the mass (and therefore the thermal time constant) of the foil is much less than that of the body to which it is attached.

An energy balance can be applied to the foil. Nomenclature is as shown in Figure (3.1b). The energy balance is

$$\text{(rate in) - (rate out) = (rate of accumulation)} \tag{3.1}$$

or in symbols

$$\dot{q}'' 2\pi\, r\Delta r - k\, 2\pi\, r\, S \left.\frac{\partial T}{\partial r}\right|_{r} + k\, 2\pi\, (r+\Delta r)\, S \left.\frac{\partial T}{\partial r}\right|_{r+\Delta r} =$$

$$= \rho\, C_p\, 2\pi\, r \Delta r S \frac{\partial T}{\partial t} \tag{3.2}$$

Rearranging, dividing by Δr and taking the limit as Δr approaches zero

Table 3.2. Bed material characteristics.

dp_{mi}, mm	fraction	
larger	trace	bulk density = 1500 kg/m^3
5.52	0.051	
4.03	0.344	solids density = 2610 kg/m^3
2.86	0.564	
2.12	0.041	bed depth = 0.61 m
1.54	0.000	$\overline{dp}$ = 3.21 mm
smaller	trace	

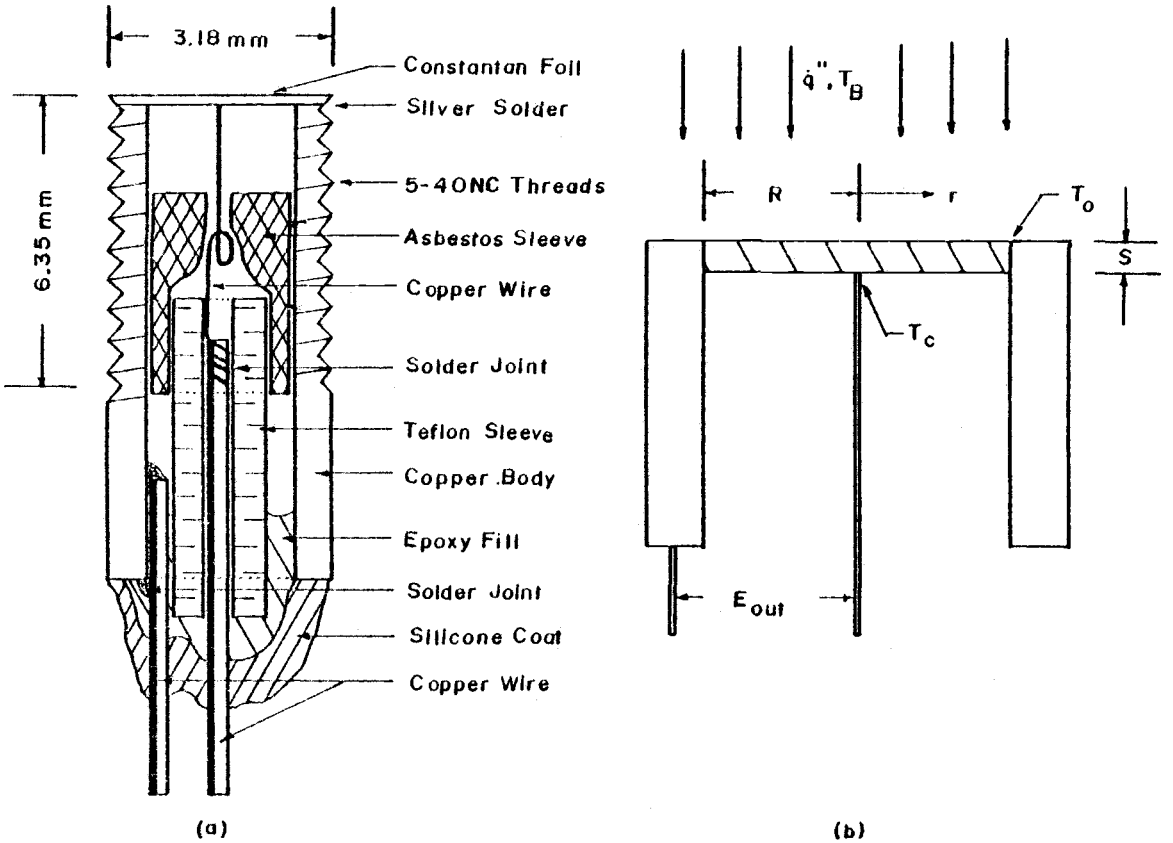

Figure 3.1 Circular Foil Heat Flux Gage.

$$\frac{\dot{q}''}{S} - \rho C_p \frac{\partial T}{\partial t} = -\frac{1}{r}\frac{\partial}{\partial r}\{kr\frac{\partial T}{\partial r}\} \tag{3.3}$$

The initial and boundary conditions are

$$T(r, 0) = T_o \tag{3.4}$$

$$T(0, t) = \text{finite} \tag{3.5}$$

$$T(R, t) = T_o \tag{3.6}$$

The steady-state response of the foil was developed by Gardon (1953) in essentially the following manner.

For the steady-state Equation (3.3) becomes

$$\frac{1}{r}\frac{\partial}{\partial r}\{kr\frac{\partial T}{\partial r}\} + \frac{\dot{q}''}{S} = 0 \tag{3.7}$$

In practice the thermal conductivity of the foil may be approximated by the form

$$k(T) = k_o [1+\beta T] \tag{3.8}$$

Making substitutions of the form

$$T' = \frac{T}{\frac{\dot{q}''}{S}\frac{R^2}{4k_o[1+\frac{\beta}{2}T]}} \tag{3.9}$$

and

$$r' = \frac{r}{R} \tag{3.10}$$

then

$$\frac{\partial T}{\partial r} = \frac{\dot{q}'' R}{4k_o S [1+\beta T]}\frac{\partial T'}{\partial r'} \tag{3.11}$$

Substituting Equations (3.8) and (3.11) into (3.7)

$$\frac{1}{r'}\frac{\partial}{\partial r'}\left\{r'\frac{\partial T'}{\partial r'}\right\} + 4 = 0 \tag{3.12}$$

The boundary conditions now are

$$T'(R) = \frac{T_o'}{\frac{\dot{q}'''}{S}\frac{R^2}{4k_o\left[1+\frac{\beta}{2}T_o\right]}} \tag{3.13}$$

$$\frac{\partial T'}{\partial r'} = 0 \quad \text{at} \quad r' = 0 \tag{3.14}$$

Equation (3.12) can be written as a total derivative. Doing so and integrating once

$$r'\frac{dT'}{dr'} = -2(r')^2 + C_1 \tag{3.15}$$

From (3.14) it is found $C_1 = 0$. Integrating again

$$T' = -(r')^2 + C_2 \tag{3.16}$$

From (3.13)

$$C_2 = 1 + T'(R) \tag{3.17}$$

Substituting in (3.16)

$$T'(r) = T'(R) + 1 - (r')^2 \tag{3.18}$$

In terms of the original variables (3.18) is

$$T[1+\frac{\beta}{2}T] - T_o[1+\frac{\beta}{2}T_o] = \frac{R^2 - r^2}{4Sk_o}\dot{q}'' \tag{3.19}$$

Rearranging (3.19) and evaluating at the foil center

$$[T_c - T_o][1+\beta\frac{T_c+T_o}{2}] = \frac{R^2\dot{q}''}{4Sk_o} \tag{3.20}$$

Equation (3.20) defines the steady-state response of the device.

The heat flux gages used in this work are constructed of constantan foil and copper bodies. The thermal conductivity of constantan is given variously by National Research Council (1929a), Gardon (1953), and Thermophysical Properties Research Center (1970) as

$$k = 8.41\ (1+6.96E\text{-}3T)\ J/m\text{-}s\text{-}K \tag{3.21a}$$

$$k = 8.11\ (1+6.18E\text{-}3T)\ J/m\text{-}s\text{-}K \tag{3.22a}$$

$$k = 8.48\ (1+5.45E\text{-}3T)\ J/m\text{-}s\text{-}K \tag{3.23a}$$

respectively.

In English engineering units these relations are

$$k = 13.5\ (1+1.39E\text{-}3T)\ Btu/hr\text{-}ft\text{-}^\circ F \tag{3.21b}$$

$$k = 12.1\ (1+1.33E\text{-}3T)\ Btu/hr\text{-}ft\text{-}^\circ F \tag{3.22b}$$

$$k = 11.7\ (1+1.27E\text{-}3T)\ Btu/hr\text{-}ft\text{-}^\circ F \tag{3.23b}$$

The thermal EMF of a copper-constantan thermocouple (Adams scale) is given by both National Research Council (1929b) and Gardon (1953) as

$$E = 0.0381\ (T-273) + 4.442E\text{-}5\ (T-273)^2$$

$$- 2.856E\text{-}8\ (T-273)^3 mV \qquad (3.24)$$

where T is in Kelvin degrees and the reference junction is maintained at 273K.

For temperatures within a few hundred degrees of 273K the last term of (3.24) can be neglected without much error, leading to

$$E = 0.0381\ (T-273)\ [1+0.0017\ (T-273)]\ mV \qquad (3.25a)$$

For Fahrenheit temperature units (3.25a) is

$$E = \{0.0203T[1+0.000678T] - 0.6634\}\ mV \qquad (3.25b)$$

The electrical output of the heat flux transducer is produced by the temperature differential between the foil center, T_c, and the foil edge, T_o. Substituting this differential in (3.25b)

$$E_{out} = \{0.0203\ T_c\ [1+0.000678\ T_c]$$

$$- 0.0203\ T_o\ [1+0.000678\ T_o]\}\ mV \qquad (3.26)$$

Substituting the constant values from (3.22a) into (3.20)

$$[T_c - T_o][1+3.09E\text{-}3(T_c+T_o)] = \frac{R^2 \dot{q}''}{32.44\ S} \qquad (3.27a)$$

and doing the same with (3.22b)

$$[T_c - T_o][1+6.65E\text{-}4\ (T_c+T_o)] = \frac{R^2 \dot{q}''}{48.4\ S} \qquad (3.27b)$$

Rearranging (3.26)

$$[T_c - T_o][1+6.78E\text{-}4\,(T_c - T_o)] = \frac{E_{out}}{0.0203} \qquad (3.28)$$

Comparing (3.27b) and (3.28)

$$\frac{R^2 \dot{q}''}{48.4\,S} \simeq \frac{E_{out}}{0.0203} \qquad (3.29)$$

In SI units (3.29) is

$$\frac{E_{out}}{\dot{q}''} = (1.09E\text{-}4)\,\frac{D^2}{S}\ \text{mV/J/m}^2\text{-s} \qquad (3.30a)$$

where D and S are in meters.

In English engineering units (3.29) is

$$\frac{E_{out}}{\dot{q}''} = 0.0314\,\frac{D^2}{S}\ \text{mV/Btu/ft}^2\text{sec} \qquad (3.30b)$$

where D and S are in inches.

The solution of the unsteady state equation for the device may be obtained by comparison to a momentum transfer problem solved by Bird et al. (1960) as follows.

An estimate of the response time of the device requires solution of (3.3) together with (3.4), (3.5), and (3.6). If the foil thermal conductivity is taken as constant, then the time dependent solution is given by Bird et al. (1960) as

$$T'' = [1-(r')^2] - 8\sum_{n=1}^{\infty} \frac{J_o(\alpha_n r')}{\alpha_n^3 J_1(\alpha_n)} \exp[-\alpha_n^2 t'] \qquad (3.31)$$

where

$$T' = \frac{T - T_o}{\frac{\dot{q}''}{S}\frac{R^2}{4k}}, \quad J_o(\alpha_n) = 0, \quad t' = \frac{kt}{\rho C_p R^2}, \quad r' = \frac{r}{R}$$

For the foil center (3.31) becomes

$$T_c'' = 1 - 8\sum_{n=1}^{\infty} \frac{1}{\alpha_n^3 J_1(\alpha_n)} \exp\left[-\alpha_n^2 t'\right] \tag{3.32}$$

Defining the time constant, τ, as the time to accomplish 63.2% of the response to a step change in heat flux, then $\tau' = k\tau/\rho C_p R^2$ and

$$0.632 = 1 - 8\sum_{n=1}^{\infty} \frac{1}{\alpha_n^3 J_1(\alpha_n)} \exp\left[-\alpha_n^2 \tau'\right] \tag{3.33}$$

Values for the first three coefficients are given in Table 3.3. Equation (3.33) can be solved with the aid of the plot given in Bird et al. (1960). According to the plot $\tau' = 0.19$ when Equation (3.33) is satisfied.

Solving for τ

$$\tau = \frac{0.19\,\rho\, C_p R^2}{k} \tag{3.34}$$

Equation (3.34) gives the approximate time constant for the device. For the particular case of copper-constantan construction

Table 3.3. Coefficients of Equation (3.33).

η	α_η	$J_1(\alpha_\eta)$	$[\alpha_\eta^3 J_1(\alpha_\eta)]^{-1}$
1	2.405	0.519	0.139
2	5.520	-0.340	-0.0175
3	8.654	0.271	0.00569

used here (3.34) is

$$\tau = 4.75\ D^2 \text{ sec} \tag{3.35}$$

where D is in inches.

A. S. T. M. (1978) gives (3.35) as $\tau = 6\ D^2$ sec. Gardon (1953) deduced an exponential decay form for (3.33) and arrived at $\tau = 5.97\ D^2$ sec for (3.35).

Equation (3.35) in SI units is

$$\tau = 7363\ D^2 \text{ sec} \tag{3.36}$$

where D is in meters.

The circular foil transducers used for these experiments are made of 0.0127 mm thick constantan foil and have diameters ranging from 1 to 2 mm.

The time constants then theoretically range between 0.0074 and 0.029 seconds for a 63.2% response to a step change in heat flux. Assuming four time constants for essentially complete response and assuming steady heat flux except when bubbles approach, the worst case bubble frequency limit is theoretically somewhat over 8 Hz (for 2 mm dia. transducers) and the best is about 33 Hz (for 1 mm dia. transducers). In the present bed the bubble frequency appears to be 2 or 3 Hz maximum at the top of the bed.

Time constants have been determined experimentally as a check

on the theory. The tests were performed as follows. A heat flux transducer is screwed into a hole in a heavy aluminum plate and connected to an instrumentation amplifier. The plate is positioned so that the transducer face is 5 or 10 cm from a 500W quartz lamp. The lamp is turned on and the amplifier output is recorded with a Visicorder while a card is first rapidly inserted between the lamp and the transducer, then is left in place for 2 seconds or so and then is rapidly withdrawn. This process is repeated for several cycles.

Analysis of the Visicorder plots shows generally good agreement between different trials for the same transducer. The experimentally determined time constants are observed to range between about 0.055 sec (Figure 3.2 shows the response time of one transducer) and 0.075 seconds versus the theoretically predicted maximum of 0.029 seconds for a 2 mm diameter device.

The observed time constants are longer than the theoretical constants because of the method of construction. The foil disk is attached to the copper body with solder. The solder wets the inside perimeter of the foil and so forms a tapered join. The join heat capacity is apparently causing the deviation from theory. In addition the 0.076 mm diameter copper wire which is welded to the foil center has a finite effect.

The transducer outputs theoretically range between 8.57 and 34.3 mV per MJ/m^2-s of outer surface flux. The outer surface flux

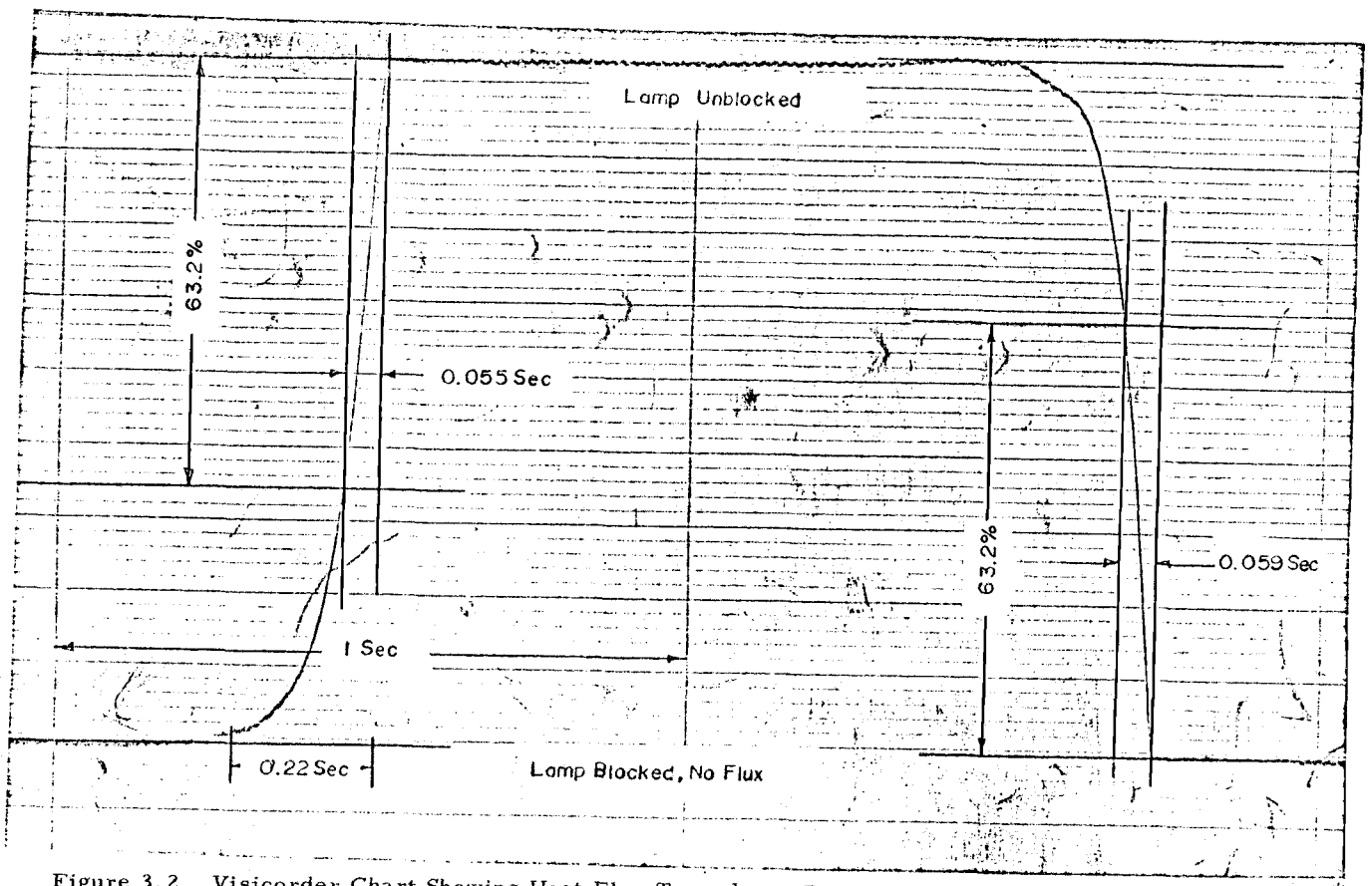

Figure 3.2 Visicorder Chart Showing Heat Flux Transducer Response Time.

ranges between about 70 and 350 KJ/m^2-s for the 3.21 mm diameter particle bed. The measured transducer outputs are presented in the next section and in Appendix E. The outputs are observed to range between 7.5 and 15 mV per MJ/m^2-s depending on the exact construction of the particular transducer under test.

The heat flux transducers, local pressure tubes (when used), and surface temperature thermocouples are screwed into three drilled and tapped stainless plugs. The three plugs screw into a port cut out of the wall of a 50.8 mm o.d. stainless steel pipe. The pipe wall is 6.35 mm thick. The plugs, the transducers, and the port are shown in the photograph of Figure 3.3. The whole assembly is schematically shown in Figure 3.4. The holes for the three plugs are at the same axial location and are spread 60° apart around the perimeter.

Local pressure is measured using any of the #5-40 threaded holes (see Figure 3.4) by screwing in a 0.20 m long piece of copper tubing which is threaded #5-40 on one end. The other end of the tube is connected to the nylon feedout tube with a small brass sleeve. The outside end is connected to a purge air supply and to a solid state differential pressure gage. Bubble presence is detected by recording the differential pressure between holes on the same plug or between different plugs, as desired. The test port locations are shown in Figure 3.5.

Dowtherm A is circulated through the pipe when the bed is in

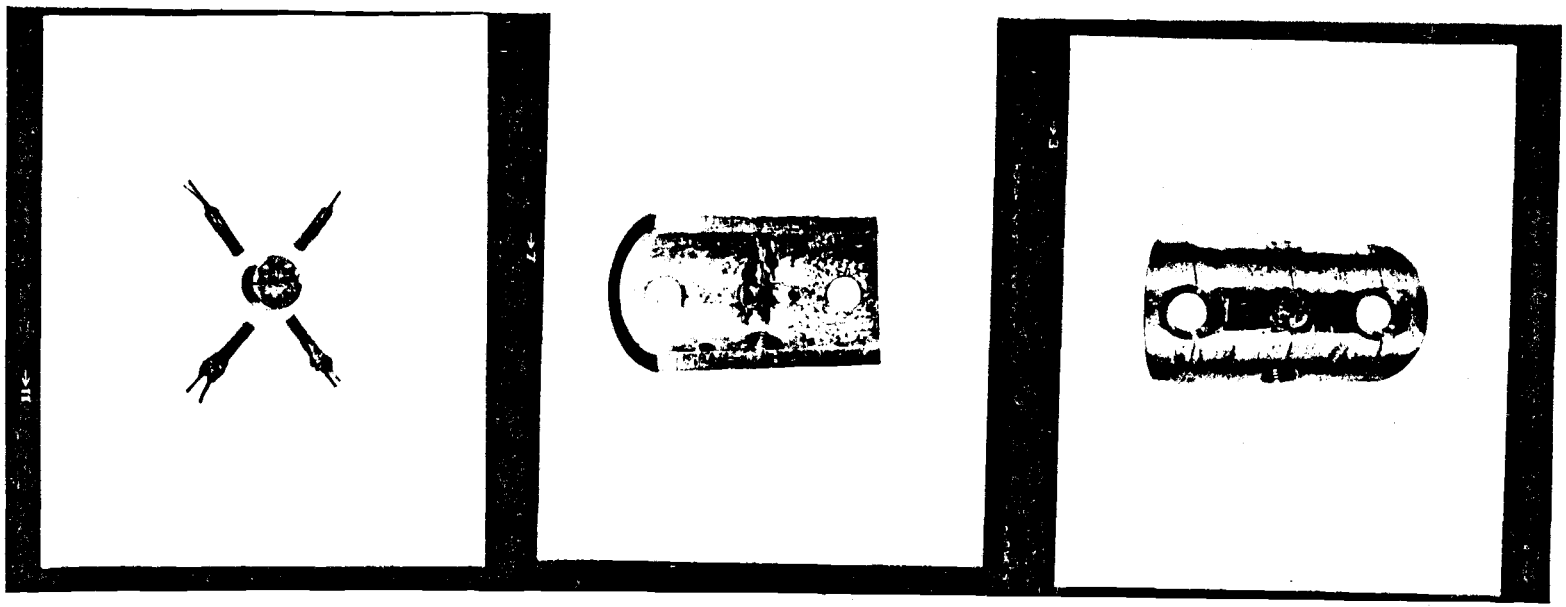

Figure 3.3 Photograph of Transducers, Plugs, and Port.

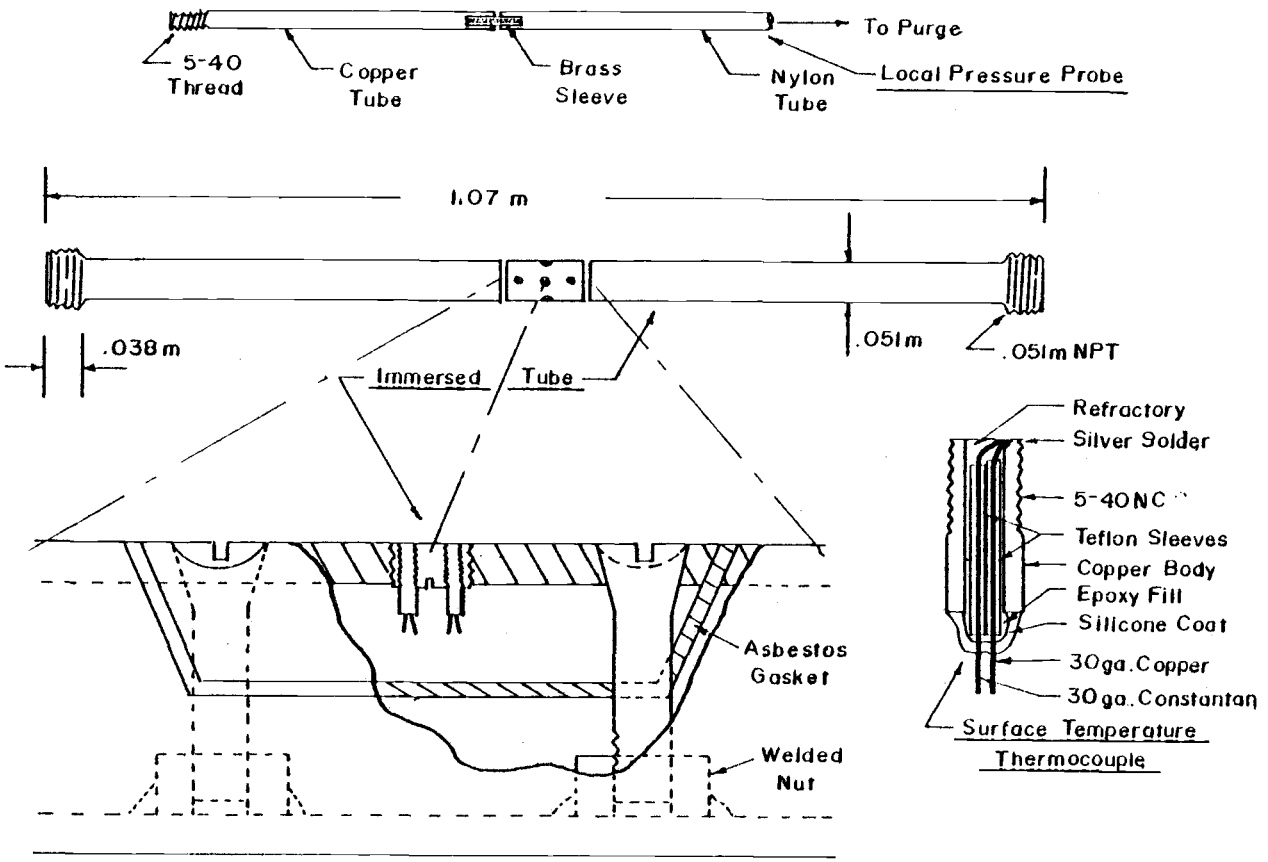

Figure 3.4 Immersed Tube and Heat Transfer Instruments.

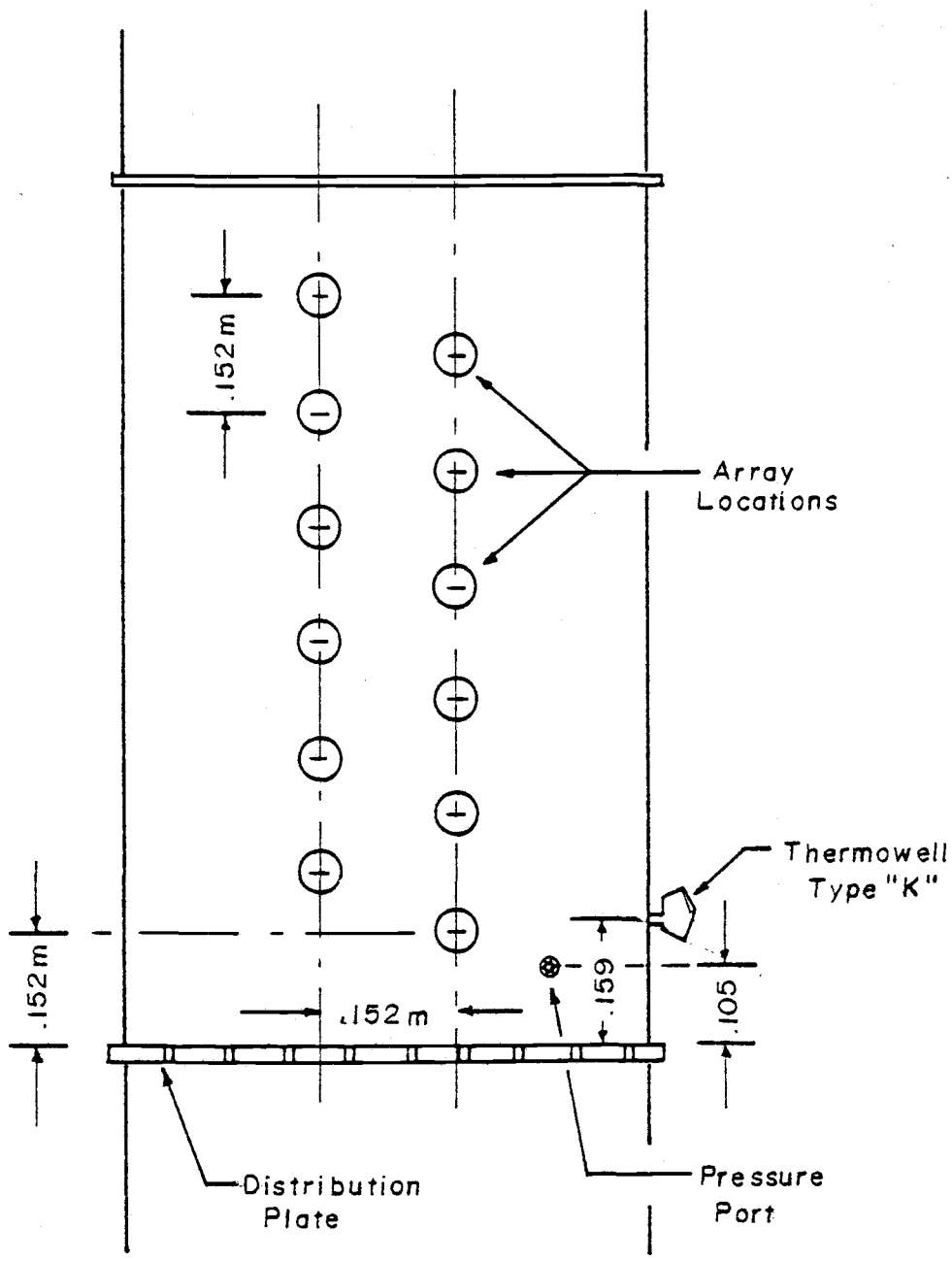

Figure 3.5 Test Port Locations.

operation. Heat is transferred from the Dowtherm to water by a shell and tube heat exchanger.

The Dowtherm flow is set at about 3.15 E-3 m^3/s (50 GPM). The water rate is then adjusted to obtain the desired Dowtherm temperature at the outlet end of the immersed tube Calibration data for the Dowtherm A orifice is located in Appendix B. The water rate is measured with a Fischer-Porter rotameter. The conversion curve for the rotameter is also given in Appendix B.

Teflon covered copper and enameled constantan wires are used to connect the various transducer leads to the feedthrough plug. The feedthrough plug consists of a short piece of 12.7 mm o.d. copper tube. It has 16 enameled copper and 4 enameled constantan 30 gage wires set in epoxy running through it. The soldered connections at the feedthrough end are covered with heat-shrunk plastic tubing. The same end is coated with Permatex brand silicone gasket material to slow the Dowtherm attack on the epoxy core.

The amplifier input cables and the thermocouple cold junctions are soldered to the outside ends of the feedthrough wires after the coolant pipes have been connected. A Swagelock brand brass fitting is used to provide the seal. This fitting is used with brass ferrules and is tightened just enough to prevent leakage Careful tightening prevents extensive crimping of the tube or ferrule and makes disassembly and reuse simple.

Analog Devices brand AD-522 instrumentation amplifiers are used to step up the output voltages of the various transducers. The outputs from the amplifiers are then recorded on a Honeywell Visicorder.

C. Experimental Procedures

The experimental heat transfer tube is placed in the desired test port pair (refer to Figure 3.5), the coolant system is connected, and bed material is added to give the desired bed depth.

The bed is brought to temperature slowly in consideration of the refractory lining. The coolant temperature is kept below 370K during the warmup to avoid unnecessary heat stress and vapor production.

Once temperature is reached, the water and/or Dowtherm A circulation rate are set to give the desired coolant exit temperature. The air flow rate into the bed is set at the desired U_o/U_{mf} ratio and time is allowed for equilibrium to develop. Equilibrium is determined by periodically recording the transducer outputs and noting the average output levels.

D. Data Analysis

Sample Visicorder trace copies are shown in Figures 3.6-3.9. Time proceeds from right to left.

Calibration of the Visicorder-amplifier setup is accomplished by feeding measured input voltages into the amplifiers and noting the

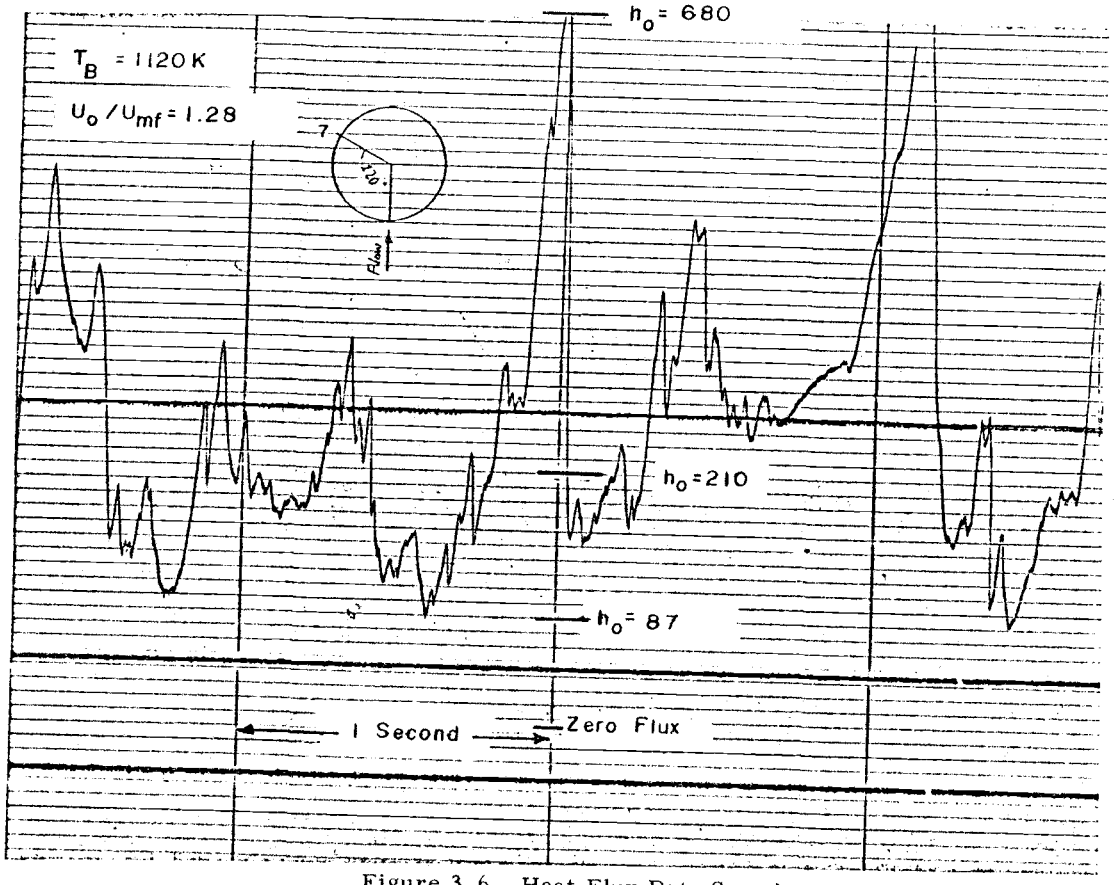

Figure 3.6 Heat Flux Data Sample.

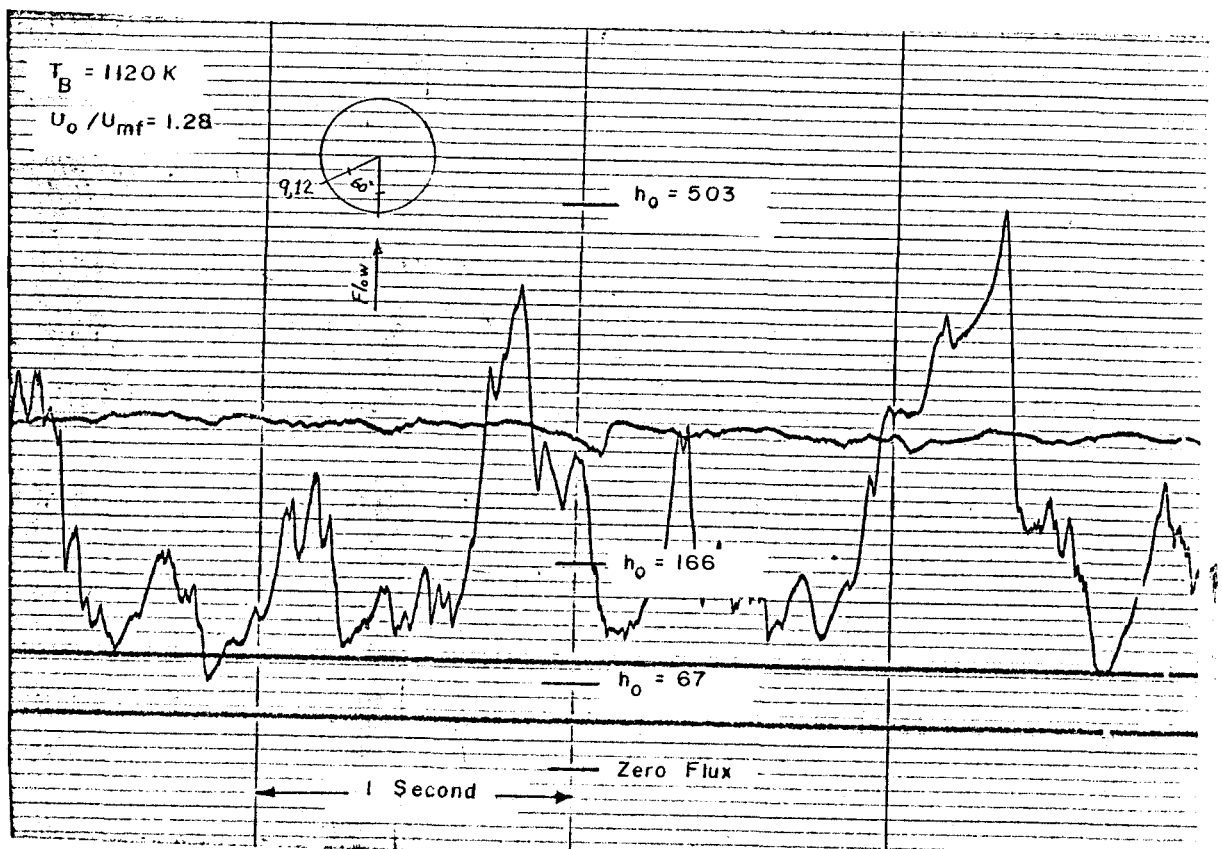

Figure 3.7 Heat Flux Data Sample.

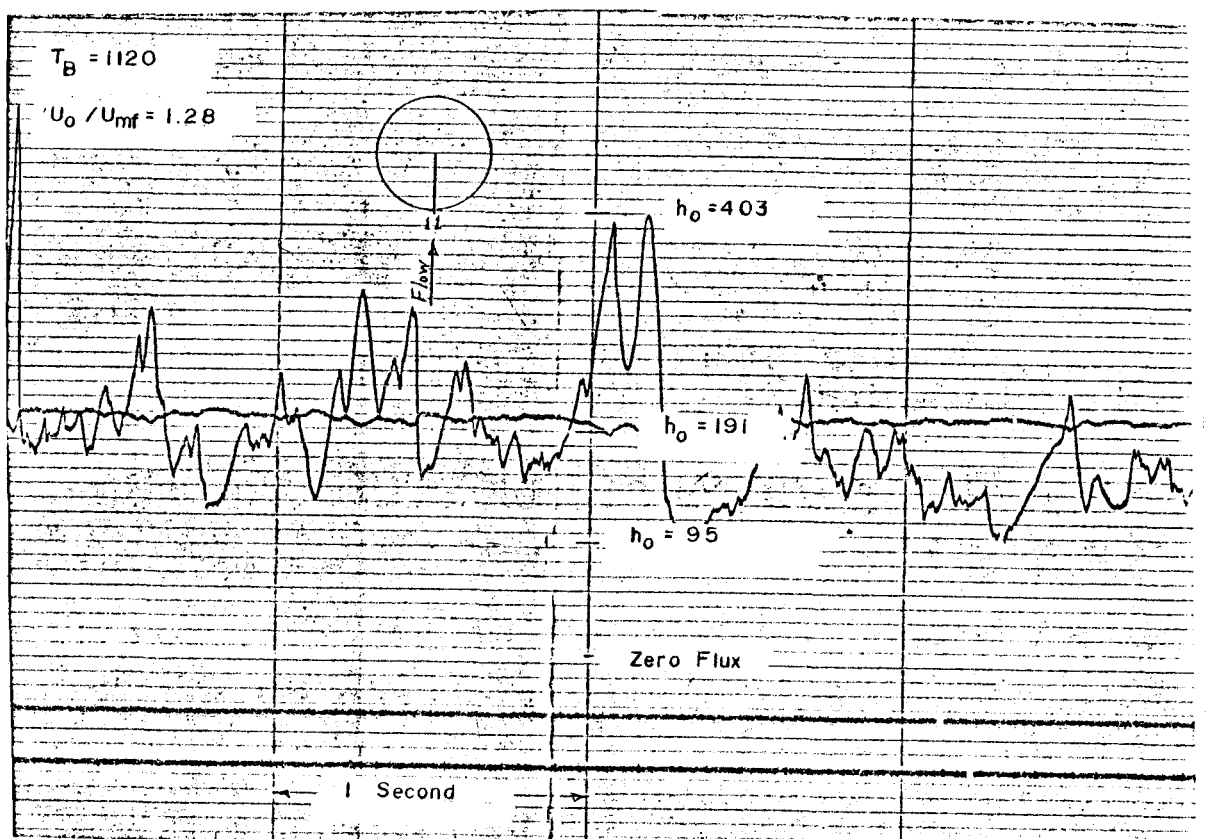

Figure 3.8 Heat Flux Data Sample.

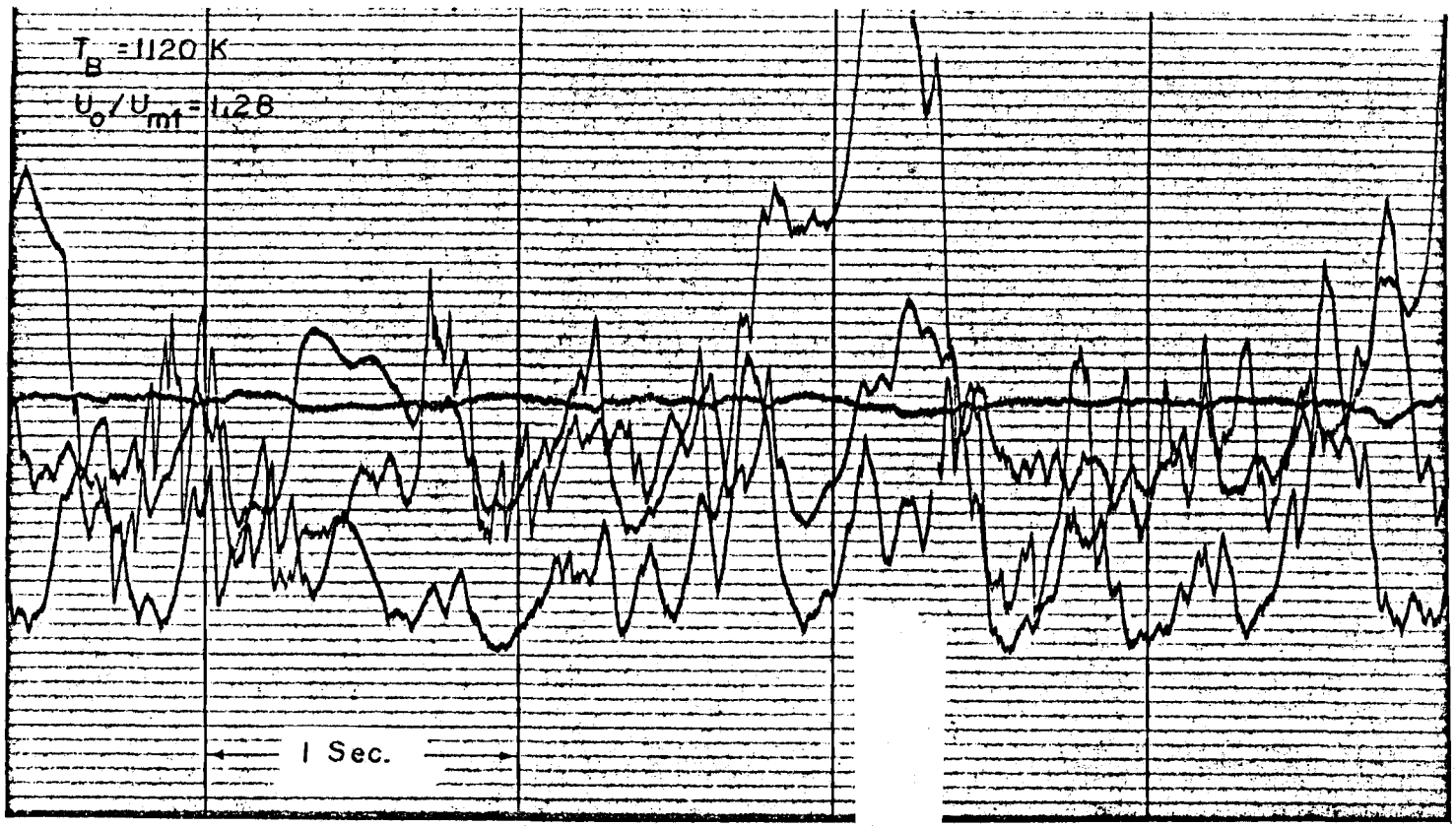

Figure 3.9 Heat Flux Data Sample.

corresponding output of the Visicorder. Overall system transfer functions are about 8500 $(J/m^2\text{-}s)$/div for the channels used with the heat flux transducers and about 0.1 mV/div for the channels used with the thermocouples. The averages of the time varying curves are estimated by inspection.

Once the outputs are determined the calibration data are used to get the actual transducer output voltages. Thermocouple voltages are converted to temperature using the tables provided by A. S. T. M. (1978). The thermocouples are provided with ice bath cold junctions for reference.

The heat flux transducer voltages are converted to heat flux using calibration data obtained prior to the run. A nice feature of the copper-constantan circular foil heat flux gage is its very linear voltage response to changes in heat flux. Within the non-linearity of the amplifiers (small) and that of the Visicorder (variable), the ratios of the Visicorder outputs correspond to actual heat flux ratios.

The heat flux transducers used in the experiments are calibrated by comparing them to a commercially produced (Hy-Cal brand) unit. Appendix C gives details on the commercial unit, including the calibration curve. The Hy-Cal unit is certified at ±3% accuracy and ±0.5% repeatability. Application of a straight edge to the Hy-Cal calibration curve in the Appendix shows just how close the linear

response predicted by Equations (3.30a) and (3.30b) is realized in practice.

The experimental heat flux transducer is calibrated against the Hy-Cal unit by mounting it next to the Hy-Cal, in a heavy aluminum plate. The surface of the experimental unit is blackened with candle soot ($\varepsilon_N \tilde{=} 0.95$, $\alpha \tilde{=} 0.95$) to provide a surface with known thermal radiative properties for calibration. The plate is placed over a 500 W quartz lamp which is connected to a rheostat and mounted in a box. The box is equipped with a stainless steel reflector and also provides protection from stray breezes. To obtain a calibration the two units are connected to the Visicorder and the lamp is turned up with the rheostat. The maximum lamp output is less than the observed maximum bed heat flux but extrapolation is justified on the basis of the observed linearity of the transducers over the calibration range. The commercial Hy-Cal unit is supplied with a calibration curve which shows a linear response to heat fluxes much higher than those encountered in the present investigation.

Calibration errors are minimized by moving the plate containing the transducers around until the position corresponding to peak outputs from both transducers is found. This position then corresponds to the position from which any further movement of the plate will result in the same or reduced level of output for both transducers. The calibration error due to positioning is less than 5% of total flux.

Figure 3.10 is a copy of the Visicorder output for part of one calibration run. The curves are obtained by setting the quartz lamp rheostat at the desired level and then turning the power on and off a couple of times while the Visicorder is running. A new level is then set and the process is repeated. Note that the quartz lamp and reflector takes about 1/4 seconds to rise or fall to 63.2% of its steady value. As noted previously the experimental heat flux transducers have time constants of 0.075 second or better so that they have no difficulty in following the quartz lamp flux. The Hy-Cal device is guaranteed to have a time constant of less than 0.15 seconds and it too shows no difficulty in following the lamp.

The transducers do not return to precisely the original no-flux level after each exposure to the lamp unless sufficient time is provided for the lamp and shield to cool completely. This presents no difficulty in calibration as both the transducer under test and the Hy-Cal unit are exposed to the same conditions.

The experimentally determined outputs of the transducers used to collect the data presented here are given in Appendix E. Calibrations over the full range of flux available from the quartz lamp apparatus shows a maximum non-linearity of the experimental transducers at 1.5% when compared to the Hy-Cal which shows no measurable deviation from the linear flux to output voltage relationship predicted by theory. This non-linearity in the experimental devices is probably

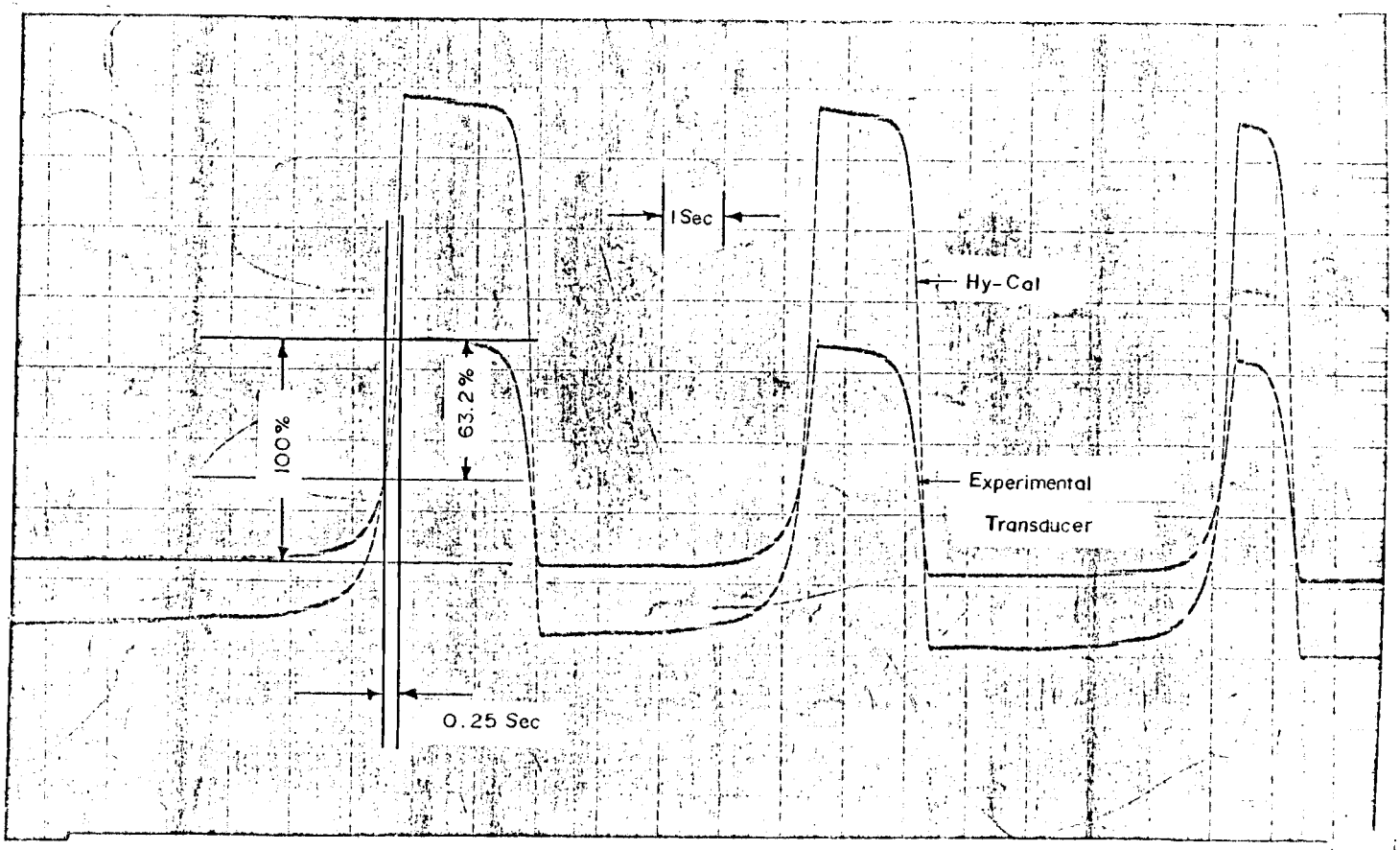

Figure 3.10 Heat Flux Transducer Calibration.

due to the relatively crude construction method of soldering the foil to the copper body. The observed transducer outputs range between 7.5 and 15 mV/[MJ/m^2-s].

The data collected with the present equipment are here presented in terms of a total (i.e. convective plus radiative) heat transfer coefficient defined by

$$h_o = \dot{q}''/(T_B - T_{LM}) \tag{3.37}$$

where T_{LM} is the average temperature of the heat flux transducer foil surface. T_{LM} is found theoretically as follows.

The steady state temperature profile across the surface of the foil is given by Equation (3.19).

From (3.19)

$$T(r) \cong \frac{R^2 - r^2}{4Sk}\, \dot{q}'' + T_o \tag{3.38}$$

and defining

$$T_{LM} = \frac{1}{\pi R^2}\int_A T(r)dA = \frac{1}{\pi R^2}\int_o^R T(r)2\pi\, r dr \tag{3.39}$$

on integrating

$$T_{LM} = T_o + \frac{1}{32}\,\frac{\dot{q}''}{Sk}\, D^2 \tag{3.40}$$

Using (3.22a) evaluated at 400K and using 2.0 mm for the foil diameter and 0.0127 mm for the foil thickness, then (3.40) in S.I.

units is

$$T_{LM} = T_o + 3.5E\text{-}4\,\dot{q}'' \qquad (3.41)$$

where $\dot{q}''$ is in J/m^2-s. Equation (3.41) is used in the calculation of heat transfer coefficients reported here.

Some of the sources of error are given in Table 3.4. The error estimate for the Visicorder chart reading does not apply to point values. Most of the results reported here are time averages of the local transient curves. The averages are obtained by inspection of the Visicorder curves. Examination of Figures 3.6-3.8 indicate a typical range around the average heat transfer coefficient of from +300 to -100 J/m^2-s-K.

Figure 3.11 shows the variation in differential local pressures relative to the variation in local heat transfer. These curves indicate that the present equipment is well capable of following both local pressure variations and heat transfer variations which may coincide with local pressure changes.

E. Results and Discussion

Appendix E contains the heat transfer data. The results are summarized in Table 3.5. Figure 3.12 shows the present experimental results versus those obtained by Catapovic (1979) for similar diameter particles in a room temperature bed. The present results should differ from those of Catapovic because of fluid property

Table 3.4. Source of errors.

Error Source	% error in "h_o"
Visicorder chart reading, ± 4 div.	$\pm \frac{4}{20} \times 100 = \pm 20\%$
Amplifier - Visicorder calibration, ±5%	±5%
" " interpolation, ±1%	±1%
" " drift, + 30 mV	$\pm \frac{0.03}{0.5} \times 100 = \pm 6\%$
Standard calorimeter, ±3% of $\dot{q}''$	±3%
Experimental calorimeters, ±5% of standard	±5%
Surface temperature, ± 20K	$\pm \frac{30}{667} \times 100 = \pm 3\%$
Bed temperature, ± 20 K	$\pm \frac{20}{667} \times 100 = \pm 3\%$
Probable accuracy	± 22.7%

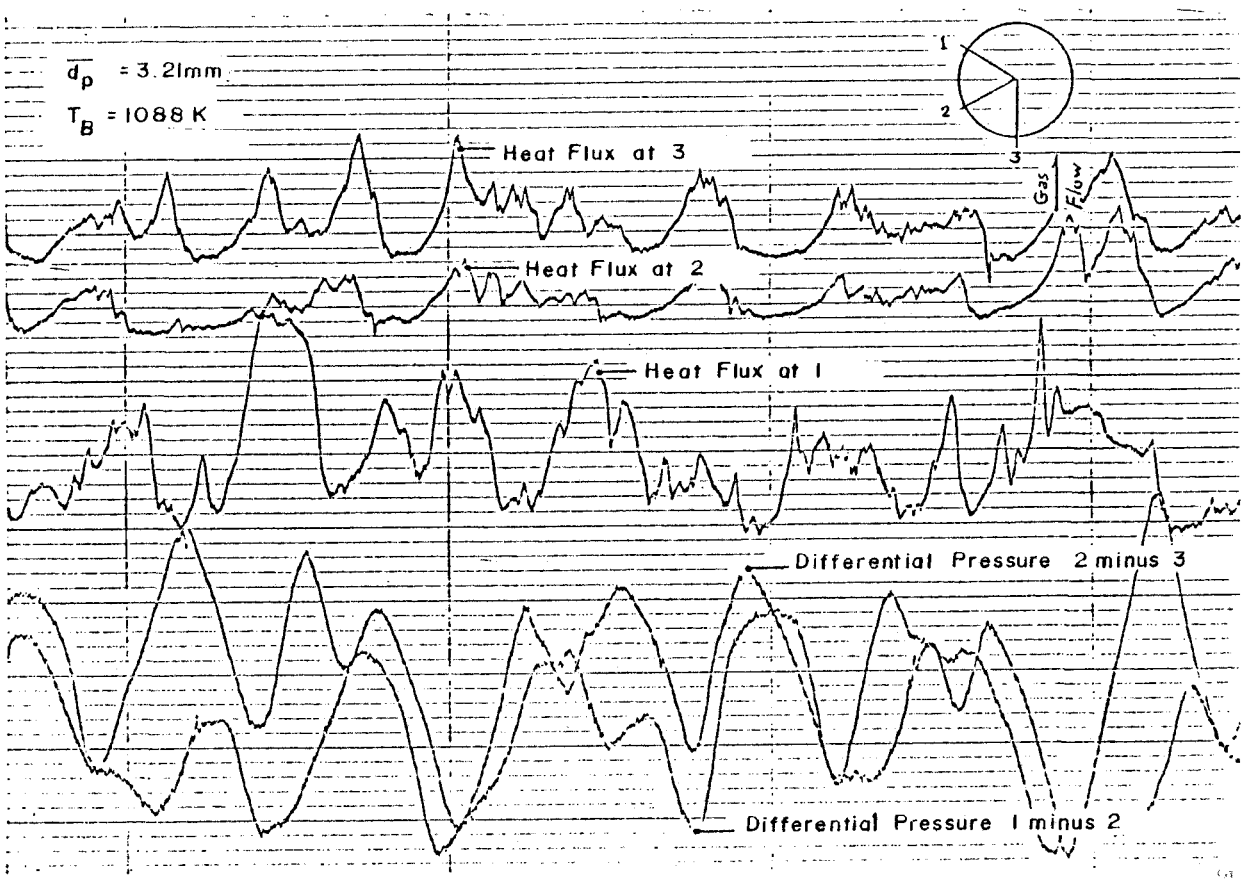

Figure 3.11 Local Pressure Versus Heat Flux Variation.

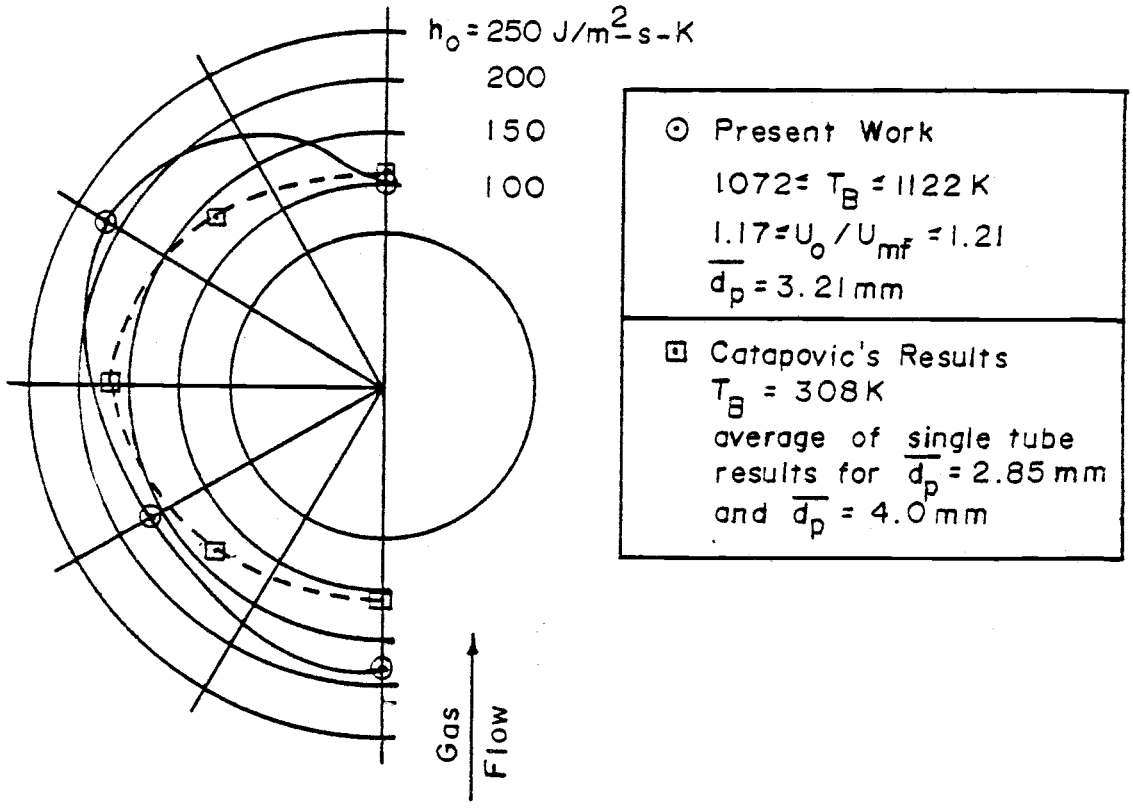

Figure 3.12 Experimental Results Versus Cold Bed Results.

Table 3.5. Heat transfer results.

Position	T_B, K	T_{LM}, K	h_o, J/m^2-s-K	U_o/U_{mf}
1	1077	358	26.0?	1.03
	1072	371	64.5?	1.20
	1077	411	228?	1.20
	1072	377	85.9	1.20
	1083	381	98.2	1.21
	1077	390	118.	1.21
2	1177	373	97.6	1.12
	1122	402	198.	1.17
3	1127	389	159.	0.96
	1077	379	115.	1.03
	1105	417	235.	1.15
	1122	421	261.	1.17
	1072	395	168.	1.20
	1077	397	165.	1.20
	1072	380	98.7?	1.20
	1083	376	76.4?	1.21
	1077	422	263.	1.21
	1122	446	398?	1.28
4	1177	387	149.	1.12
	1122	392	156.	1.17
5	1127	370	84.5	0.96
	1077	372	86.9	1.03
	1105	400	161.	1.15
	1122	402	179.	1.17
	1116	399	170.	1.16
	1072	385	119?	1.20
	1077	382	100?	1.20
	1072	392	156.	1.20
	1083	391	141.	1.21
	1077	399	154	1.21
	1122	396	166	1.28
	1122	378	101?	1.28
6	1177	368	78.8	1.12
	1122	386	133.	1.17
7	1127	373	94.3	0.96
	1105	401	168	1.15
	1116	425	284?	1.16
	1122	402	179	1.17
	1122	402	191	1.28
	1122	401	194	1.28

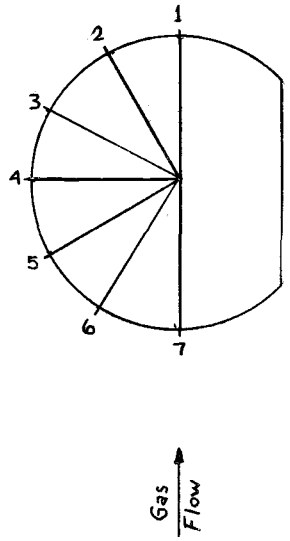

differences and radiant heat transfer caused by the present high temperature conditions. Catapovic shows very little effect of particle diameter on heat transfer for particles 2 to 6 mm diameter. Assuming that the effect of fluid property changes due to temperature is small then the bulk of the difference should be due to radiative transfer. A theoretical estimate of the radiative contribution is gotten as follows.

Sucec (1975) gives Christiansen's equation

$$\dot{q}'' = \frac{\sigma (T_2^4 - T_1^4)}{\frac{1}{\varepsilon} + \frac{A_1}{A_2}(\frac{1}{\varepsilon_2} - 1)} \qquad (3.42)$$

as the solution to the problem of radiative transfer between the outer wall of a gray cylinder or sphere of surface area A_1, temperature T_1, and emissivity ε_1 and the inner wall of a concentric cylinder or sphere of subscript 2 properties.

Since ε, ε_2, A_1, σ, T and T_2 are fixed by physical properties and experimental conditions it is apparent that if gas radiation is neglected then the maximum radiative flux to the inner cylinder occurs when the outer cylinder (i.e. the bed particles) is adjacent. The analysis is only applicable to effect of the presence of a concentric bubble which extends the length of the whole immersed tube or the absence of such a bubble. Never-the-less an estimate of the radiative heat

transfer rate is then given by

$$\dot{q}_1'' = \frac{\sigma(T_B^4 - T_{LM}^4)}{\frac{1}{\varepsilon_1} + \frac{1}{\varepsilon_2} - 1} \tag{3.43}$$

where σ is a constant with the value 5.676 E-8 J/s-m^2-K^4.

ε_2 is the emissivity of the bed and is taken as 0.65. T_1 is taken as 400K and T_2 as 1080K as representative of the values reported with the data.

The surface emissivity of the heat flux transducer has been measured experimentally by comparing the output when the metal surface was bare (9.21 mV/[MJ/m^2-s]) to that when the surface was coated with candle soot (14.56 mV/[MJ/m^2-s]). The soot emissivity has a handbook value of 0.95 (Morrison and Ingle (1962)) and so the constantan foil emissivity is

$$\varepsilon_1 = \frac{9.721}{14.56}(0.95) = 0.63 \tag{3.44}$$

Now from (3.37) and (3.43)

$$h_R = 52 \text{ J/m}^2\text{-s-K} \tag{3.45}$$

Figure 3.13 shows a plot of Catapovic's cold-bed results subtracted from the present results. The curve should be of the order of magnitude of 52 J/m^2-s-K provided that the tube surface and adjacent bed temperaturs are uniform around the perimeter of the tube. The figure indicates that the bed temperature in the vicinity of the

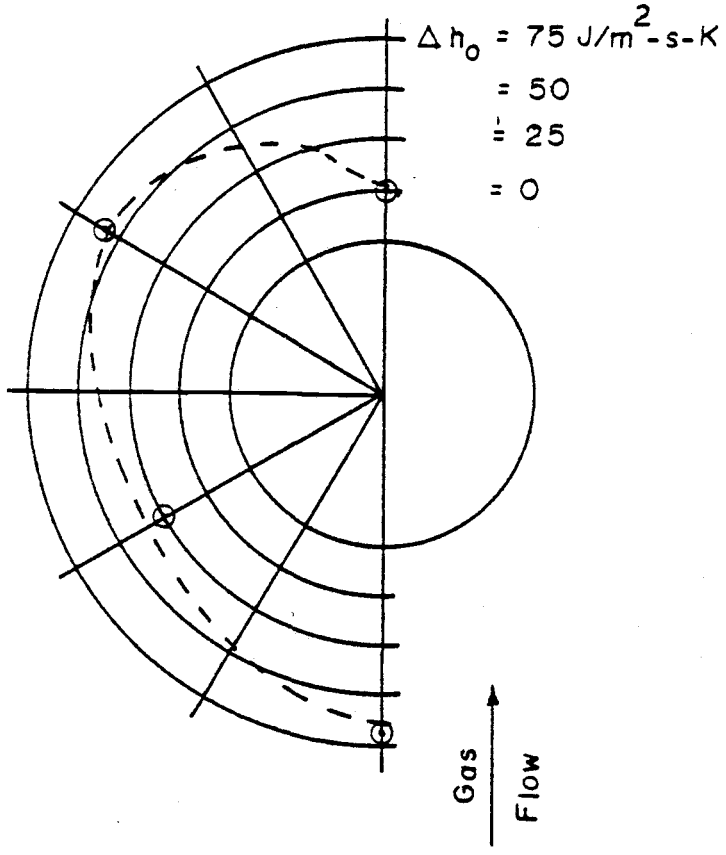

$\Delta h_o = h_o - h_{cold\ bed}$
$1072 \leq T_B \leq 1122$ K
$1.17 \leq U_o / U_{mf} \leq 1.21$
$\overline{d_p} = 3.21$ mm

Figure 3.13 Experimental Results Minus Cold Bed Results.

lee stack area of the tube surface is probably less than the average bed temperature since the tube surface temperatures are measured as fairly uniform.

F. Summary

An experimental method for measuring local transient heat transfer coefficients in a heated, large particle fluidized bed has been developed and tested. Examination of the data in Appendix E indicates that the heat flux transducers produce self consistent results. This assertion is based on the fact that the overlapping results of the individual transducers are generally similar for a given radial position. The time averaged coefficients reported here are thought to be as much as ±23% inaccurate. This is largely due to the difficulty in accurately integrating the Visicorder plotted transient flux curves. The precision of the 19 accepted trials for locations 1, 3, 5, and 7 and for $1.15 \leq U_o/U_{mf} \leq 1.28$ is ±13%.

The experimental heat flux transducers have measured response times (for 63.2% of the change due to a step change in flux) of between 0.055 and 0.075 seconds. The transducer sensitivities have been measured as ranging between 7.5 and 15 $mV/[MJ/m^2\text{-}s]$.

Local pressures can be measured at any point around the tube perimeter which is near a heat flux transducer. Simultaneous recording of local pressure and heat flux indicates that the heat flux

probes are capable of following flux changes which occur sumultaneously with local pressure changes.

IV. SUMMARY AND CONCLUSIONS

An experimental system has been developed and tested which is able to measure local, transient heat transfer coefficients in a high temperature fluidized bed.

In the course of this development data has been collected which indicates that the Wen and Yu (1966) correlation gives a good estimate for the minimum fluidization velocity of the material used, regardless of bed temperature.

The heat flux transducers have been shown to exhibit response times at 0.075 seconds or better for a 63.2% response to a step change in heat flux. The device sensitivities have been measured as ranging between 7.5 and 15 mV per MJ/m^2-s.

Transient heat transfer data has been collected and the time averaged results have been presented as a function of radial position. The values reported range between 101 and 218 J/m^2-s-K for the total heat transfer coefficient. These values have been compared to room temperature bed results obtained by Catapovic (1979) and an estimate of the radiant heat transfer effect is given. A preliminary conclusion, based on the results, is that the bed material adjacent to the lee area of the tube is at a lower temperature than that adjacent to the rest of the tube wall. The highest velocity ratio used was $U_o/U_{mf} = 1.28$.

BIBLIOGRAPHY

Adams, R. L., and J. R. Welty, "A Gas Convective Model of Heat Transfer in Large Particle Fluidized Beds," A. I. Ch. E. Journal, 25, 395-405 (1979).

A. S. M. E., "Flow Measurement," Power Test Codes, PTC 19.5, Ch. 4 (1959).

A. S. T. M., "Standard Method for Measurement of Heat Flux Using a Copper-Constantan Circular Foil Heat-Flux Gage," Ann. Book of Standards, Part 41 (E511), 731-739 (1978).

Avedesian, M. M., and J. F. Davidson, "Combustion of Carbon Particles in a Fluidized Bed," Trans. Instn. Chem. Engrs., 51, 121-131 (1973).

Bartel, W. J., and W. E. Genetti, "Heat Transfer from a Horizontal Bundle of Bare and Finned Tubes in an Air Fluidized Bed," Chem. Eng. Progr. Symposium Ser. No. 128, 69, 85-93 (1973).

Bird, R. B., W. E. Stewart, and E. N. Lightfoot, Transport Phenomena, Wiley, New York (1960).

Botterill, J. S. M., Fluid-Bed Heat Transfer, Academic Press, London (1975).

Catapovic, N. M., "Heat Transfer to Horizontal Tubes in Fluidized Beds: Experiment and Theory," Ph. D. thesis, Oregon State Univ., Corvallis (1979).

Chen, J. C., and J. G. Withers, "An Experimental Study of Heat Transfer from Plain and Finned Tubes in Fluidized Beds," Chem. Eng. Progr. Symposium Ser. No. 174, 74, 327-333 (1978).

Doheim, M. A., and C. N. Collinge, "Effect of Temperature on Incipient Fluidization and Study of Bed Expansion," Powder Technology, 27, 289-293 (1978).

Gardon, R., "An Instrument for the Direct Measurement of Intense Thermal Radiation," Review Sci. Ins., 24, 366-370 (1953).

Gardon, R., "A Transducer for the Measurement of Heat-Flow Rate," Trans. A.S.M.E., J. of Heat Transfer, 82, 396-398 (1960).

Genetti, W. E., R. A. Schmall, and E. S. Grimmett, "The Effect of Tube Orientation on Heat Transfer with Bare and Finned Tubes in a Fluidized Bed," Chem. Eng. Progr. Symposium Ser. N. 116, 67, 90-96 (1971).

Junge, D. C., Design and Operation - High Temperature Fluidized Bed Test Facility, Dept. Mech. Engr. Oregon State University, Corvallis (1978).

Kunii, D., and O. Levenspiel, Fluidization Engineering, Wiley, New York (1962).

McLaren, J., and D. F. Williams, "Combustion Efficiency, Sulphur Retention, and Heat Transfer in Pilot-Plant Fluidized Bed Combustors," J. Inst. Fuel, 42, 303-308 (1969).

Morrison, R. B., and M. J. Ingle, Design Data for Aeronautics, Wiley, New York (1962).

National Research Council, E. W. Washburn, Ed., International Critical Tables, 5, McGraw-Hill, New York (1929a).

National Research Council, E. W. Washburn, Ed., International Critical Tables, 6, McGraw-Hill, New York (1929b).

Pruden, B. B., D. Crosbie, and B. J. P. Whalley, "Circulation of Large Bodies in an Aggregatively Fluidized Bed," Fluidization Technology, D. L. Keairns, Ed., 65-86, Hemisphere, Washington (1976).

Saxena, S. C., and G. J. Vogel, "The Properties of a Dolomite Bed of a Range of Particle Sizes and Shapes at Minimum Fluidization," Can. J. Chem. Eng., 54, 453-455 (1976).

Saxena, S. C., and G. J. Vogel, "Segregation and Fluidization Characteristics of a Dolomite Bed with a Range of Particle Sizes and Shapes," Chem. Eng. Journal, 14, 59-63 (1977).

Sucec, J., Heat Transfer, Simon and Schuster, New York (1975).

Thermophysical Properties Research Center, Thermophysical Properties of Matter, 1, IFI/Plenum, New York (1970).

Wen, C. Y., and Y. H. Yu, "Mechanics of Fluidization," Chem. Eng. Progr. Symposium Ser. No. 62, 62, 100-111 (1966a).

Wen, C. Y., and Y. H. Yu, "A Generalized Method for Predicting the Minimum Fluidization Velocity," A. I. Ch. E. Journal, 12, 610-612 (1966b).

Wright, S. J., H. C. Ketley, and R. G. Hickman, "The Combustion of Coal in Fluidized Beds for Firing Shell Boilers," J. Inst. Fuel, 42, 235-240 (1969).

Wright, S. J., R. Hickman, and H. C. Ketley, "Heat Transfer in Fluidized Beds of Wide Size Spectrum at Elevated Temperatures," Brit. Chem. Eng., 15, 1551-1555 (1970).

APPENDICES

APPENDIX A

Figure A1 gives the block diagram of the overall system. Figure A2 gives copies of the engineering drawings made by the system designer, Professor D. Junge of Oregon State University.

The bed is basically a cast refractory lined steel shell. Hot air and combustion products enter the firebox from the burner assembly. The firebox allows completion of combustion. The burner is normally operated with about 100% excess air.

Gases leaving the firebox are conducted through a flared 90° turn and encounter the distribution plate assembly.

The plate assembly, illustrated in Figure A3, consists of two punched stainless steel plates separated by a stainless steel screen. The screen openings are approximately 1.3 mm. The plate hole grid, with dimensions as shown on the figure, provides a total opening of about 6.7% of the fluidized zone superficial area. The fluidized zone has a cross-section of 0.31 x 0.61 m. The plate assembly was fabricated by Western Wire Works of Portland, OR.

Gas leaving the distribution plate enters the fluidization zone. There are twelve sets of test port locations cast into the walls of this zone. In addition there are ten small diameter ports which are used to measure bed pressures. The locations of these ports are shown in Figure A2. Figure A4 shows the bottom thermowell and

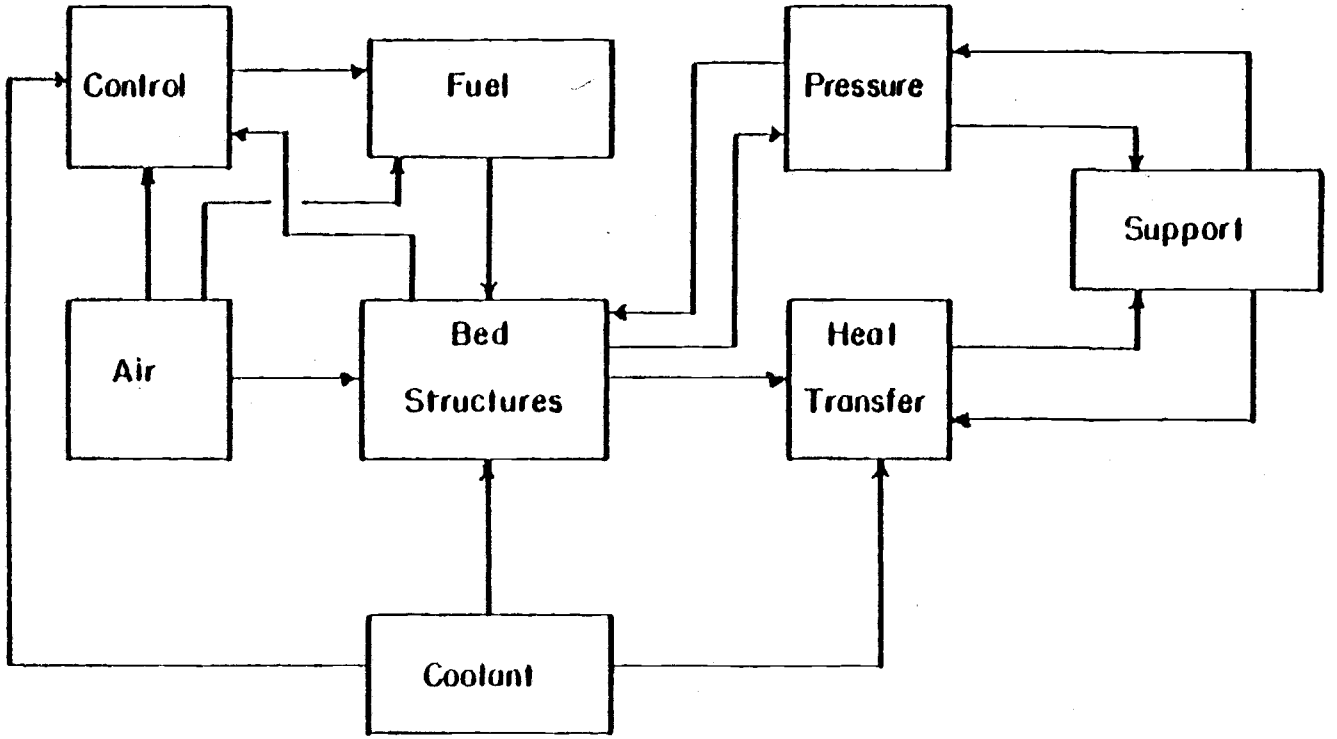

Figure A1. System block diagram.

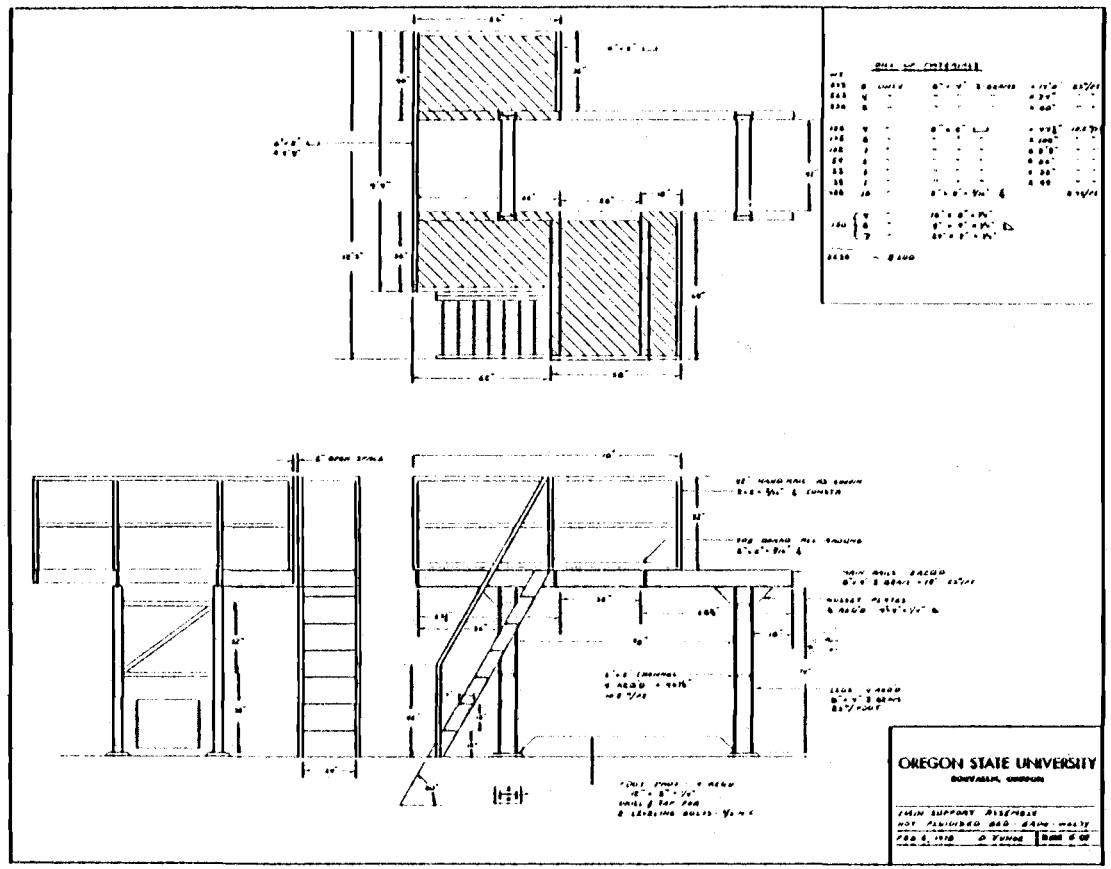

Figure A2. Engineering drawings of bed superstructure.

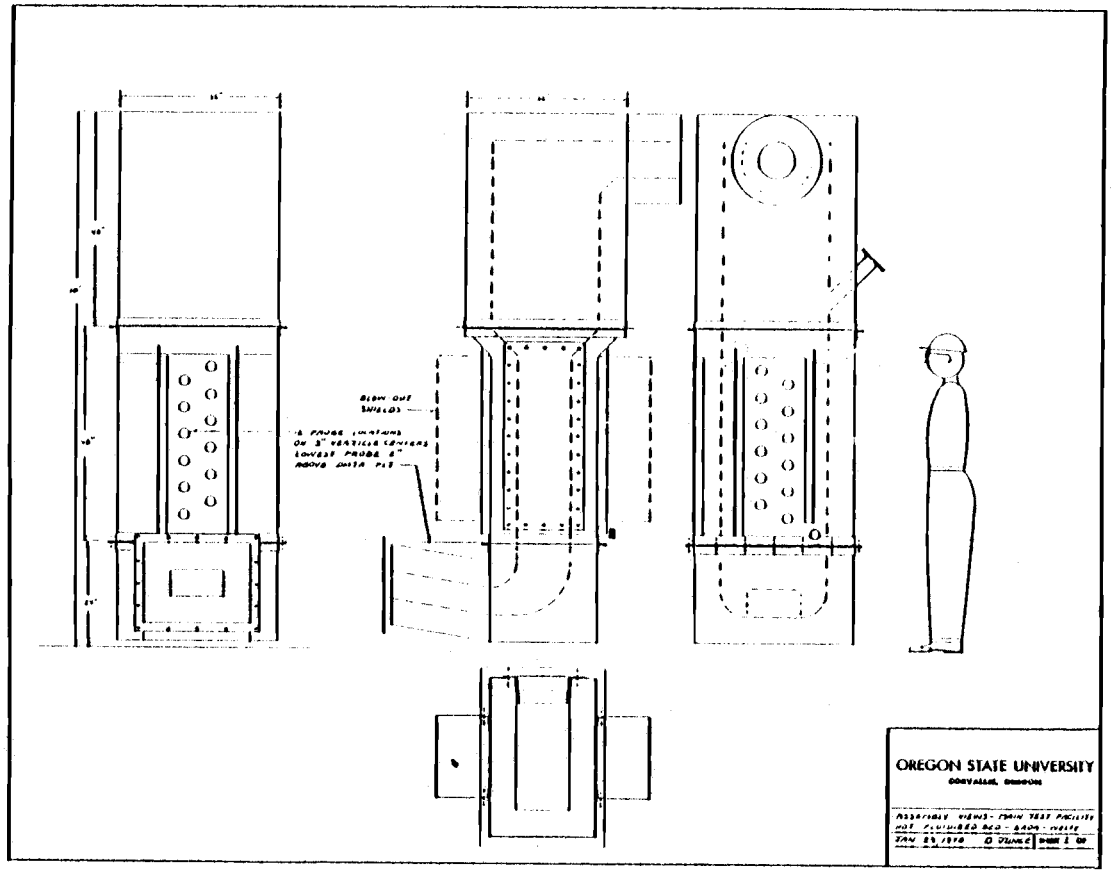

Figure A2. (Continued)

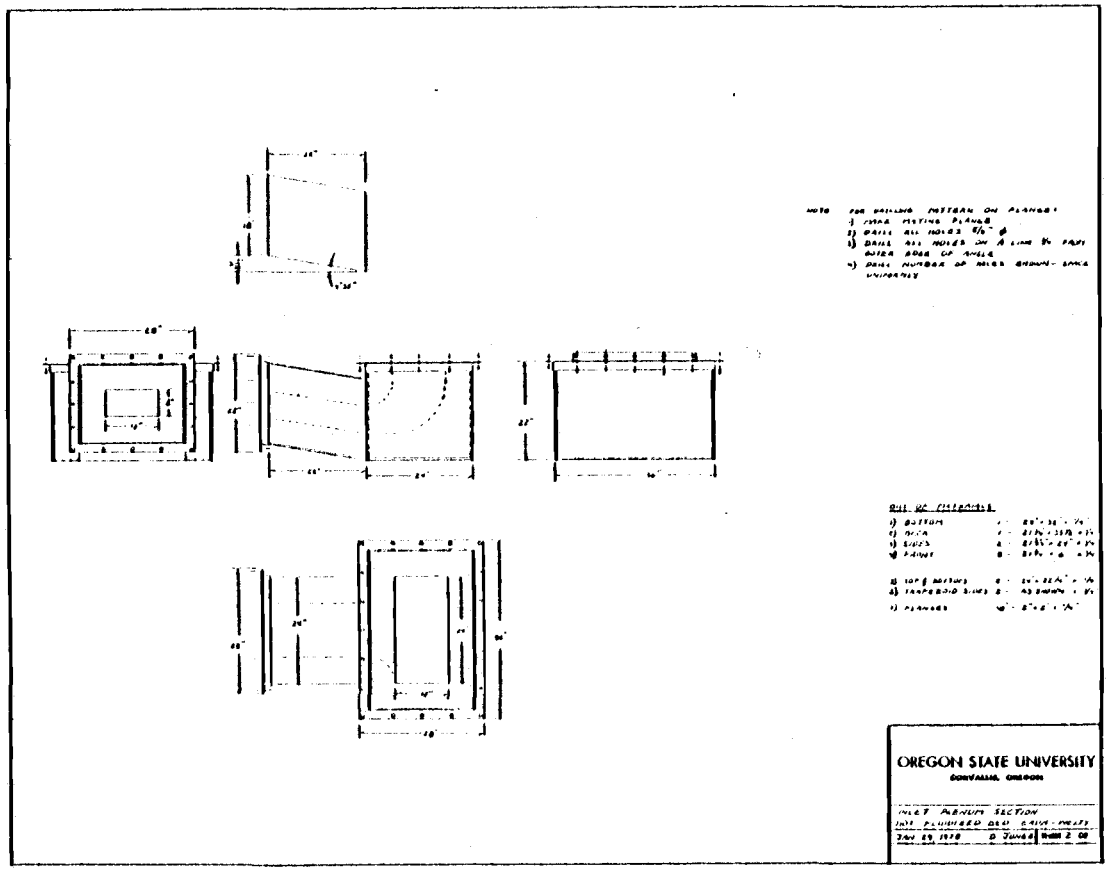

Figure A2. (Continued)

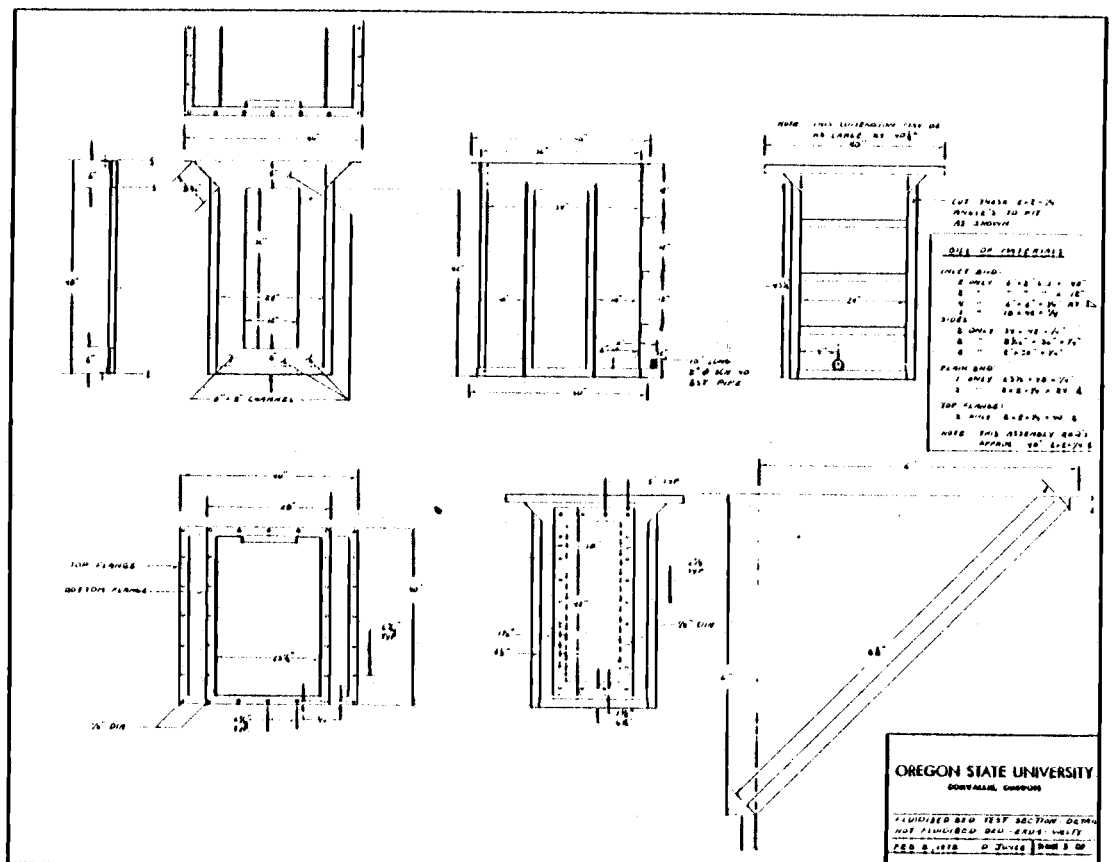

Figure A2. (Continued)

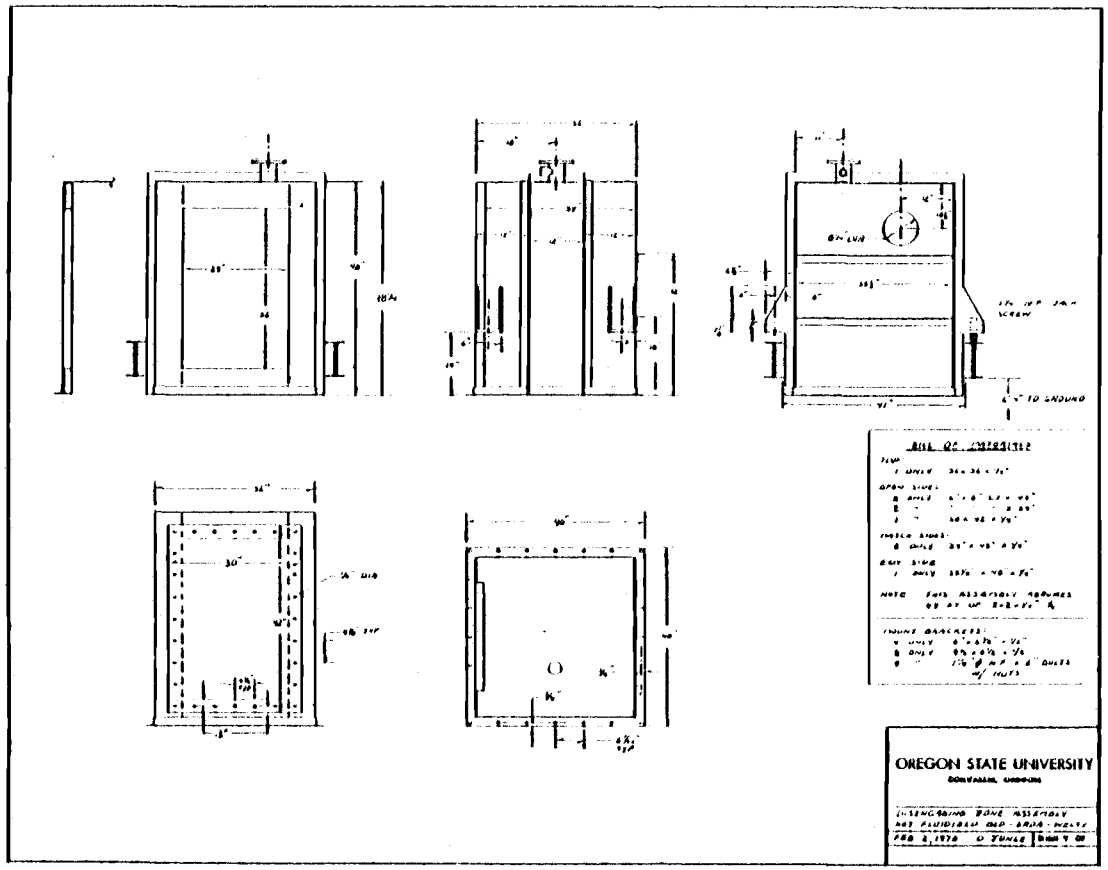

Figure A2. (Continued)

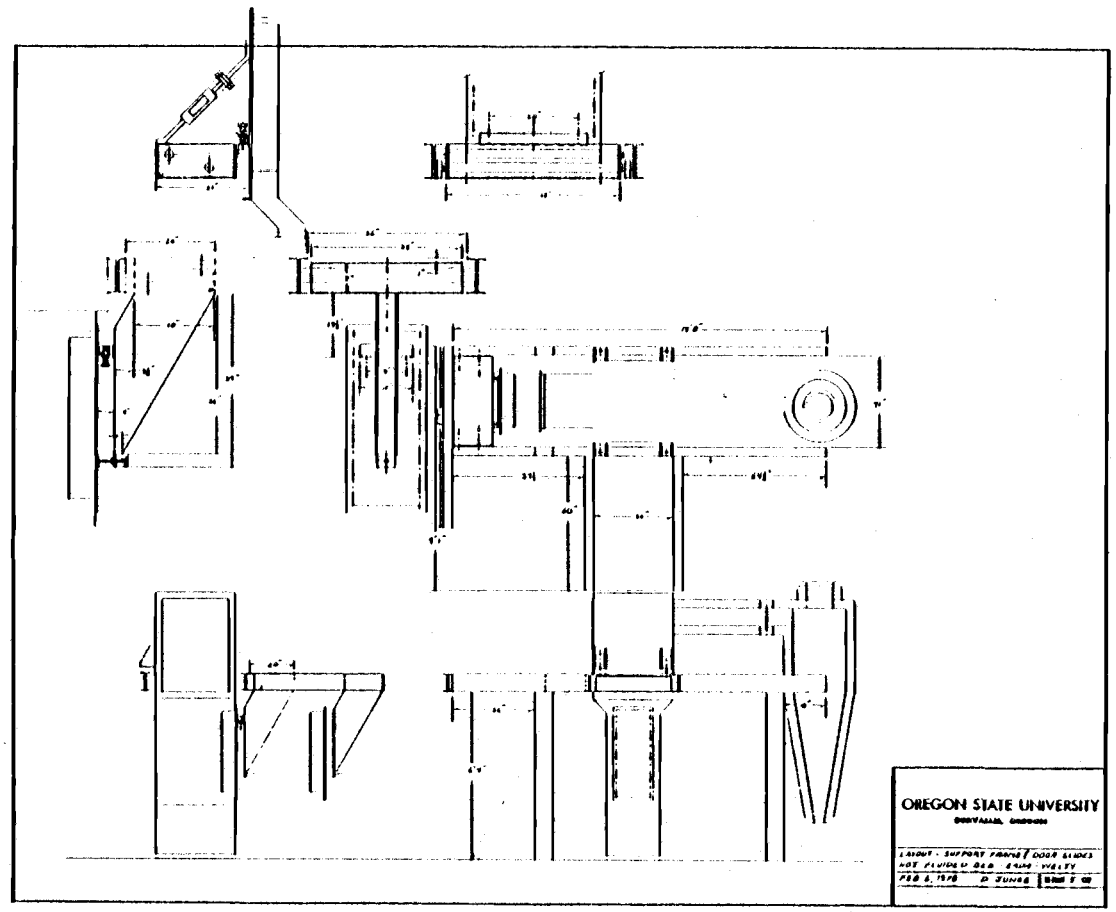

Figure A2. (Continued)

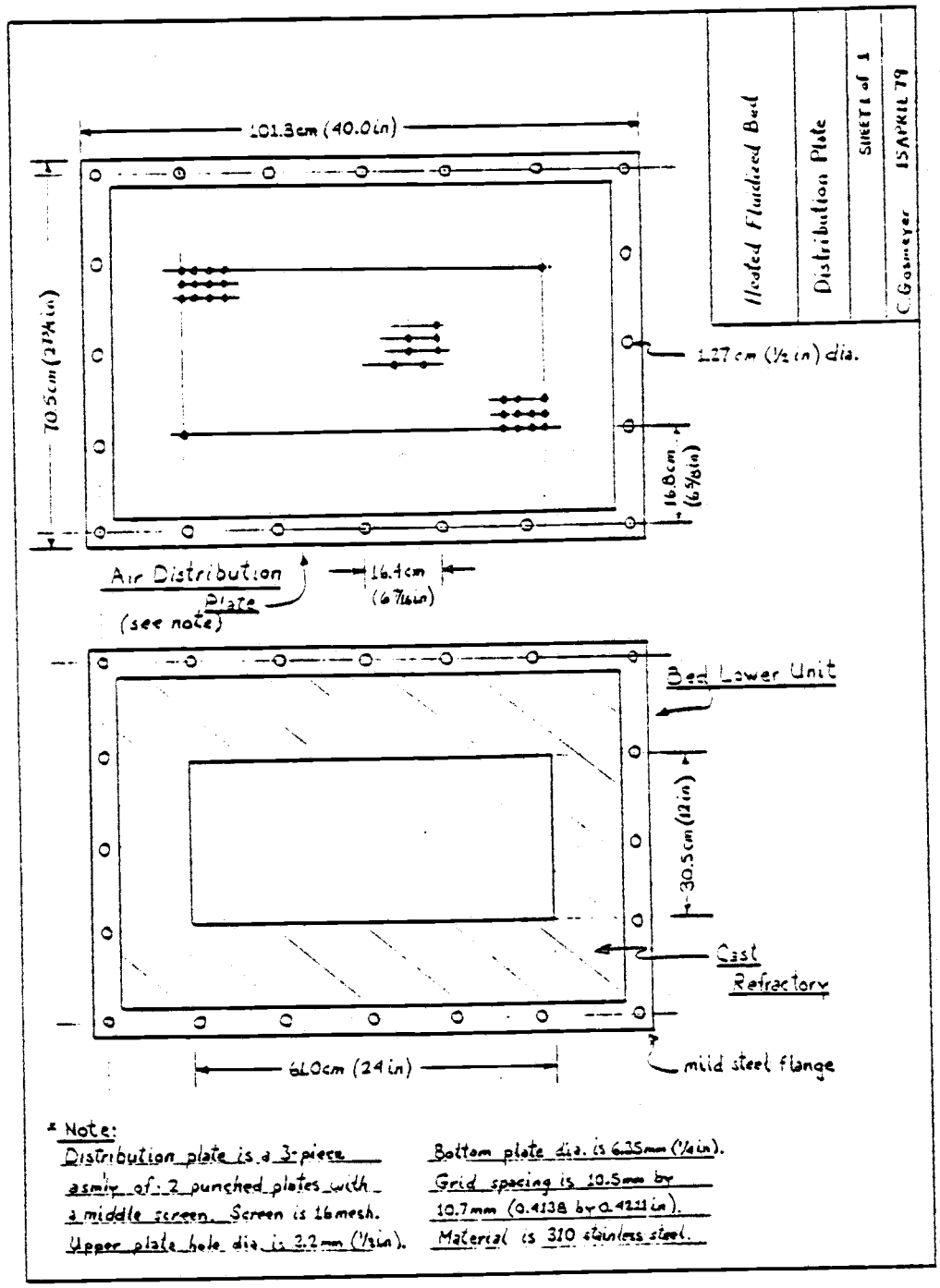

Figure A3. Air distribution plate detail.

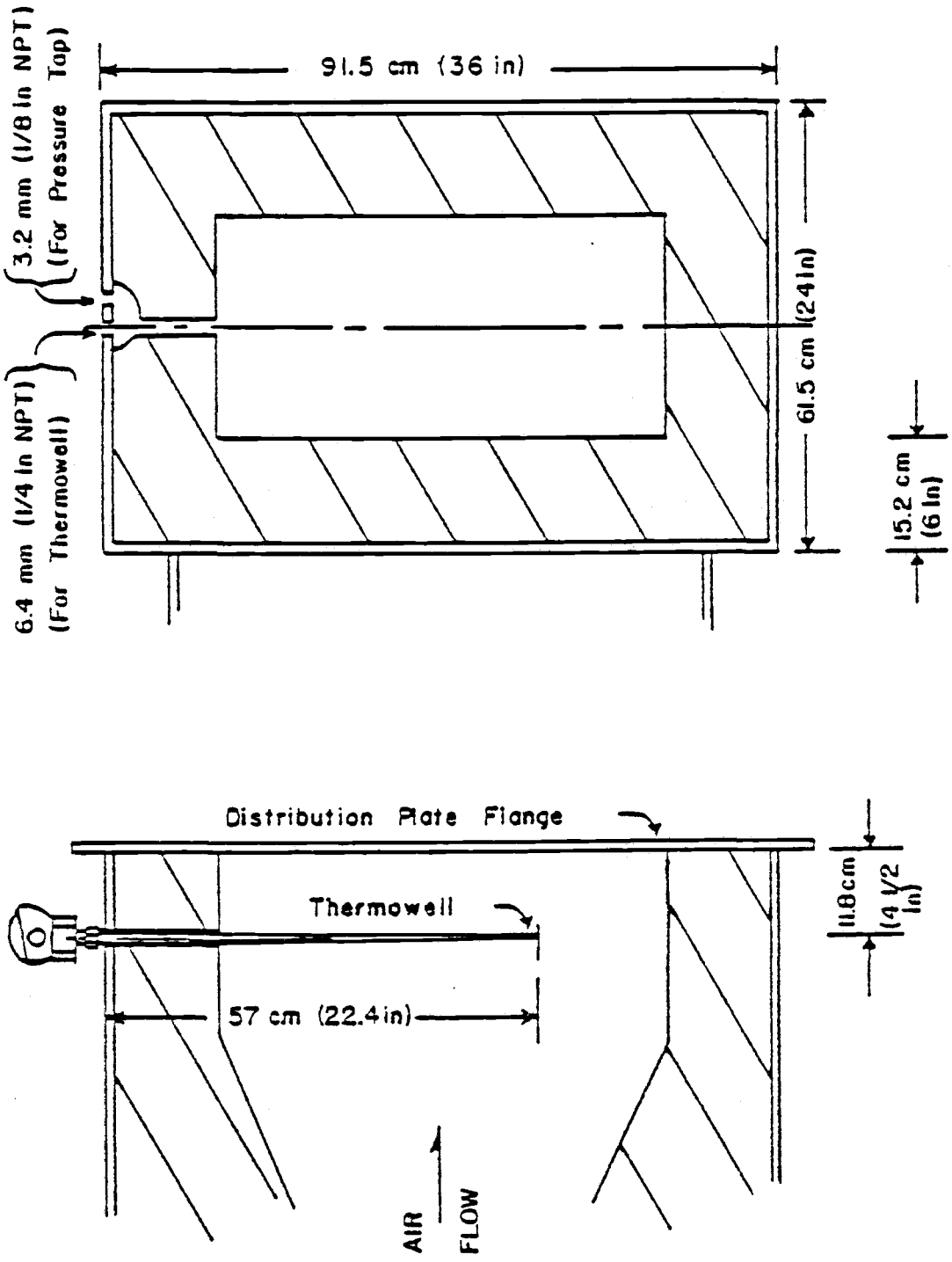

Figure A4. Lower thermowell and pressure port.

pressure port locations.

Hot gases leaving the fluidized section (as well as some solids) enter the transport disengaging zone. In this zone the superficial cross-section expands from 0.186 m^2 to 0.372 m^2, resulting in a decreased superficial velocity. This velocity decrease seems to prevent much carryover of all but the very finest particles.

A 0.171 m diameter tempered glass viewport is located to one side of the top of the transport disengaging zone. Gases leaving this zone exit through a round side duct which directs them to a stainless steel cyclone. Exhaust from the cyclone exits out the building roof. Solids are collected in a sealed bucket. There is no direct solids recycle. The majority of solids collected in the cyclone appears to be very fine pieces of refractory material eroded from the bed walls.

Filling of the bed is done through the viewport flange. The upper portions of the bed are surrounded by a steel deck which simplifies the filling process.

Both the fluidization zone and the disengaging zone are provided with large doors which roll on a track and caster arrangement and provide access to the bed interior.

The main air system, illustrated by Figure A5, provides air for fluidization and viewport cooling. A small piston type air compressor supplies higher pressure air for port purging.

The main air is provided by a Sutorbilt brand blower driven by

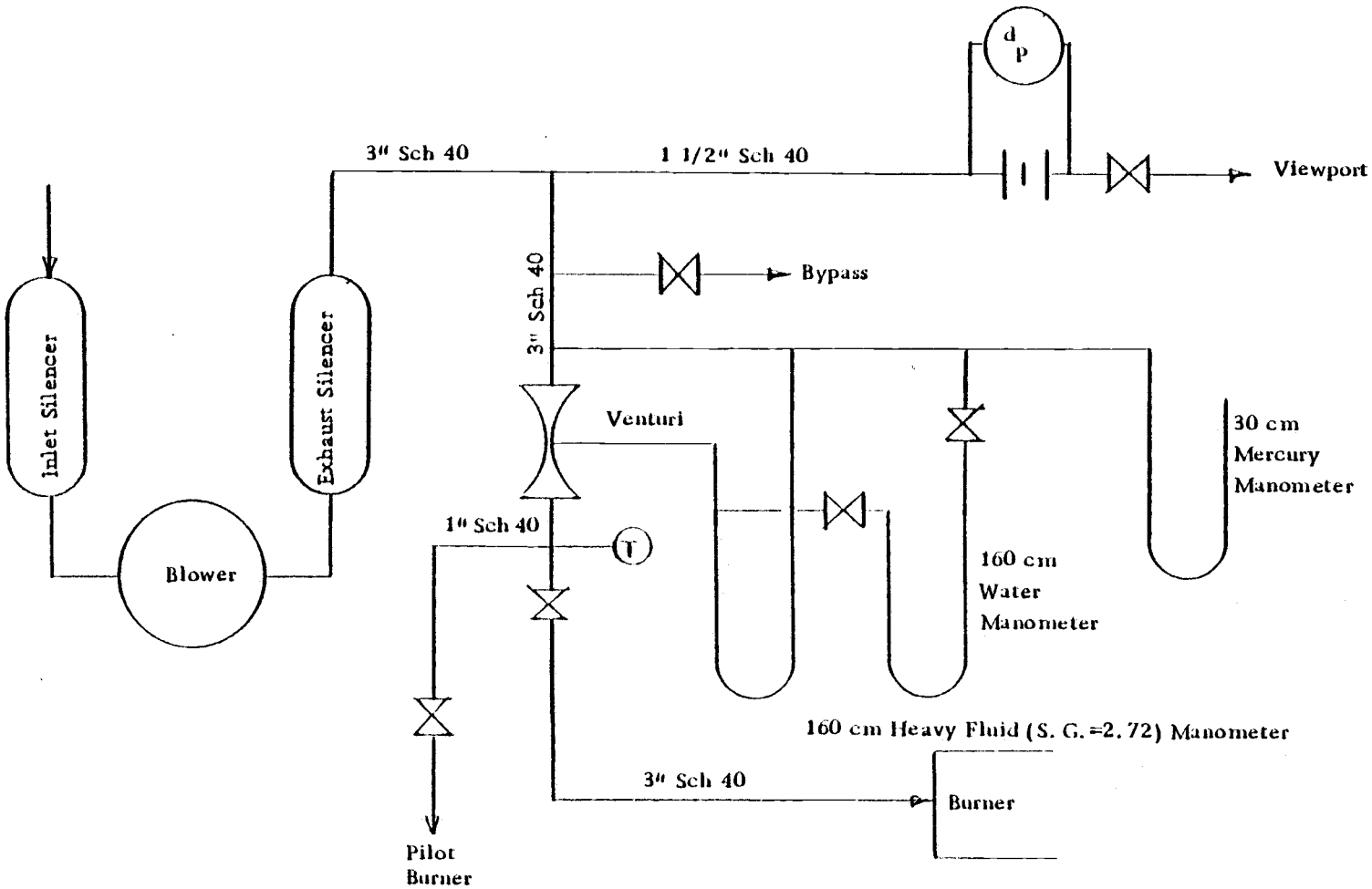

Figure A5. Main air system.

a 22.4 KW electric motor. The blower is equipped with inlet and exit silencers.

Air pressure on the downstream side of the blower is limited by a weight controlled pressure relief valve.

Air flow may be bypassed to the environment through a 76 mm gate valve.

The air flow measuring system consists of a venturi and three manometers connected as shown in Figure A5. The venturi was supplied by Oregon Electro-Mec of Corvallis. Venturi calibration was done with a pitot tube and micromanometer. A five point traverse was used to find average air velocities. The pitot results agreed well with published venturi data. The calibration results have been written into a computer program and this program is used to convert manometer data into air flow rates. A copy of this program and a limited table of the calibration results are included in Appendix B.

Air leaving the venturi passes through a 76 mm gate valve and goes to the burner. A small portion of the air is directed to the pilot burner and so enters the bed through this route.

Upstream of the venturi is a takeoff for a 38 mm diameter pipe which supplies cooling air to the glass viewport. This line is equipped with an orifice connected to a magnahelic type differential pressure gage. A calibration curve for this orifice is given in Appendix B. When conducting tests the viewport air flow is kept to a very small

fraction (< 5%) of the fluidizing flow rate.

Gaseous propane is supplied from a tank which has a capacity of about 28 m^3 of propane liquid. Inlet line pressure is controlled at 239 kP_a by a regulator at the tank. The propane flowrate is metered by a rotameter. The rotameter scale is calibrated for oxygen flow and the necessary conversion curve is given in Appendix B.

Propane leaving the rotameter passes through another pressure regulator and then goes to the main gas valve. This valve is an electrically enabled, manually reset type. A side stream, controlled by an electric solenoid and a globe valve is taken off at the main valve. This side stream supplies propane to the pilot burner.

Propane leaving the main gas valve flows through an electric servo-operated valve and/or a manually operated bypass valve.

The electric valves are automatically operated by the control system. The control system schematic is given by Figure A6. The system was supplied by the Grant Edgel Company of Portland, OR. The original system has been modified to provide additional safety features.

The system performs two main functions. It operates as a sequencer and shut-off circuit to provide safe and orderly ignition and firing procedures and it operates as a control circuit to maintain constant bed temperature.

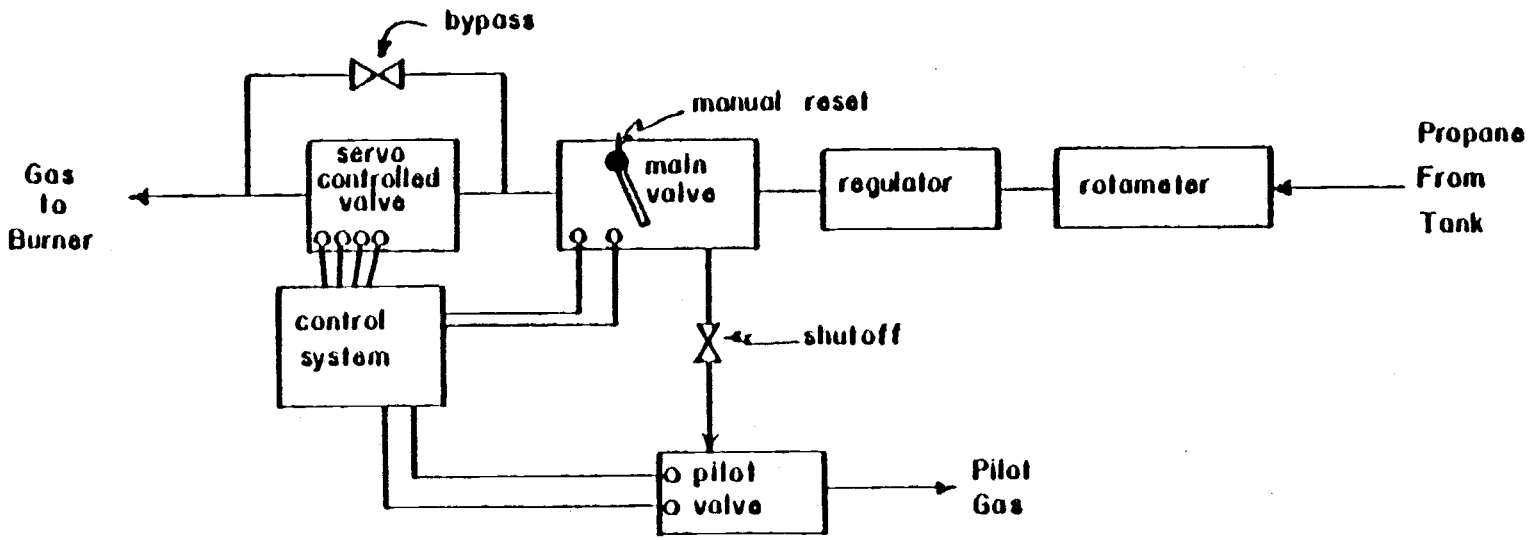

Figure A6. Fuel control system.

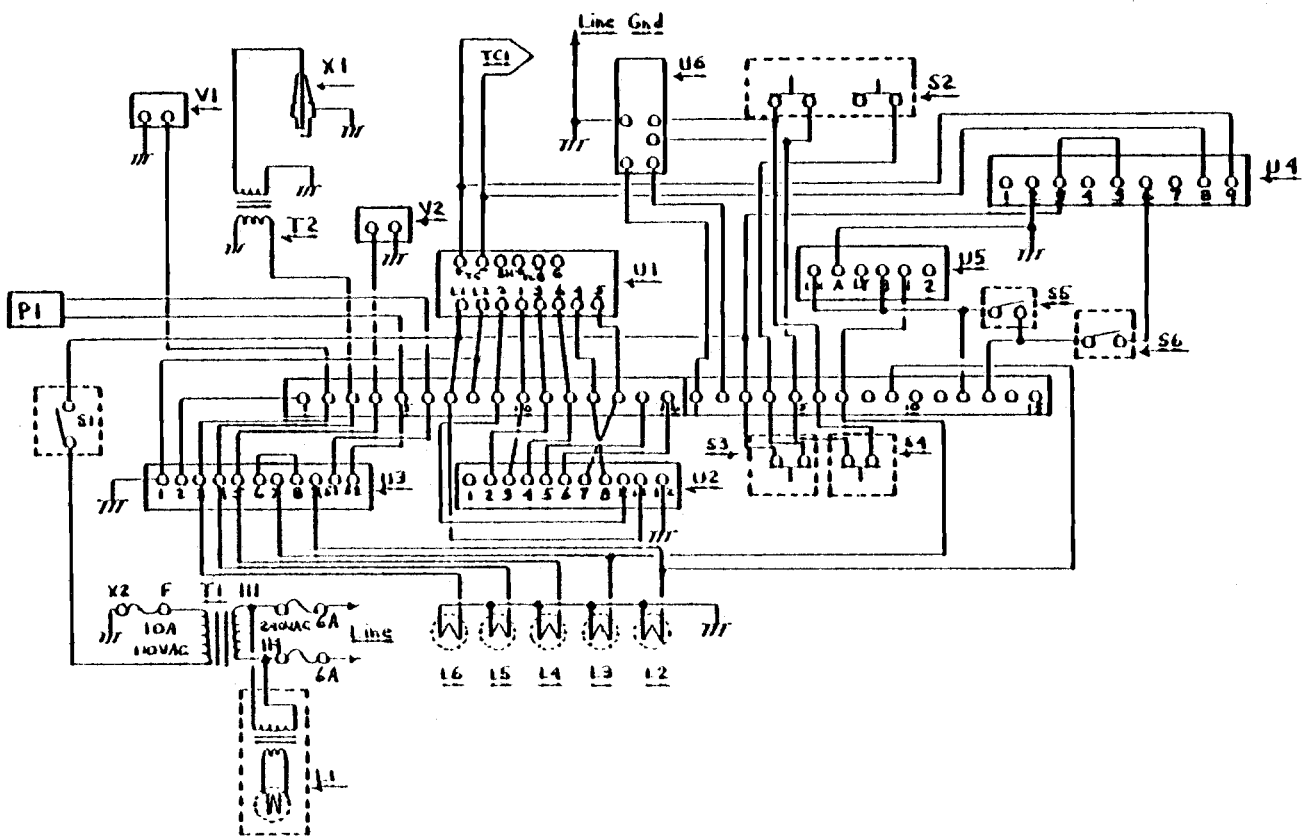

Figure A6. (Continued)

SYMBOL	DESCRIPTION
P1	Flame photo-dectector
X1	Ignitor plug
V1	Pilot gas solenoid valve
V2	Main gas solenoid valve
T1	pri 240 VAC, sec 110 VAC
T2	Ignition transformer
TC1	Thermocouple, type K
U1	Wheelco proportional control
U2	Barber Colman servo
U3	Fireye unit
U4	Partlow hi-limit switch
U5	Eagle purge timer
U6	Cutler-Hammer motor control
S1	ON-OFF
S2	START-STOP, west wall
S3	STOP
S4	START
S5	Dwyer minimum flow
S6	Coolant flow
L1	"ON", green
L2	ALARM, red
L3	LIMIT, white
L4	FUEL, green
L5	IGNITION, amber
L6	PILOT, white

Figure A6. (Continued)

Startup and maintenance procedures are covered in Junge (1978). They will not be repeated here except to cover some changes and additions dealing with the high limit safety switch and the coolant flow system and safety switch.

The Partlow brand high limit switch is used to shut the propane system down if the adjustable setpoint temperature is exceeded. This switch is used to protect the bed from damage due to control system malfunctions or operator errors. In normal operation the high limit setpoint is set about 100K above the temperature controller setpoint. This allows room for minor transients to occur without the bed automatically shutting down.

The cooland system schematic is given by Figure A7. It is a simple circulation system designed to provide more than 0.0038 m^3/s of Dowtherm A at pressures up to 377 kP_a.

The Dowtherm is circulated from a 0.473 m^3 capacity stainless steel tank located on the upper deck. The tank is provided with a top to help limit fume escape. A 200 W immersion heater is used to thaw the tank during cold weather. The tank is insulated with about 0.1 m of fiberglass.

About 0.132 m^3 of Dowtherm A are kept in the system during operation. The Dowtherm was obtained from Van Waters and Rogers of Portland, OR.

The system pump is a 2.2 kW Jacuzzi brand centrifugal type

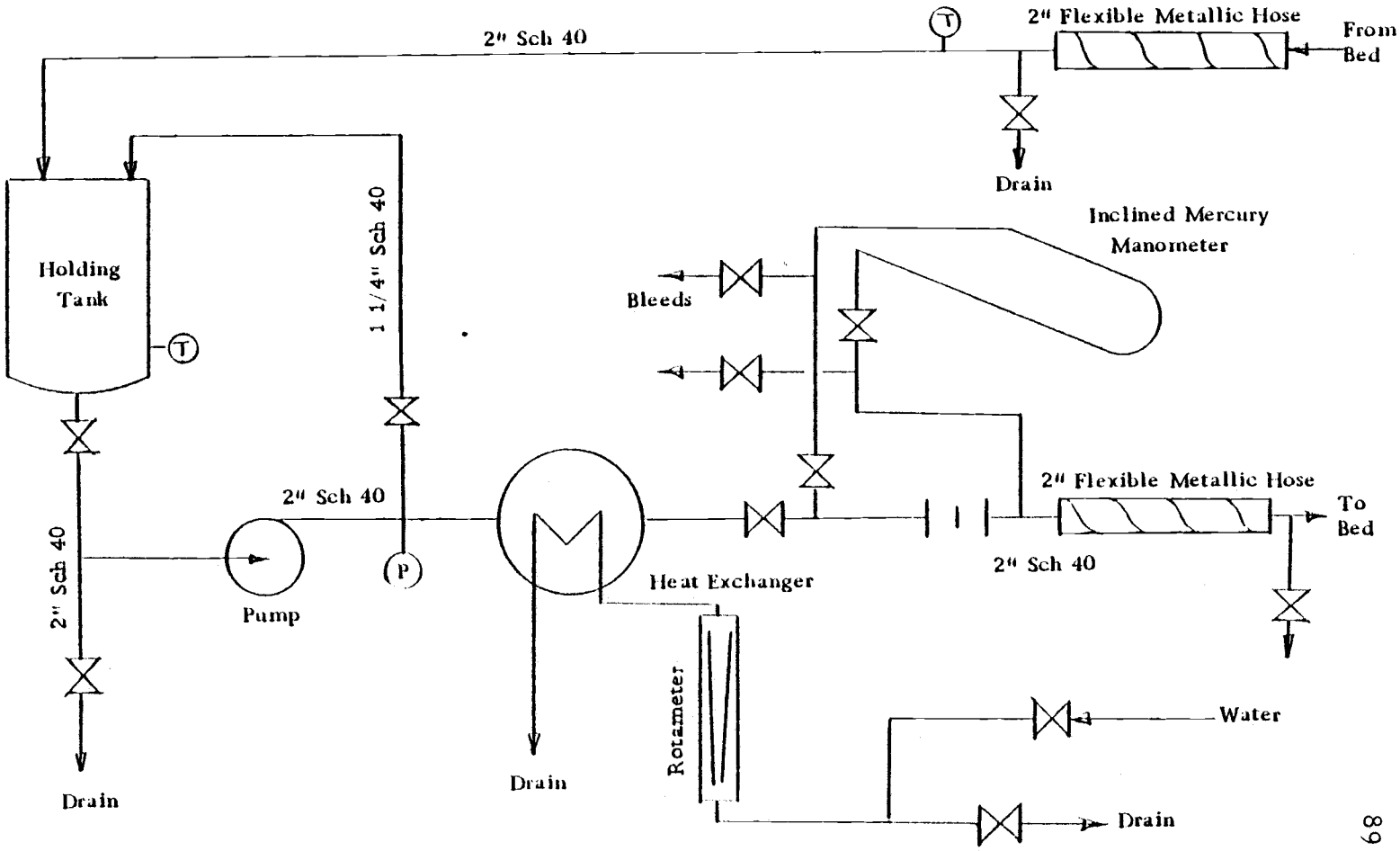

Figure A7. Coolant system schematic.

equipped with special viton elastomer mechanical seals. The seal is available from Queen Pump Company of Portland, OR as U.S. Seal Mfg. Corp. #PS-358-Viton. A spare seal set is kept on hand.

Coolant out of the pump can be bypassed back to the tank or directed to the bed. The coolant flows through the shell side of the shell and tube exchanger. Water flows through the tube side. The cooling water rate is measured with a rotameter (calibration curve, in Appendix B). The rotameter full scale corresponds to a flow of 4.95E-4 m^3/s. The heat exchange system has considerable excess capacity and water rates are low during normal operation.

Coolant flow rate is measured with an in-line orifice plate and an inclined mercury manometer. Appendix B has the calibration curve for the manometer.

The coolant flow safety switch also operates off this inclined manometer. The safety switch schematic is given by Figure A8. When the switch is in the "OFF" position or when it is disconnected from line power the propane supply is shut off. When the switch is in the "TEST" position the propane control system behaves as if the coolant safety switch was not there, provided the switch is connected to line power. When the safety switch is in the "NORMAL" position the propane flow cannot be established until enough coolant flow is provided to break the mercury switch circuit. If coolant flow rate drops below this level the safety switch shuts the burner down.

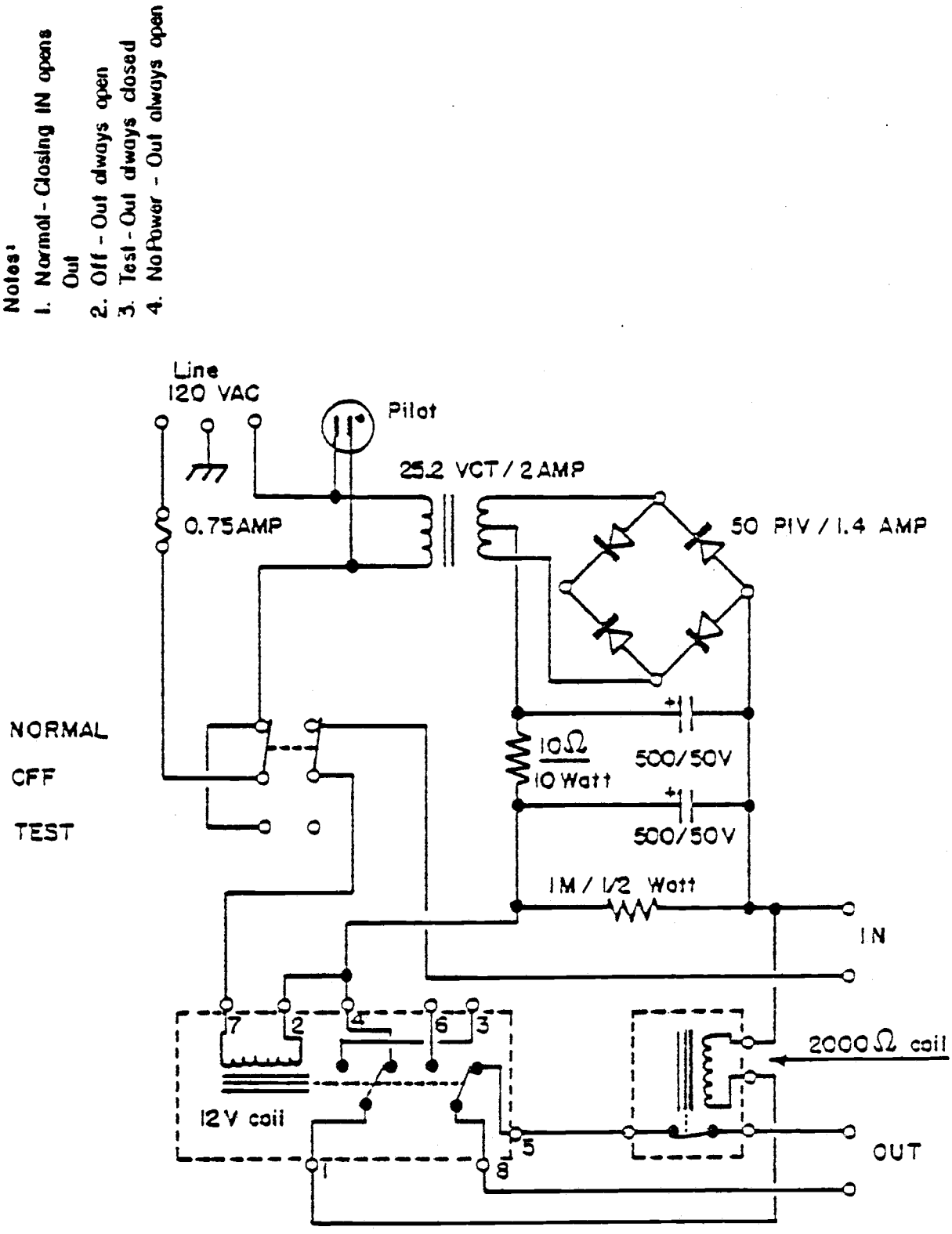

Figure A8. Coolant flow safety switch schematic.

Connections to and from the test pipe in the bed are made through 51 mm diameter flexible metal hoses.

The Dowtherm exit temperature is measured by a well type thermometer located in the line immediately past the bed exit point. Dowtherm A boils at about 531 K at atmospheric pressure and care is taken that the immersed tube inner wall does not exceed this temperature. The mixed Dowtherm exit temperature will be somewhere between 340 K and 394 K when the inner wall temperature reaches the boiling point. The exact temperature depends on the flowrate and the heat flux through the wall.

Some of the physical properties of Dowtherm A are given in Table A1. Materials found suitable for use in contact with hot Dowtherm A include metals, teflon, nylon, viton, dense asbestos gaskets, Permatex brand silicone gasket material, and some epoxies.

The coolant system should not be started up until it has been determined that the Dowtherm is not frozen and that the various valves are properly adjusted. A good rule-of-thumb is to start with the bypass valve wide open and the heat exchanger valve fully closed.

The system is usually kept drained when not in use. The drained Dowtherm is returned to the holding tank. The holding tank valve is kept closed except while the system is in use to prevent an accident from spilling the whole tank.

Kitty litter makes a good absorbent for minor spills and drips.

Table A1. Physical properties of Dowtherm A.

Property	Specification
Atmospheric Boiling Point	531 K (495.8°F)
Freezing Point	285 K (53.6°F)
Flash Point, c.o.c.	397 K (255°F)
Fire Point, c.o.c.	408 K (275°F)
Auto Ignition Temp., A.S.T.M	894 K (1150°F)
Density at 289 K (60°F)	1068 kg/m^3 (66.7 lbm/ft^3)
Heat of Fusion	98000 J/kg (42.2 Btu/lbm)
Specific Resistivity at 313 K (104°F)	3.9 E13 Ω/m
Heat Capacity at 339 K (150°F)	1704 J/kg-K (0.407 Btu/lb_m°F)
Viscosity at 339 K (150°F)	1.8 E-3 Pa-s (1.8 cps)

A Class B (Flammable liquids approved) fire extinguisher is available at the lab. Also available are two organic mist approved respirators with spare cartridges.

Dowtherm A toxicity is a matter of debate. According to the manufacturer it is not especially hazardous but prolonged breathing of vapors and skin contact must be avoided. Under no conditions should the area be entered without the proper respirator if there is visible Dowtherm vapor. The best policy is to avoid any contact with the material or its vapor.

APPENDIX B

This appendix consists of calibration information for the various flow measuring systems on the bed.

Figure B1 is a copy of one of the computer programs used to translate manometer and temperature readings into superficial velocities. The particular program shown also calculates the Wen and Yu prediction for U_{mf} at the prevailing bed conditions. The program uses gas property relations that are modified from those for pure air in order to account for the presence of combustion products. The modified relations were constructed on an average mole fraction basis. The rate of propane combustion is taken as the theoretical minimum plus 30%. The latter factor was determined from operating experience.

Table B1 gives the results of the final venturi calibration runs. The table compares the results obtained from the pitot tube traverses with the venturi flowrates. The venturi flowrates are calculated by the method of A. S. M. E. (1959).

Figure B2 through B5 gives the calibration curves for the other orifices and rotameters.

Table B1. Venturi calibration results.

Pitot Tube SCFM	Venturi SCFM	Factor
197.7	197.5	1.0010
450.1	447.8	1.0051
194.4	195.9	0.9923
464.7	461.9	1.0061
198.0	200.3	0.9885
440.9	441.2	0.9993
Average Factor = 0.9987		

```
      PROGRAM UMO(INPUT,OUTPUT,DATAMO,LPM,TAPE4=INPUT,TAPE5=DATAMO,
     *  TAPE10=LPM)
      REAL MUG
      G=980.6
      OS=2.4414
      FA=1.000
      F=1.0342
      C=0.984
      SY2=3.5
      BETA=0.5050505
      READ(4,*)RHOS,PC
   10 CONTINUE
      READ(5,100)TB,T,DP,P
  100 FORMAT(9X,F7.2,3(1X,F7.2))
      IF(EOF(5).NE.0.)GO TO 20
      TFAC=(0.020*TB-1.29)/(1663.1-0.085*TB)
      RHOG=0.6297/(459.7+TB)
      MUG=3.934E-4+1.376E-7*(TB-1200.0)
      A1=MUG/(PC*RHOG)
      A2=PC*PC*PC*G*RHOG*(RHOS-RHOG)/(MUG*MUG)
      A3=SQRT(33.7*33.7+0.148*A2)
      UMF=A1*(A3-33.7)
      UMFF=UMF/30.48
      P=P*0.4912
      P1=14.697+P
      P2=P1-0.03613*DP
      R=P2/P1
      SY1=R**1.429
      SY3=(1.-R**0.2857)/(1.-R)
      SY4=(1.0-BETA**4)/(1.0-(BETA**4)*(R**1.429))
      YA=SQRT(SY1*SY2*SY3*SY4)
      GA=39.626/(T+459.7)
      GZ=GA*P1*0.068041
      WM=3.983*C*F*OS*FA*YA*SQRT(DP*GZ)
      ACFM=WM/GZ
      SCFM=ACFM*30.0414*P1/(T+459.7)
      P=P/0.4912
      B=SCFM*TFAC
      UO=(SCFM+2.0*B)*(459.7+TB)/529.7
      UO=UO/120.0
      UOF=UO/UMFF
      WRITE(10,200)RHOS,RHOG,MUG,UMF,UMFF,PC,P,T,TB,DP,WM,ACFM,
     *  SCFM,B,UO,UOF
  200 FORMAT(1X,F5.2,2(1X,E12.4),1X,F7.2,1X,F7.3,2(1X,F5.3),
     *  1X,F7.1,1X,F7.0,1X,F5.2,1X,F7.3,2(1X,F6.1),3(1X,F5.2))
      GO TO 10
   20 CONTINUE
      CALL EXIT
      END
```

Figure B1. Computer program for venturi data processing.

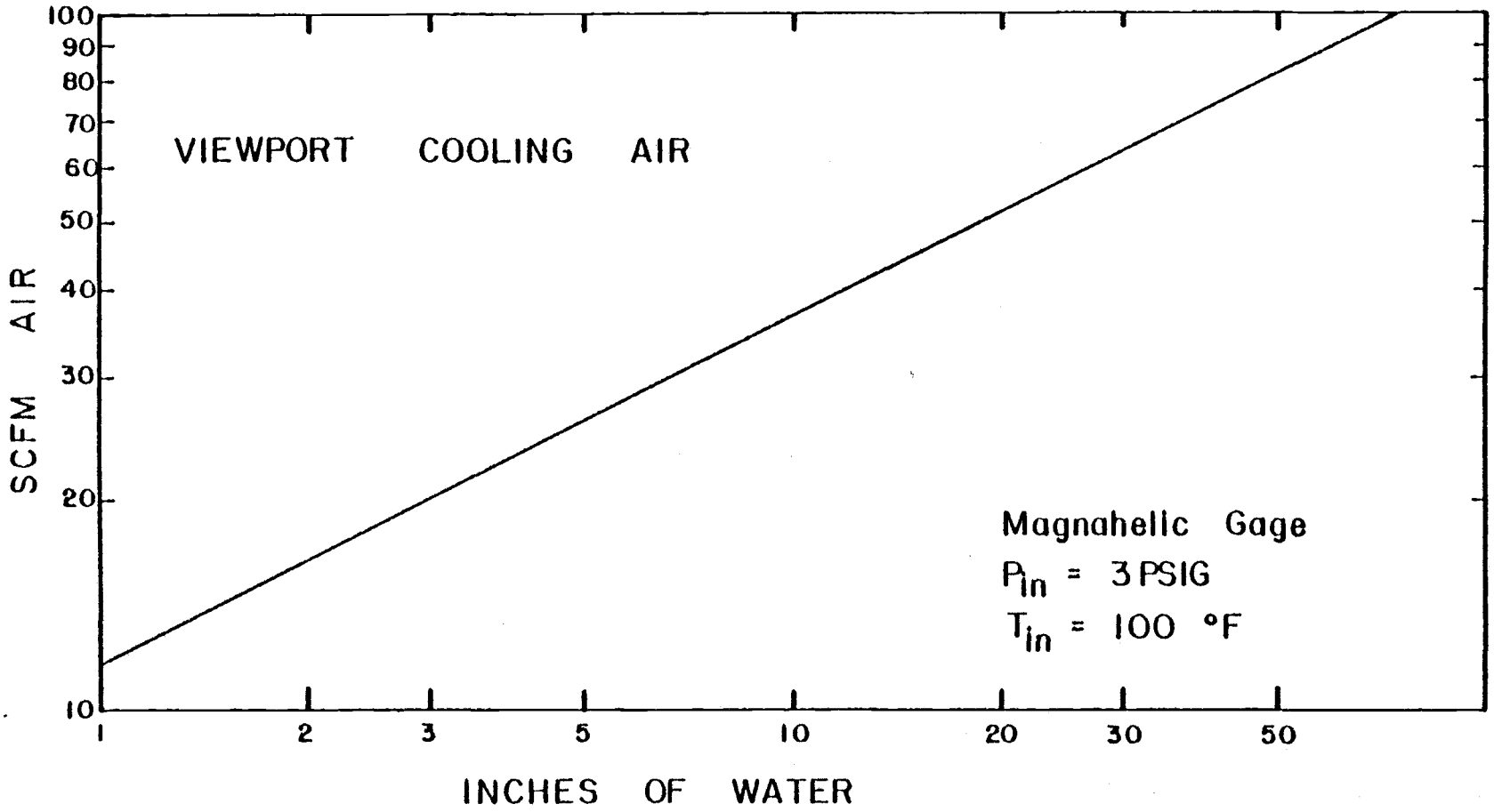

Figure B2. Viewport cooling air flowrate calibration curve.

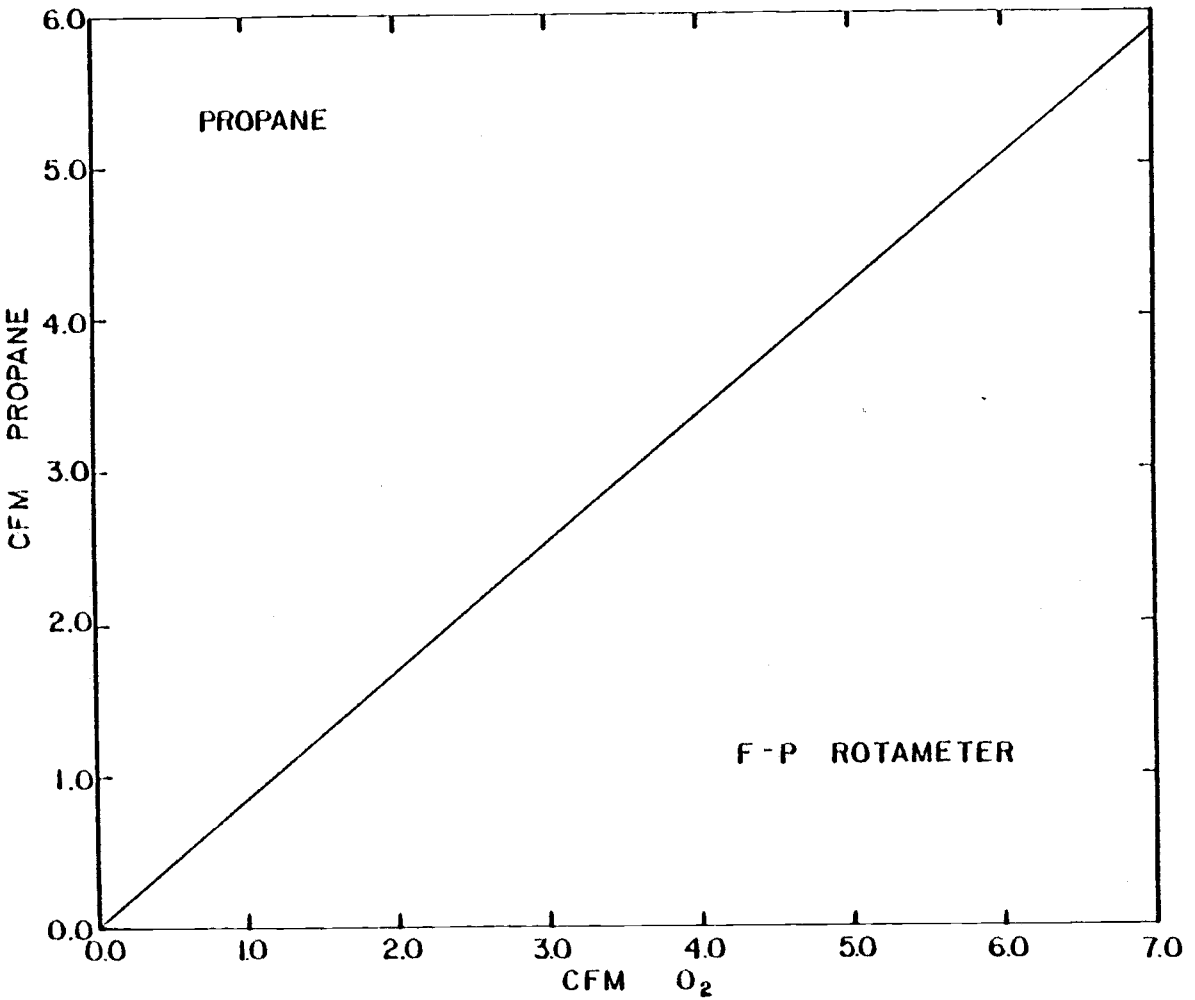

Figure B3. Propane rotameter calibration curve.

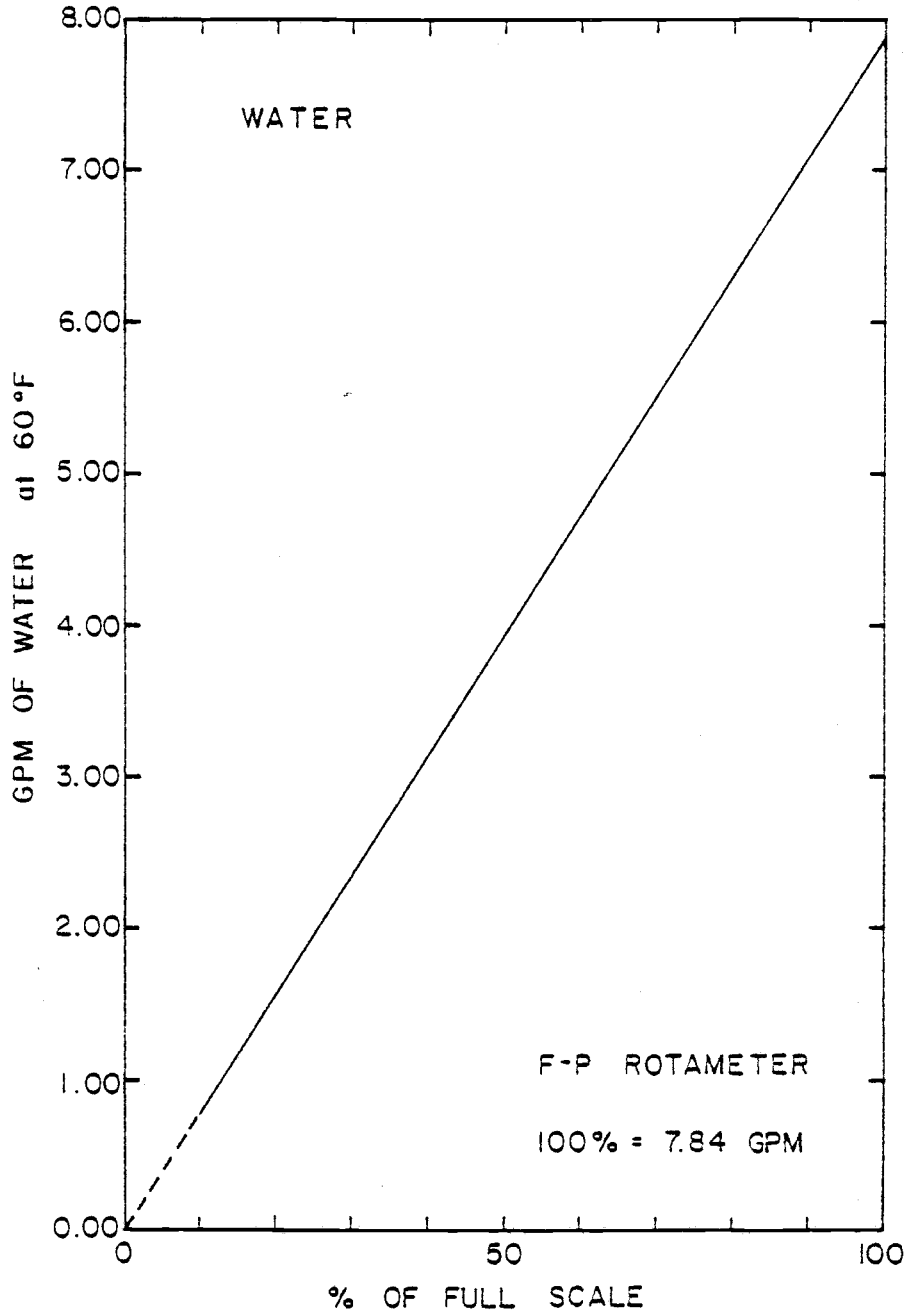

Figure B4. Water rotameter calibration curve.

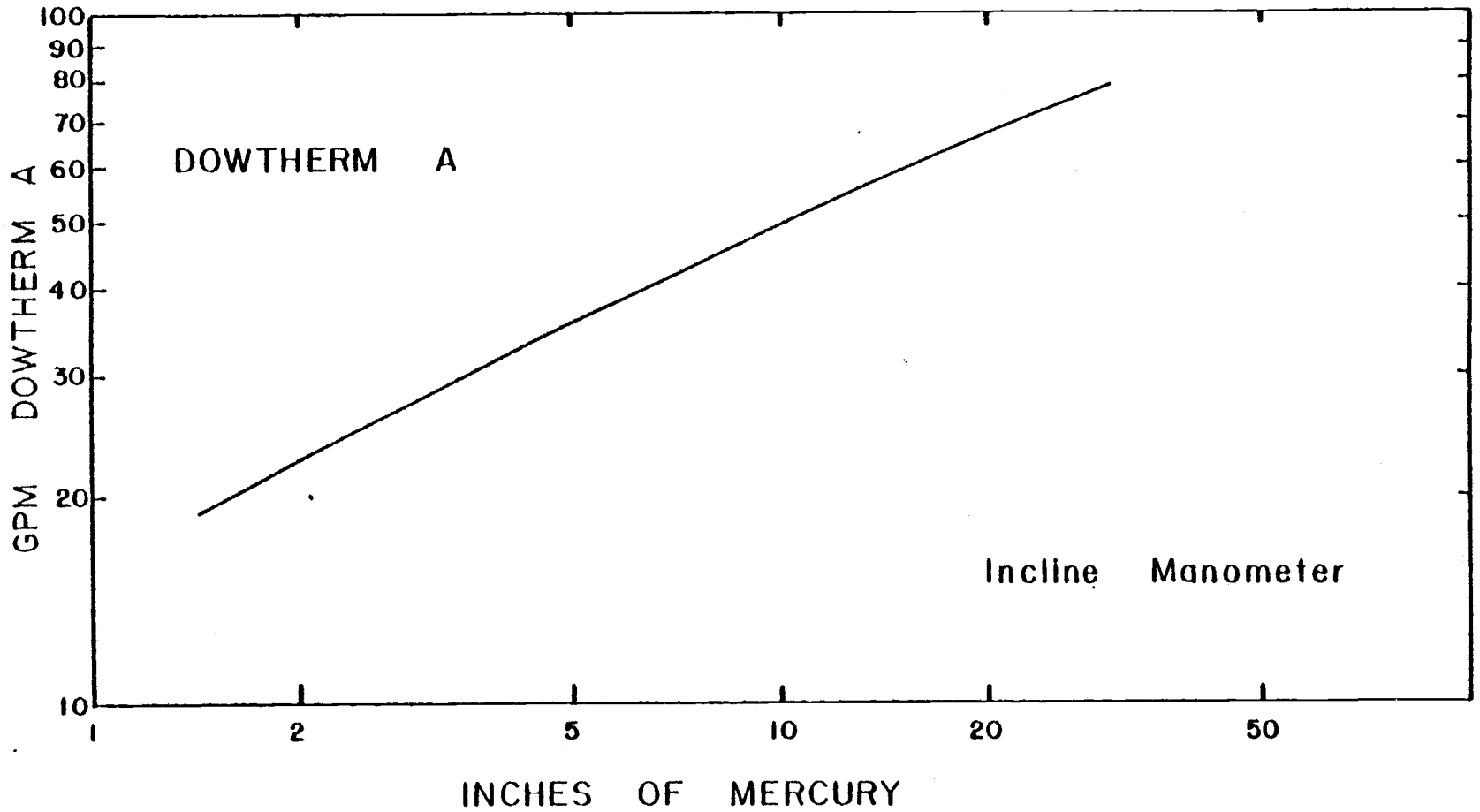

Figure B5. Dowtherm A flowrate calibration curve.

APPENDIX C

This appendix covers the Hy-Cal brand heat flux transducer which is used as the calibrated standard for this work.

Figure C1 is a line drawing of the Hy-Cal device. Figure C2 is a copy of the calibration curve supplied with the instrument. Table C1 is a summary of the device specifications.

The Hy-Cal brand transducers are available from Hy-Cal Engineering, Santa Fe Springs, CA., (213)-698-7785.

Table C1. Hy-Cal model #C-1221-A specifications.

Item	
Response Time	less than 150 ms
Maximum Heat Flux	3.41E5 J/m^2-s
Full Scale Output	10± 1.5 mV
α, ε_N (λ =0.2-20 μm)	0.89 flat
Accuracy	±3%
Repeatability	±0.5%

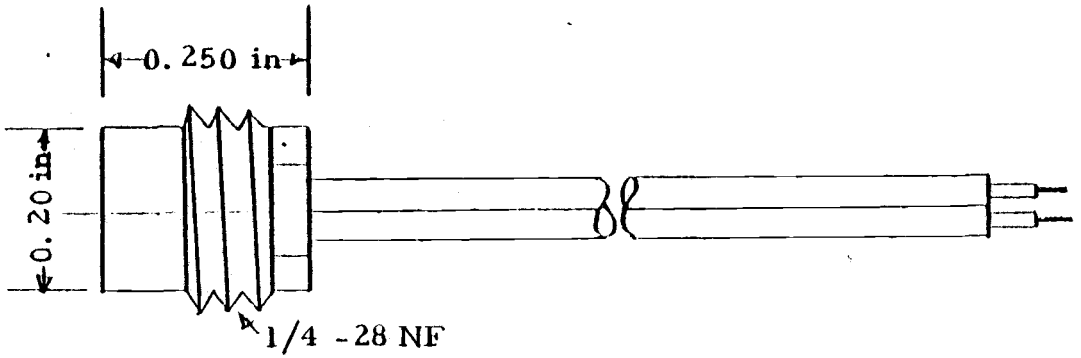

Figure C1. Hy-Cal heat flux transducer outline.

Best scan available.

CERTIFICATE OF CALIBRATION

DATE 2-15-79

CUSTOMER Oregon State Univ.

P.O. NO. 30-262-2130

DESCRIPTION Calorimeter

MODEL G-1221-A-30-060

ABSORPTIVITY .89

NOTE TO RECIPIENT OF CALIBRATION DATA: IT IS RECOMMENDED RECIPROCAL CALIBRATION BE PERFORMED AT REGULAR INTERVALS TO INSURE CONTINUED ACCURACY OF THIS TRANSDUCER.

CALIBRATED STANDARD 9791

CALIBRATED BY

QUALITY APPROVAL

OFFICIAL SEAL
JULIE A. HANGO
NOTARY PUBLIC - CALIFORNIA
LOS ANGELES COUNTY
My comm. expires JUN 28, 1982

SUBSCRIBED AND SWORN TO BEFORE ME THIS 15th DAY OF February 1979

NOTARY PUBLIC

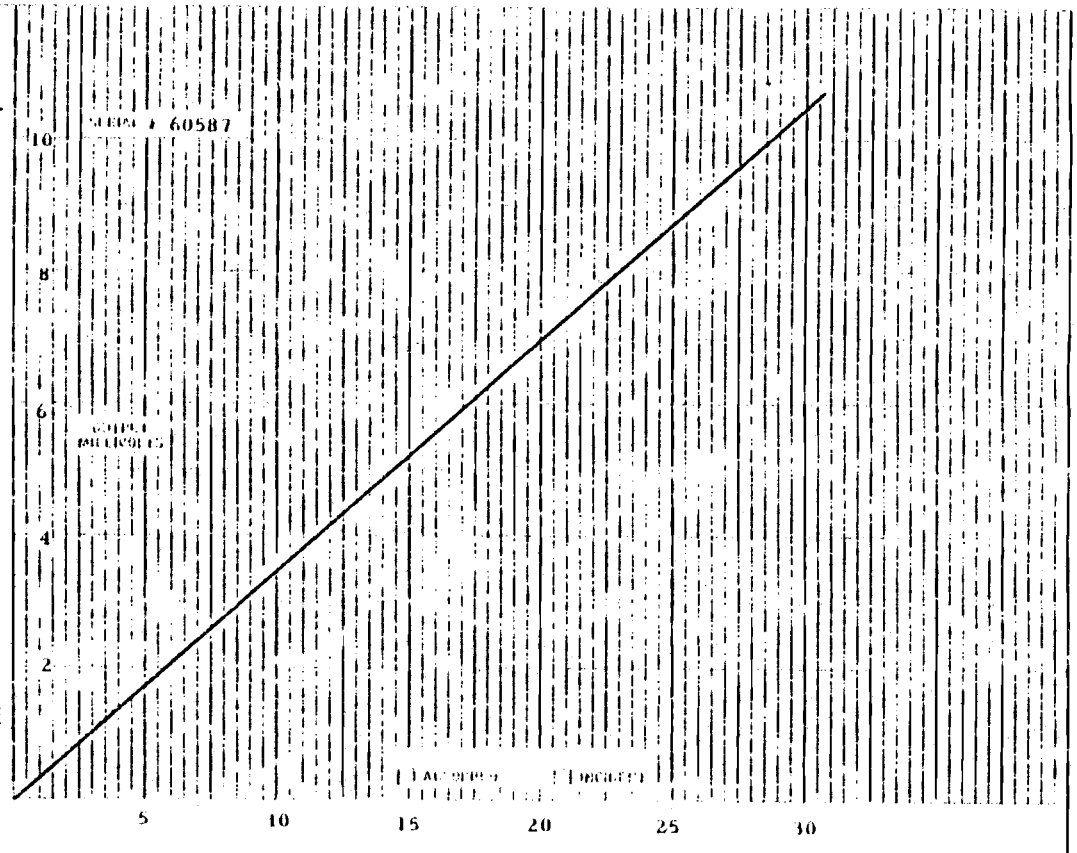

Figure C2. Hy-Cal transducer calibration curve.

PA

APPENDIX D

This appendix presents the U_{mf} raw data. The tables present both the array and open bed data, as taken from the Visicorder charts.

It will be noted that the open bed data have an individual set of calibration data for each bed temperature. Four separate measurements were obtained for each bed temperature.

The runs made with the tube array in place have only one set of calibration data listed which corresponds to an average of several sets made during the course of the runs. The array runs produce U_{mf} values that are very dependent on array geometry.

Tables D1 and D2 present the open bed U_{mf} and calibration data. Tables D3 and D4 present the array data and calibration information.

Table D1. U_{mf} data for open bed runs.

Run #	d_{p_v} Ch 1	p_v Ch 2	$d_{p_{bed}}$ Ch 4		d_{p_v} Ch 1	p_v Ch 2	$d_{p_{bed}}$ Ch 4	T_v, °F
1a	35.5	30.6	28.7		36.98	30.88	28.68	96
1b	37.9	31.2	28.6	ZERO	-3.50	-8.35	-10.5	
1c	37.9	30.8	28.7	NET	33.48	22.53	18.18	
1d	36.6	30.9	28.7					
2a	27.45	28.7	28.7		28.52	28.63	28.70	98
2b	30.5	29.0	28.7		3.4	8.35	10.6	
2c	27.6	28.2	28.7		25.12	20.28	18.10	
2d	-glitch on chart-							
3a	32.05	28.7	28.7		32.29	28.83	28.68	106
3b	31.5	28.7	28.7		6.6	8.4	10.5	
3c	32.7	29.0	28.6		25.69	20.43	18.18	
3d	32.9	28.9	28.7					
4a	30.7	28.5	28.7		29.60	28.10	28.70	110
4b	29.6	28.2	28.7		6.15	8.4	10.7	
4c	29.3	28.2	28.7		23.45	19.70	18.00	
4d	28.8	27.5	28.7					
5a	27.05	28.0	28.7		26.38	27.73	28.70	108
5b	25.75	27.4	28.7		6.3	9.1	10.8	
5c	26.6	27.8	28.7		20.08	18.63	17.90	
5d	26.1	27.7	28.7					
6a	24.4	27.75	29.5		24.98	27.80	29.50	108
6b	26.0	27.9	29.5		6.7	9.0	11.3	
6c	24.6	27.8	29.5		18.28	18.80	18.20	
6d	24.9	27.75	29.5					
7a	23.4	27.0	29.5		23.30	26.87	29.50	107
7b	23.4	26.9	29.5		6.3	9.0	11.3	
7c	23.1	26.7	29.5		17.00	17.87	18.20	
7d	- no data-							
8a	19.5	26.1	29.5		21.28	26.60	29.50	108
8b	21.5	26.5	29.5		6.7	8.3	11.5	
8c	21.8	26.9	29.5		14.58	18.30	18.00	
8d	22.3	26.9	29.5					
9a	19.1	26.0	29.5		19.28	26.00	26.93	110
9b	18.95	25.6	29.5		6.9	8.6	12.1	
9c	19.4	26.0	29.5		12.38	17.40	17.53	
9d	19.65	26.4	30.0					
10a	17.6	25.5	29.5		18.14	25.66	29.50	109
10b	18.75	26.05	29.5		7.0	8.65	11.9	
10c	18.0	25.5	29.5		11.4	17.01	17.60	
10d	18.2	25.6	29.5					

Table D1. (Continued)

Run #	T_{Bed} K	T_v °F	d_{p_v} in H_2O	P_v in Hg	$d_{p_{Bed}}$ psia	U_{mf} m/s
1	583	96	55.67	3.22	0.860	1.97
2	633	98	43.79	3.00	0.868	1.92
3	689	106	39.45	2.94	0.846	1.98
4	744	110	35.01	2.85	0.880	2.03
5	797	108	30.22	2.72	0.869	2.04
6	861	108	27.91	2.75	0.885	2.13
7	905	107	25.76	2.63	0.890	2.16
8	955	108	22.01	2.37	0.858	2.11
9	1016	110	18.71	2.47	0.852	2.08
10	1091	109	17.06	2.39	0.844	2.15

Table D2. Calibration data for open bed runs.

Run #	Zeros or Net Divisions Ch 1	Ch 2	Ch 4	Calibration Levels in H_2O/div Ch 1	in Hg/div Ch 2	psia/div Ch 4
1	3.5	8.35	10.5	θ	θ	θ
	8.5	7.85	10.1	2.4000 ?	0.2038	0.04505
	22.0	17.15	15.0	1.7864	0.1516	0.04700
	36.5	24.25	18.8	1.6301	0.1402	0.04894
2	3.4	8.35	10.6	θ	θ	θ
	22.7	17.75	16.0	1.7665	0.1521	0.04719
	37.4	23.85	18.5	1.6257	0.1426	0.04811
3	6.6	8.4	10.5	θ	θ	θ
	19.9	15.6	14.8	1.5377	0.1506	0.04595
	28.8	22.5	18.6	1.5347	0.1333	0.04720
	35.35	24.0	18.8	1.5348	0.1375	0.04707
4	6.15	8.4	10.7	θ	θ	θ
	17.6	15.35	14.55	1.5057	0.1498	0.04625
	24.35	20.1	17.6	1.4908	0.1443	0.04756
	29.95	22.1	18.0	1.4925	0.1403	0.04889
5	6.3	9.1	10.8	θ	θ	θ
	13.5	12.8	13.8	1.4963	0.1602	0.04688
	20.2	19.4	18.1	1.5050	0.1443	0.04862
	26.9	21.2	18.3	1.4870	0.1415	0.04891
6	6.7	9.0	11.3	θ	θ	θ
	13.85	13.7	14.6	1.5235	0.1642	0.04692
	20.1	19.4	18.1	1.5274	0.1443	0.04834
	26.1	21.3	18.3	1.5019	0.1455	0.04891
7	6.3	9.0	11.3	θ	θ	θ
	16.4	16.9	17.1	1.4695	0.1479	0.04678
	20.7	20.0	18.7	1.4879	0.1450	0.04786
	27.0	21.25	18.3	1.4741	0.1459	0.04891
8	6.7	8.3	11.5	θ	θ	θ
	7.1	9.05	11.3	1.5211	0.1657	0.04425
	13.0	16.1	15.9	1.5154	0.1366	0.04673
	19.1	20.5	18.65	1.4921	0.1220	0.04799
9	6.9	8.6	12.1	θ	θ	θ
	8.5	12.25	13.7	1.5529	0.1551	0.04693
	13.1	17.7	17.4	1.5038	0.1412	0.04862
	17.2	20.1	18.65	1.5581	0.1393	0.04779
10	7.0	8.65	11.9	θ	θ	θ
	9.8	15.3	16.0	1.5408	0.1438	0.04750
	12.9	19.15	18.6	1.5194	0.1358	0.04823
	17.0	20.15	18.6	1.5000	0.1390	0.04812

Table D3. U_{mf} data for tube array runs.

Run #	d_{p_v} Ch 1	P_v Ch 2	$d_{p_{bed}}$ Ch 4	d_{p_v} Ch 1	P_v Ch 2	$d_{p_{bed}}$ Ch 4	T_v, °F
1a	41.7	34.2	30.0	41.95	34.30	29.85	117
1b	42.2	34.4	29.7 ZERO	-4.2	-7.8	-10.8	
			NET	37.75	26.50	19.05	
2a	31.2	31.1	29.6	31.60	31.35	29.65	117
2b	32.0	31.6	29.7	4.2	7.8	10.8	
				27.40	23.55	18.85	
3a	27.1	31.1	30.0	27.10	30.95	29.95	116
3b	27.1	30.8	29.9	4.2	7.8	10.8	
				22.90	23.15	19.15	
4a	24.2	30.0	29.9	24.35	30.10	30.05	120
4b	24.5	30.2	30.2	4.2	7.8	10.8	
				20.15	22.30	19.25	
5a	22.5	30.2	30.6	22.15	29.95	30.25	125
5b	21.8	29.7	29.9	4.2	7.8	10.8	
				17.95	22.15	19.45	
6a	20.6	29.8	30.5	20.85	29.80	30.50	134
6b	21.1	29.8	30.5	4.2	7.2	10.8	
				16.65	22.00	19.70	
7a	20.0	29.7	30.6	20.10	29.65	30.50	144
7b	20.2	29.6	30.4	4.2	7.8	10.8	
				15.90	21.85	19.70	
8a	18.2	29.7	30.5	18.35	29.75	30.45	130
8b	18.5	29.8	30.4	4.2	7.8	10.8	
				14.15	21.95	19.65	
9a	17.3	29.8	30.8	17.30	29.60	30.70	137
9b	17.3	29.4	30.6	4.2	7.8	10.8	
				13.10	21.80	19.90	
10a	15.0	28.0	29.5	14.75	28.15	29.65	123
10b	14.5	28.3	29.8	4.2	7.8	10.8	
				10.55	20.35	18.85	

Table D3. (Continued)

Run #	T_{bed} K	T_v °F	dp_v in H_2O	P_v in Hg	dp_{bed} psia	U_{mf} m/s
1	561	117	53.70	3.46	0.932	1.83
2	614	117	41.20	3.07	0.922	1.78
3	672	116	35.25	3.02	0.937	1.83
4	714	120	31.45	2.91	0.942	1.83
5	758	125	28.33	2.89	0.951	1.85
6	808	134	26.42	2.87	0.964	1.90
7	872	144	25.28	2.85	0.964	2.00
8	919	130	22.60	2.86	0.961	2.03
9	966	137	20.98	2.84	0.973	2.05
10	1030	123	17.13	2.66	0.922	2.01

Table D4. Calibration data for tube array runs.

Run E	Zeros or Net Divisions Ch 1	Ch 2	Ch 4	Calibration Levels in H_2O/div Ch 1	in Hg/div Ch 2	psia/div Ch 4
all runs	4.2	7.8	10.8	θ	θ	θ
	8.3	13.7	14.5	1.7108	0.1460	0.04724
	9.0	18.1	16.5	1.6389	0.1326	0.05218
	12.4	18.3	17.8	1.6048	0.1311	0.04831
	17.1	22.9	20.8	1.5848	0.1310	0.04952
	35.4	27.7	21.5	1.4407	0.1300	0.05023

APPENDIX E

This appendix presents the heat transfer data run results. Table E1 gives the heat flux, surface temperature, bed temperature, and heat transfer coefficient as a function of radial position. Figure E1 defines each radial position.

Table E2 gives calibration data for each of the heat flux transducers used to generate the data of Table E1.

No page 114

Table E1. Heat flux data.

1122	24.2	4.0	110	1.17
2		4		6
7		9		8
16.7		13.5		12.0
0		0		0
16.7		13.5		12.0
142384		113643		98028
402		392		386
720		730		736
198		156		133
1077	24.0	4.0	112	1.20
1		3		5
10		9		8
17.5		13.3		8.5
0		0		0
151988		111959		69437
411		397		382
666		680		695
228		165		100
1177	17.15	3.4	110	1.12
2		4		6
7		9		8
9.2		14.0		7.8
0		0		0
9.2		14.0		7.8
78439		117852		63718
373		387		368
804		790		809
97.6		149		78.8

1072	24.0	4.0	113	1.20
1		3		5
1		4		8
20.5		13.3		10.0
.15		.05		0
20.65		13.35		10.0
59699		68312		81690
377		380		385
695		692		687
85.9		98.7		119
1105	20.2	3.8	108	1.15
3		5		7
7		9		8
19.0		13.5		14.5
0		0		0
161994		113643		118451
417		400		401
688		705		704
235		161		168
1083	24.0	4.0	114	1.21
1		3		5
1		4		11
23.7		10.5		11.0
.15		.05		0
23.85		10.55		11.0
68950		53984		97823
381		376		391
702		707		692
98.2		76.4		141

				4
				12
				28.4
				0
				28.4
				3.292
				352
				3
				12
				31.0
				0
				3.593
				358
				3
				12
				26.0
				0
				26.0
				3.013
				346
				3
				12
				30.0
				0
				30.0
				3.477
				356
				5
				12
				28.0
				0
				3.245
				360
				3
				12
				30.5
				0
				30.5
				3.535
				357

Table E1. (Continued)

1072	24.0	4.0	112	1.20		1077	24.0	4.0	112	1.21	
1		3		5	3	1		3		5	3
1		9		8	12	7		9		8	12
15.5		13.5		13.0	29.2	9.5		20.5		12.8	32.5
.15		0		0	0	0		0		0	0
15.65		13.5		13.0	29.2	9.5		20.5		12.8	32.5
45244		113643		106197	3.384	80997		172569		104563	3.767
371		395		392	355	390		422		399	362
701		677		680		687		655		678	
64.5		168		156		118		263		154	
1077	17.3	3.4	112	1.03		1122	24.8	4.0	107	1.28	
1		3		5	3	3		5		7	5
7		9		8	12	7		9		11	12
2.2		9.5		7.5	28.0	17.6		14.3		15.5	29.5
0		0		0	0	0		0		0	0
2.2		9.5		7.5	28.0	17.6		14.3		15.5	29.5
18757		79971		61268	3.245	150058		120377		137842	3.418
358		379		372	351	407		396		402	354
719		698		705		715		726		720	
26.0		115		86.9		210		166		191	
1116	20.3	3.8	108	1.16		1122	24.8	4.0	109	1.28	
3		5		7	5	3		5		7	5
7		9		8	12	10		4		11	12
18.5		14.5		24.0	30.0	30.8		14.7		15.7	28.5
0		0		0	0	.2		.05		0	0
18.5		14.5		24.0	30.0	31.0		14.75		15.7	28.5
157731		122061		196056	3.477	269235		75478		139620	3.303
411		399		425	356	446		378		401	352
705		717		691		676		744		721	
224		170		284		398		101		194	

Table E1. (Continued)

1127	13.9	2.8	107	0.96		1122	20.5	3.8	108	1.17	
3		5		7	5	3		5		7	5
7		9		8	12	7		9		11	12
13.8		7.6		8.7	27.0	21.5		15.3		14.5	30.3
0		0		0	0	0		0		0	0
13.8		7.6		8.7	27.0	21.5		15.3		14.5	30.3
117659		63973		71070	3.129	183309		128795		128949	3.512
389		370		373	348	421		402		402	357
738		757		754		701		720		720	
159		84.5		94.3		261		179		179	

Note. The data is in the following order:

(T_B, K) (venturi data) (U_o/U_{mf})
(transducer locations)
(transducer numbers)
(gross chart divisions)
(offset divisions)
(heat flux, J/m^2-s) (thermocouple mV)
(T_{LM}, K) (T_o, K)
(ΔT, K)
(h_o, J/m^2-s-K)

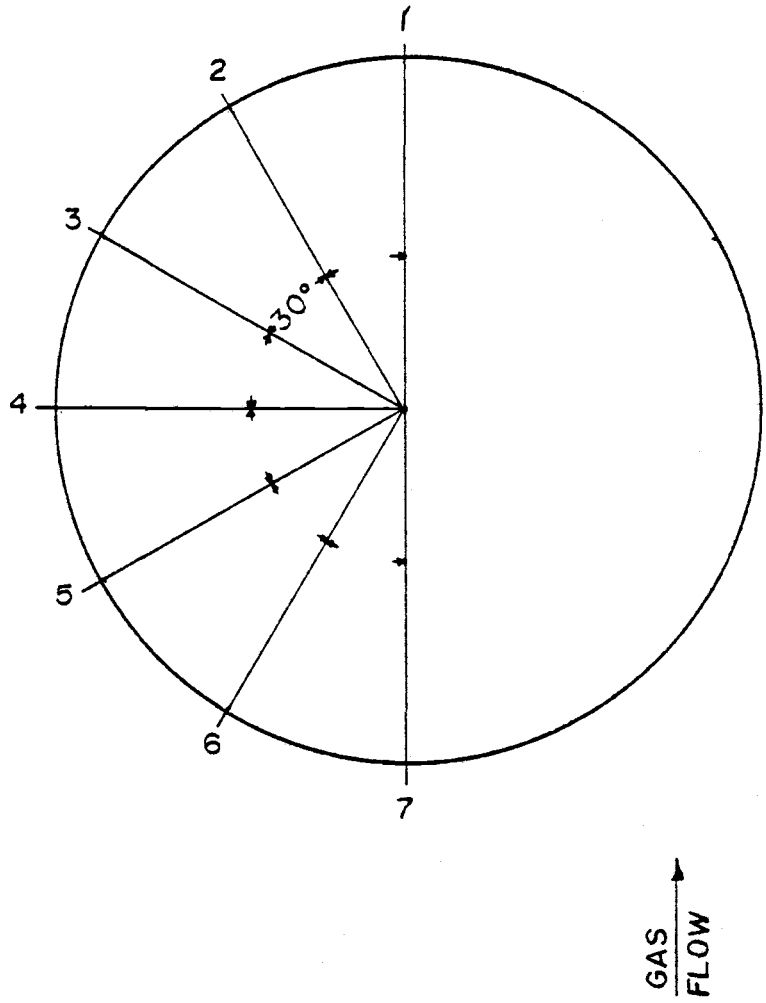

Appendix Figure E1 Radial Position Key for Heat Flux Data.

Table E2. Heat flux calibration data.

Radial Position #	Transducer #	Transducer Gain mV / J/m^2-s	Amplifier Visicorder Gain mV/ div	Overall Gain J/m^2-s / div	Visicorder Offset divisions
1, 2, 3	1	1.275E-5	0.03686	2891	-0.15
1, 2, 3	7	1.275E-5	.1087	8526	0
1, 2, 3	10	1.455E-5	.1264	8685	-0.2
3, 4, 5	4	7.510E-6	.03843	5117	-0.05
3, 4, 5	9	1.5074E-5	.1269	8418	0
5, 6, 7	8	1.3833E-5	.1130	8169	0
5, 6, 7	11	1.4159E-5	.1259	8893	0

Transducer #	Trial #	Observed Gain, mV / J/m^2-s	Transducer #	Trial #	Observed Gain, mV / J/m^2-s
1, 7	1	1.2635E-5	9	1	1.5303E-5
	2	1.2829		2	1.5066
	3	1.2935		3	1.4705
	4	1.2715		4	1.5189
	5	1.2653		5	1.5118
	avg	1.2750E-5		avg	1.5074E-5
4	1	7.6305E-6	10	1	1.4458E-5
	2	7.5478		2	1.4608
	3	7.4624		3	1.4599
	4	7.4905		avg	1.4555E-5
	5	7.4571			
	6	7.4712			
	avg	7.5099E-6			
8	1	1.3692E-5	11	1	1.4282E-5
	2	1.3736		2	1.4238
	3	1.3657		3	1.4414
	4	1.4159		4	1.4053
	5	1.3912		5	1.3877
	avg	1.3833E-5		6	1.4097
				avg	1.4159E-5

APPENDIX F

The experimental heat flux transducers are manufactured as follows.

The first step is to obtain the materials of construction. The constantan foil is obtained from Micro-Tek Associates Inc. of Los Angeles, CA. The copper body is fabricated from copper tubing of 1/8 inch o.d. originally intended for refrigeration service. The silver solder used is of the type known as "easy" hard solder (m.p. = 1125°F). A self pickling flux (Batterns brand) is used for the soldering. A miniature torch is used for soldering although a standard sized propane or butane torch is also used. The latter torch requires more finesse to avoid overheating the copper or foil. A few transducers have been made using 600°F m.p. cadmium solder and are satisfactory except when there is a possibility of some pressure head from the inside of the transducer (e.g. due to gas expansion on heating or to coolant leakage). The lower m.p. solder appears to form a much weaker bond than the 1125°F m.p solder does and several transducers made with the former have failed due to clean foil separation after a fairly short time in service. The 1125°F solder is also necessary if the outer surface of the transducer is to be operated at temperatures over 450°F or so. The transducer bodies should be kept cooled to 500°F or less lest the

center junction temperature run into the non-linear region of the device response curve in any case. The alternative is to calibrate over the full range of flux and temperature at which operation is contemplated.

The center conductor is made of the smallest diameter copper wire which is convenient to handle. In general the center conductor diameter should be of the same order of magnitude as the foil thickness to facilitate the electrical welding which is to be done.

The device electrical attachments are made with teflon sleeved, solid 26 gage copper wire. A short piece of asbestos sleeving of a diameter to be a sliding fit inside the copper tube bore and a tight fit on the outside of the teflon sleeve is also used in the present design. It will be seen that there is considerable flexibility in the exact configuration used and it all depends on what the operating environment is to be.

Conventional rosin core solder and a 20 watt soldering iron are also used in the construction.

A variable voltage power supply which has fold-back or similar current limiting and which puts out 6-10 VDC is also needed. The current limit is necessary to prevent burning the weld which the power supply is used to produce. A 1000 μf electrolytic capacitor of 12 WVDC or higher rating is also used.

The actual construction starts with fabrication of the threaded

holes into which the transducers will fit. Each transducer is custom fitted to its location to minimize surface irregularities in the completed assembly. The 1/8" copper tube is threaded with a #5-40 NC die so that it will protrude 1/16" or more from the outer surface of the hole into which it is screwed. The non-threaded end is then hacksawed off so that 3/16 to 1/4 inch of unthreaded copper is left.

The threaded end is fully screwed into its location and the protrusion is carefully filed down to the level of the surface. A small tapered round jeweler's file is used to clean up the tube bore. The non-threaded end is also filed until it is flat and then the full bore is cleaned with the round file.

The copper piece is removed from its receptacle and the threaded end (which has been filed to conform to the outer surface) is now carefully filed as uniformly as possible to sufficient degree so that when the foil is soldered on and the device is screwed into its receptacle it will be flush with the surface.

Soldering of the foil is accomplished with the aid of a jeweler's type coiled asbestos soldering ring which has a short pin stuck in the surface. The pin is used to support the copper body during the soldering operation. The general method is to flux and tin the outer end of the copper tube, allow to cool, file very lightly, reflux lightly and then heat the body only, with a small square of foil placed on the tube end. When the solder wets the foil a bright ring (in the case of

the 1125 m. p. solder) or a dark ring (in the case of the 600 m. p. solder) will appear on the outer surface of the foil and the success or failure of the operation is fairly readily apparent. The solder is allowed to cool for a few seconds until it solidifies and then the whole assembly is pickled by dropping it into dilute sulphuric acid. The pickling can be repeated as necessary. Thorough flushing with clean water follows. A small piece of paper towel is used to clean and dry the bore of the tube. Examination of the bore under a strong light permits examination of the inside foil surface. The flux must be completely removed and the solder must not bridge the foil.

The next step is to take a piece of the 26 gage bare copper wire and a few inches of the very fine copper wire and to wrap the latter around one end of the former a few times. This joint is lightly soldered with the electronic type rosin core solder and one end of the fine wire is cut back so that only one end is left. The remaining fine wire is looped around a small round object (the round tapered jeweler's file is used here) a few times to form loops that permit expansion or contraction of the device without breaking the wire.

A 1/2 inch or so long piece of teflon sleeving is slipped over the free end of the 26 gage wire and is slid up to (and over as much as possible) the solder joint. The sleeving should be a very tight fit if the device is to be fluid-tight from the back.

The next step is to slide a very short piece of the asbestos

sleeving over the fine wire and slide it down so that it covers the loops and the solder joint and is firmly butted against or over the teflon sleeve. The function of the asbestos is to provide guidance and support for the fine wire during insertion and welding. Once the asbestos sleeve is on, the fine wire is clipped off to protrude 1/16" or so from the end of the sleeve. The sleeve end is rolled with the fingers to work the asbestos down and to center the wire. The sketch shows the state of affairs at this point.

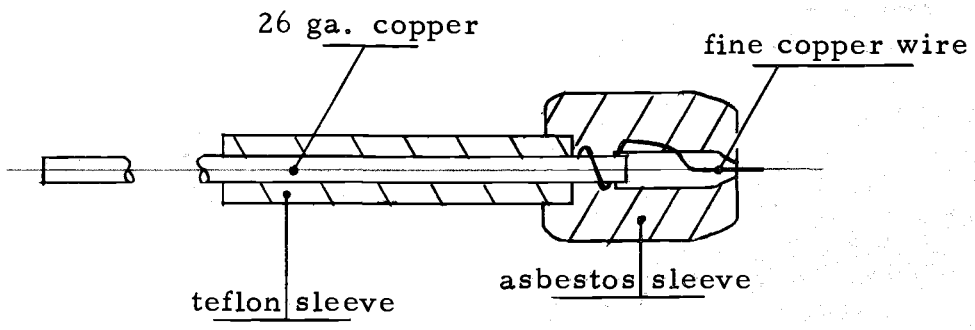

The 1000 μf capacitor is connected across the output terminals of the power supply and the output is set to 8 Volts DC (this may not be optimum for all foil/wire thickness combinations). The negative side of the supply is connected to the copper body with an alligator head and the positive terminal is connected to the free end of the 26 gage wire assembly. The latter unit is slid into the copper body until contact between the fine wire and the foil occurs. If a weld occurs the power supply will go into the limit mode and the output voltage should drop to some low value. The weld is tested by withdrawing

the wire a small fraction of an inch and noting that the power supply voltage stays at the low level. The power supply lead is gently disconnected from the center conductor and a pair of needle nose pliers are used to crimp the unthreaded end down on the teflon sleeve until the wire is firmly anchored in the body. The worst is over now, provided the job has been done right.

A razor blade is used to cut the teflon sleeve back so that it just protrudes past the back of the body. A short piece of bare 26 gage copper wire is slid into the body, in the space beside the sleeving, and this is soldered to the body end, avoiding excessive solder (using rosin core solder).

The present experimental facility uses Dowtherm A as the heat transfer medium in the immersed tube and this requires the following additional steps.

A small amount of two-part epoxy is beaded around the protruding electrical connections and the body is lightly heated with the soldering iron and then allowed to cool so that gas contraction pulls the epoxy somewhat inside the body and around the wires. Sufficient additional epoxy is added to seal the teflon sleeve and form a small bead. After the epoxy hardens the transducer is oven baked at 200 or 300°F for several hours to thoroughly cure the epoxy. For Dowtherm A service it has been found necessary to coat the epoxy with a thin layer of silicone gasket material (Permatex brand will

work) to slow the attack on the epoxy. While the silicone appears to be completely inert to the Dowtherm there is still some penetration and it is necessary to re-epoxy those transducers which have not failed due to coolant penetration after each data run. It is quite possible that some superior material is available to form this seal.

If the electric welding process did not puncture the foil end at the point of contact then it may be a good idea to put a very small hole in the foil to relieve gas pressure if the device is to be operated at high body temperature.

A high temperature large particle fluidized bed is a very hostile environment and no claim is made that these devices function for long periods without problems. Slugging in the bed has caused foil failure. Occasionally a device fails apparently due to a poor electric weld but it has been found that the main cause of failure is due to coolant leakage past the inside seal (coolant pressure is kept as low as possible with large diameter lines and short runs but nevertheless runs up to 15 psig in this equipment). Dowtherm A appears to be a fair to excellent solvent for all epoxies tried and so any leakage past the silicone coat is eventually fatal.

A few suggestions should be made here. The foil used to this point in these experiments is much thinner than necessary (0.0005 inches). New foil is to be ordered (0.0020 inches thick) and will be used for future construction. The foil thickness does not affect the

device time constant (within limits) and the four-fold reduction in electrical output which will result from the thicker foil should be no problem, even for the very simple electronics in use (Analog Devices brand AD522 amplifiers with gain and offset trimmers) here. The thicker foil should provide better performance for high air velocity, large particle runs.

The other major suggestion is that electric welding be used to attach the foil to the body if the equipment is available. This should result in a much faster responding device compared to one produced by the present soldering method. This should also eliminate the annealing of the copper which occurs when the device is soldered and pickled. This annealing eliminates the advantageous work hardening of the copper which occurs during the threading operation and results in a transducer which must be handled carefully when inserting or removing to avoid excessive distortion.

A further suggestion that does not appear to be really important is that the A. S. T. M. recommends oxygen free copper be used throughout. This may eliminate the slight ($< 1.5\%$) non-linearity in the output voltage versus flux observed in the experimental transducers when calibrated against the Hy-Cal standard which has no measurable non-linearity. It seems quite possible that the solder joint is the culprit however.